POR-2015-V2(EX)
(WT-2015-V2)(EX)
EXTRACTED VERSION

OPERATION DOMINIC, FISH BOWL SERIES

Project Officer's Report—Project 6.1

Fireball Attenuation and Refraction

R. J. Clawson, Project Officer
S. G. Hoihjelle
C. R. Yalkut
U. S. Army Electronics Research and Development Activity
White Sands Missile Range, NM

D. J. Pearce
C. L. Gardenhire
Physical Science Laboratory
New Mexico State University
University Park, NM

24 March 1965

NOTICE:

This is an extract of POR-2015 (WT-2015), Operation DOMINIC, Volume 2, Fish Bowl Series, Project 6.1.

Extracted version prepared for
Director
DEFENSE NUCLEAR AGENCY
Washington, DC 20305-1000

1 September 1985

UNCLASSIFIED
SECURITY CLASSIFICATION OF THIS PAGE

AD-A995426

REPORT DOCUMENTATION PAGE

1a. REPORT SECURITY CLASSIFICATION UNCLASSIFIED	1b. RESTRICTIVE MARKINGS
2a. SECURITY CLASSIFICATION AUTHORITY	3. DISTRIBUTION/AVAILABILITY OF REPORT Approved for public release; distribution is unlimited.
2b. DECLASSIFICATION/DOWNGRADING SCHEDULE	
4. PERFORMING ORGANIZATION REPORT NUMBER(S)	5. MONITORING ORGANIZATION REPORT NUMBER(S) POR-2015-V2 (EX) (WT-2015-V2) (EX)
6a. NAME OF PERFORMING ORGANIZATION 1-Army Electronics R&D Activity 2-Physical Science Lab, New Mexico State U.	6b. OFFICE SYMBOL (If applicable)
7a. NAME OF MONITORING ORGANIZATION Defense Atomic Support Agency	
6c. ADDRESS (City, State, and ZIP Code) 1-White Sands Missile Range, NM 2-University Park, NM	7b. ADDRESS (City, State, and ZIP Code) Washington, DC
8a. NAME OF FUNDING/SPONSORING ORGANIZATION	8b. OFFICE SYMBOL (If applicable)
9. PROCUREMENT INSTRUMENT IDENTIFICATION NUMBER	
8c. ADDRESS (City, State, and ZIP Code)	10. SOURCE OF FUNDING NUMBERS PROGRAM ELEMENT NO. / PROJECT NO. / TASK NO. / WORK UNIT ACCESSION NO.

11. TITLE (Include Security Classification) OPERATION DOMINIC, FISH BOWL SERIES; PROJECT OFFICER'S REPORT, Project 6.1 - Fireball Attenuation and Refraction, Extracted Version

12. PERSONAL AUTHOR(S)
S. G. Hoihjelle, R. J. Clawson, C. R. Yalkut, D. G. Pearce, and C. L. Gardenhire

13a. TYPE OF REPORT	13b. TIME COVERED FROM TO	14. DATE OF REPORT (Year, Month, Day)	15. PAGE COUNT
		650324	178

16. SUPPLEMENTARY NOTATION This report has had sensitive military information removed in order to provide an unclassified version for unlimited distribution. The work was performed by the Defense Nuclear Agency in support of the DoD Nuclear Test Personnel Review Program.

17. COSATI CODES		
FIELD	GROUP	SUB-GROUP
18	3	
14	3	

18. SUBJECT TERMS (Continue on reverse if necessary and identify by block number)
Dominic, Fish Bowl, Fireball Attenuation, Refraction, Blue Gill, King Fish, Tight Rope

19. ABSTRACT (Continue on reverse if necessary and identify by block number)

A prime objective of the experiment was the quantitative measurement of the attenuation suffered by radar beams passing near or through the fireball of a nuclear detonation. During the test series, measurements were also made of effects produced in regions not directly associated with the fireball proper.

A second prime objective of the experiment was to investigate possible phase differences which were expected to develop in nearly parallel radar rays passing through ionized regions.

Ballistic rockets were used to place CW beacons, radiating at 1-, 5-, and 10-kMc frequencies. Five receiving stations, four on ships and one on Johnston Island, made signal strength measurements. An interferometer on the island made phase-front measurements at 1 and 5 kMc.

20. DISTRIBUTION/AVAILABILITY OF ABSTRACT ☒ UNCLASSIFIED/UNLIMITED ☐ SAME AS RPT. ☐ DTIC USERS	21. ABSTRACT SECURITY CLASSIFICATION UNCLASSIFIED
22a. NAME OF RESPONSIBLE INDIVIDUAL MARK D. FLOHR	22b. TELEPHONE (Include Area Code) 202-325-7559
22c. OFFICE SYMBOL DNA/ISCM	

DD FORM 1473, 84 MAR 83 APR edition may be used until exhausted. All other editions are obsolete.

SECURITY CLASSIFICATION OF THIS PAGE
UNCLASSIFIED

FOREWORD

Classified material has been removed in order to make the information available on an unclassified, open publication basis, to any interested parties. The effort to declassify this report has been accomplished specifically to support the Department of Defense Nuclear Test Personnel Review (NTPR) Program. The objective is to facilitate studies of the low levels of radiation received by some individuals during the atmospheric nuclear test program by making as much information as possible available to all interested parties.

The material which has been deleted is either currently classified as Restricted Data or Formerly Restricted Data under the provisions of the Atomic Energy Act of 1954 (as amended), or is National Security Information, or has been determined to be critical military information which could reveal system or equipment vulnerabilities and is, therefore, not appropriate for open publication.

The Defense Nuclear Agency (DNA) believes that though all classified material has been deleted, the report accurately portrays the contents of the original. DNA also believes that the deleted material is of little or no significance to studies into the amounts, or types, of radiation received by any individuals during the atmospheric nuclear test program.

OPERATION DOMINIC

FISH BOWL SERIES

PROJECT OFFICERS REPORT — PROJECT 6.1

FIREBALL ATTENUATION AND REFRACTION

Robert J. Clawson, Project Officer

Sylvia G. Hoihjelle
Carl R. Yalkut

U.S. Army Electronics Research and Development Activity
White Sands Missile Range, New Mexico

and

David G. Pearce
Charles L. Gardenhire

Physical Science Laboratory
New Mexico State University
University Park, New Mexico

CONTENTS

APPENDIX A AZIMUTH AND ELEVATION PEDESTAL INFORMATION ---- 11

APPENDIX B SUPPORT DATA ---- 53

B.1 Ship Position Data ---- 53
B.2 Fireball Data ---- 53
B.3 Trajectory Tracking Systems and Data ---- 54
B.3.1 Cubic Corporation Missile Tracking Systems ---- 54
B.3.2 Cubic Corporation Trajectory Data ---- 57

APPENDIX C SHIPBOARD REFRACTION MEASUREMENTS ---- 118

C.1 Calibration Method I ---- 118
C.2 Calibration Method II ---- 119

APPENDIX D INTERFEROMETER DESCRIPTION ---- 127

D.1 Data Reduction ---- 127
D.1.1 Angular Position Solution ---- 129
D.1.2 White Sands Missile Range Firing Data ---- 134
D.1.3 Dominic Data Problems ---- 134
D.1.4 Least-Squares Solution ---- 137
D.1.5 Short-Term Refraction ---- 139
D.2 Sources of System Error ---- 144
D.2.1 Lead-In Cables ---- 145
D.2.2 Doppler Shift ---- 146
D.2.3 Atmospheric Refraction ---- 147
D.2.4 Antenna Misalignment ---- 147
D.2.5 Phase Shift Between Receivers ---- 147
D.2.6 Multipath ---- 148

REFERENCES ---- 176

TABLES

B.1 Positions of Ships Relative to Reference Ship S-1, Blue Gill ---- 59
B.2 Positions of Ships Relative to Johnston Island, Blue Gill ---- 59
B.3 Ship Bearing and Speed, Blue Gill ---- 60
B.4 Positions of Ships Relative to Ground Zero, Blue Gill ---- 61
B.5 Positions of Ships Relative to Johnston Island, King Fish ---- 61
B.6 Positions of Ships Relative to Ground Zero, King Fish ---- 61
B.7 Ship Bearing and Speed, King Fish ---- 62
B.8 Positions of Ships Relative to Johnston Island at H-Hour, Tight Rope ---- 62
B.9 Positions of Ships Relative to Ground Zero, Tight Rope ---- 63
B.10 Ship Bearing and Speed, Tight Rope ---- 63

B.11 Location of Reentry Vehicle at Event, Blue Gill ---------- 64
B.12 Location of Reentry Vehicle at Event, King Fish ---------- 64
B.13 Location of Reentry Vehicle at Event, Tight Rope ---------- 65
B.14 Cubic Corporation Trajectory, Blue Gill, Missile A, H - 195 -------- 66
B.15 Cubic Corporation Trajectory, Blue Gill, Missile B, H - 190 -------- 70
B.16 Cubic Corporation Trajectory, Blue Gill, Missile C, H - 112 -------- 75
B.17 Cubic Corporation Trajectory, Blue Gill, Missile D, H - 108 -------- 78
B.18 Cubic Corporation Trajectory, Blue Gill, Missile E, H+ 290 -------- 80
B.19 Cubic Corporation Trajectory, Blue Gill, Missile F, H+ 905 -------- 81
B.20 Cubic Corporation Trajectory, King Fish, Missile B, H -155 -------- 83
B.21 Cubic Corporation Trajectory, King Fish, Missile C, H -85 --------- 87
B.22 Cubic Corporation Trajectory, Tight Rope, Missile A, H -50 -------- 88
B.23 Cubic Corporation Trajectory, Tight Rope, Missile C, H -40 -------- 93
B.24 Cubic Corporation Trajectory, Tight Rope, Missile D, H -40 -------- 99
C.1 Calibration Method II, Tracking Sequence ---------- 122
D.1 Equivalent Wavelengths of Interferometer Legs, Blue Gill, Missile A, H -195 Sec ---------- 149
D.2 Equivalent Wavelengths of Interferometer Legs, King Fish, Missile C, H -85 Sec ---------- 149
D.3 Equivalent Wavelengths of Interferometer Legs, Tight Rope, Missile A, H -50 Sec ---------- 149
D.4 Dispersion of Sample Recorded Deviations for the Fourteen System Combinations, Blue Gill ---------- 150
D.5 Dispersion of Sample Recorded Deviations for the Fourteen System Combinations, King Fish ---------- 151

FIGURES

A.1 Azimuth and elevation versus time, Blue Gill, Missile C, Ship 1, H -120 to H +50---------- 12
A.2 Azimuth and elevation versus time, Blue Gill, Missile C, Ship 1, H +50 to H +220---------- 13
A.3 Azimuth and elevation versus time, Blue Gill, Missile C, Ship 2, H -120 to H +50---------- 14
A.4 Azimuth and elevation versus time, Blue Gill, Missile C, Ship 2, H +50 to H +220---------- 15
A.5 Azimuth and elevation versus time, Blue Gill, Missile C, Ship 3, H -120 to H +50---------- 16
A.6 Azimuth and elevation versus time, Blue Gill, Missile C, Ship 3, H +50 to H +220---------- 17
A.7 Azimuth and elevation versus time, Blue Gill, Missile C, Ship 4, H -120 to H +50---------- 18
A.8 Azimuth and elevation versus time, Blue Gill, Missile C, Ship 4, H +50 to H +220---------- 19
A.9 Azimuth and elevation versus time, Blue Gill, Missile E, Ship 1, H +290 to H +460---------- 20
A.10 Azimuth and elevation versus time, Blue Gill, Missile E, Ship 1, H +460 to H +630---------- 21
A.11 Azimuth and elevation versus time, Blue Gill, Missile E, Ship 2, H +290 to H +460---------- 22

A.12 Azimuth and elevation versus time, Blue Gill, Missile E, Ship 2, H+460 to H+630 ---- 23
A.13 Azimuth and elevation versus time, Blue Gill, Missile E, Ship 3, H+290 to H+460 ---- 24
A.14 Azimuth and elevation versus time, Blue Gill, Missile E, Ship 3, H+460 to H+630 ---- 25
A.15 Azimuth and elevation versus time, Blue Gill, Missile E, Ship 4, H+290 to H+460 ---- 26
A.16 Azimuth and elevation versus time, Blue Gill, Missile E, Ship 4, H+460 to H+630 ---- 27
A.17 Azimuth and elevation versus time, Blue Gill, Missile F, Ship 1, H+900 to H+1070 ---- 28
A.18 Azimuth and elevation versus time, Blue Gill, Missile F, Ship 1, H+1070 to H+1240 ---- 29
A.19 Azimuth and elevation versus time, Blue Gill, Missile F, Ship 2, H+900 to H+1070 ---- 30
A.20 Azimuth and elevation versus time, Blue Gill, Missile F, Ship 2, H+1070 to H+1240 ---- 31
A.21 Azimuth and elevation versus time, Blue Gill, Missile F, Ship 3, H+900 to H+1070 ---- 32
A.22 Azimuth and elevation versus time, Blue Gill, Missile F, Ship 3, H+1070 to H+1240 ---- 33
A.23 Azimuth and elevation versus time, Blue Gill, Missile F, Ship 4, H+900 to H+1070 ---- 34
A.24 Azimuth and elevation versus time, Blue Gill, Missile F, Ship 4, H+1070 to H+1240 ---- 35
A.25 Azimuth and elevation versus time, King Fish, Missile B, Ship 1, H-170 to H-20 ---- 36
A.26 Azimuth and elevation versus time, King Fish, Missile B, Ship 1, H-20 to H+130 ---- 37
A.27 Azimuth and elevation versus time, King Fish, Missile B, Ship 2, H-170 to H-20 ---- 38
A.28 Azimuth and elevation versus time, King Fish, Missile B, Ship 2, H-20 to H+130 ---- 39
A.29 Azimuth and elevation versus time, King Fish, Missile B, Ship 3, H-170 to H-20 ---- 40
A.30 Azimuth and elevation versus time, King Fish, Missile B, Ship 3, H-20 to H+130 ---- 41
A.31 Azimuth and elevation versus time, King Fish, Missile B, Ship 4, H-160 to H+30 ---- 42
A.32 Azimuth and elevation versus time, King Fish, Missile B, Ship 4, H+30 to H+220 ---- 43
A.33 Azimuth and elevation versus time, King Fish, Missile C, Ship 1, H+150 to H+300 ---- 44
A.34 Azimuth and elevation versus time, King Fish, Missile C, Ship 2, H+150 to H+300 ---- 45
A.35 Azimuth and elevation versus time, King Fish, Missile C, Ship 3, H+150 to H+300 ---- 46
A.36 Azimuth and elevation versus time, Tight Rope, Missile A, Ship 1, H-60 to H+110 ---- 47

A.37 Azimuth and elevation versus time, Tight Rope, Missile A, Ship 1, H+110 to H+280 ---- 48
A.38 Azimuth and elevation versus time, Tight Rope, Missile B, Ship 3, H-60 to H+110 ---- 49
A.39 Azimuth and elevation versus time, Tight Rope, Missile B, Ship 3, H+110 to H+280 ---- 50
A.40 Azimuth and elevation versus time, Tight Rope, Missile D, Ship 4, H-60 to H+110 ---- 51
A.41 Azimuth and elevation versus time, Tight Rope, Missile D, Ship 4, H+110 to H+280 ---- 52
B.1 Blue Gill fireball radius, early time ---- 104
B.2 Blue Gill fireball radius ---- 105
B.3 Angular diameter of Blue Gill fireball referenced to Point John ---- 106
B.4 Blue Gill fireball rise rates, early time ---- 107
B.5 Blue Gill fireball rise rates ---- 108
B.6 King Fish fireball horizontal radius ---- 109
B.7 King Fish fireball vertical radius ---- 110
B.8 King Fish fireball diameter ---- 111
B.9 King Fish fireball rise rates, early time ---- 112
B.10 King Fish fireball rise rates ---- 113
B.11 Tight Rope fireball radius, early time ---- 114
B.12 Tight Rope fireball radius ---- 115
B.13 Tight Rope fireball angular diameter referenced to Point John ---- 116
B.14 Tight Rope fireball rise rates ---- 117
C.1 Calibration Method I, test procedure ---- 123
C.2 Calibration Method II, test procedure ---- 124
C.3 Calibration Method II, error angles ---- 125
C.4 Calibration Method II, multipath interference ---- 126
D.1 Interferometer geometry ---- 152
D.2 Wave front incident to an interferometer antenna pair ---- 153
D.3 Slant plane lobe diagram, interferometer, Leg AB ---- 154
D.4 Slant plane lobe diagram, interferometer, Leg AC ---- 155
D.5 Slant plane lobe diagram, interferometer, Leg CD ---- 156
D.6 Slant plane lobe diagram, interferometer, Leg BD ---- 157
D.7 Slant plane lobe diagram, interferometer, Leg AD ---- 158
D.8 Slant plane lobe diagram, interferometer, Leg BC ---- 159
D.9 Trajectory and interferometer lobe numbers, WSMR test, Leg AB ---- 160
D.10 Trajectory and interferometer lobe numbers, WSMR test, Leg AC ---- 161
D.11 Trajectory and interferometer lobe numbers, WSMR test, Leg AD ---- 162
D.12 Trajectory and interferometer lobe numbers, WSMR test, Leg BC ---- 163
D.13 Trajectory and interferometer lobe numbers, WSMR test, Leg BD ---- 164
D.14 Trajectory and interferometer lobe numbers, WSMR test, Leg CD ---- 165
D.15 Interferometer and radar angular comparison, WSMR test, Interferometer Combination AC-BD ---- 166
D.16 Interferometer and radar angular comparison, WSMR test, Interferometer Combination AB-BC ---- 166
D.17 Interferometer and radar angular comparison, WSMR test, Interferometer Combination AC-CD ---- 167
D.18 Interferometer and radar angular comparison, WSMR test, Interferometer Combination AB-BD ---- 167

D.19 Interferometer and radar angular comparison, WSMR test, Interferometer Combination AD-BD ---------- 168
D.20 Interferometer and radar angular comparison, WSMR test, Interferometer Combination BC-AC ---------- 168
D.21 Interferometer and radar angular comparison, WSMR test, Interferometer Combination AD-CD ---------- 169
D.22 Interferometer and radar angular comparison, WSMR test, Interferometer Combination AB-AC ---------- 169
D.23 Interferometer and radar angular comparison, WSMR test, Interferometer Combination BC-BD ---------- 170
D.24 Interferometer and radar angular comparison, WSMR test, Interferometer Combination AC-AD ---------- 170
D.25 Interferometer and radar angular comparison, WSMR test, Interferometer Combination BC-CD ---------- 171
D.26 Interferometer and radar angular comparison, WSMR test, Interferometer Combination AB-AD ---------- 171
D.27 Interferometer and radar angular comparison, WSMR test, Interferometer Combination BD-CD ---------- 172
D.28 Interferometer and radar angular comparison, WSMR test, Interferometer Combination BC-AD ---------- 172
D.29 Interferometer and radar angular comparison, WSMR test, least-squares combination. ---------- 173
D.30 Ray-path directional components ---------- 174
D.31 Perturbation component in azimuth plane, Blue Gill---------- 175

APPENDIX A

AZIMUTH AND ELEVATION PEDESTAL INFORMATION

Azimuth and elevation pedestal information, recorded by the four shipboard stations (when available), are presented in Figures A.1 to A.41. The actual tracking data is indicated by a solid line with interpolated point plots describing pedestal angles to the missile. Some significant relative power points of the X-, C-, and L-band antenna patterns are also presented to indicate the extent of attenuation caused by antenna-pointing errors in each of the directional planes.

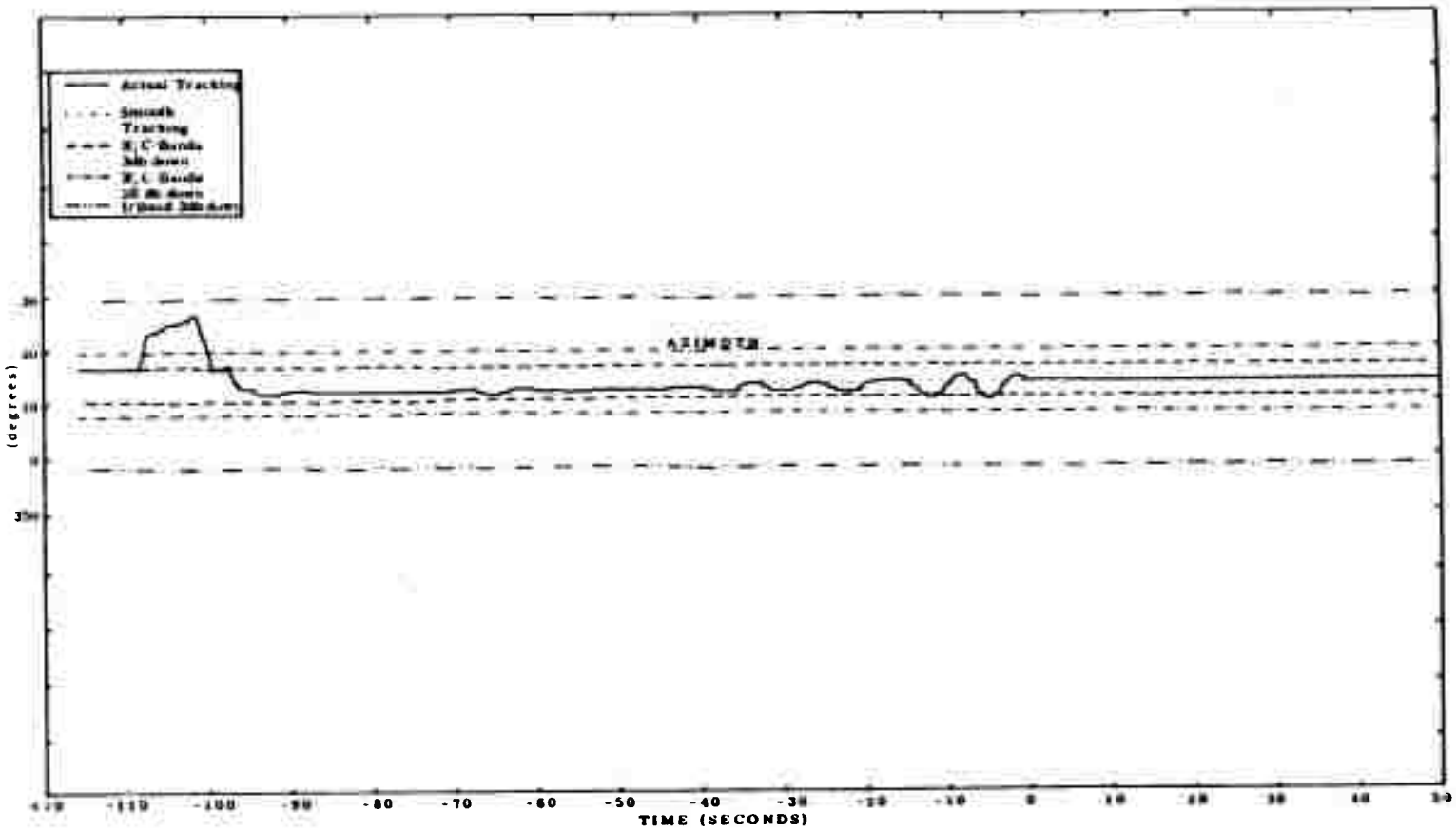

Figure A.1 Azimuth and elevation versus time, Blue Gill, Missile C, Ship 1, H - 120 to H + 50.

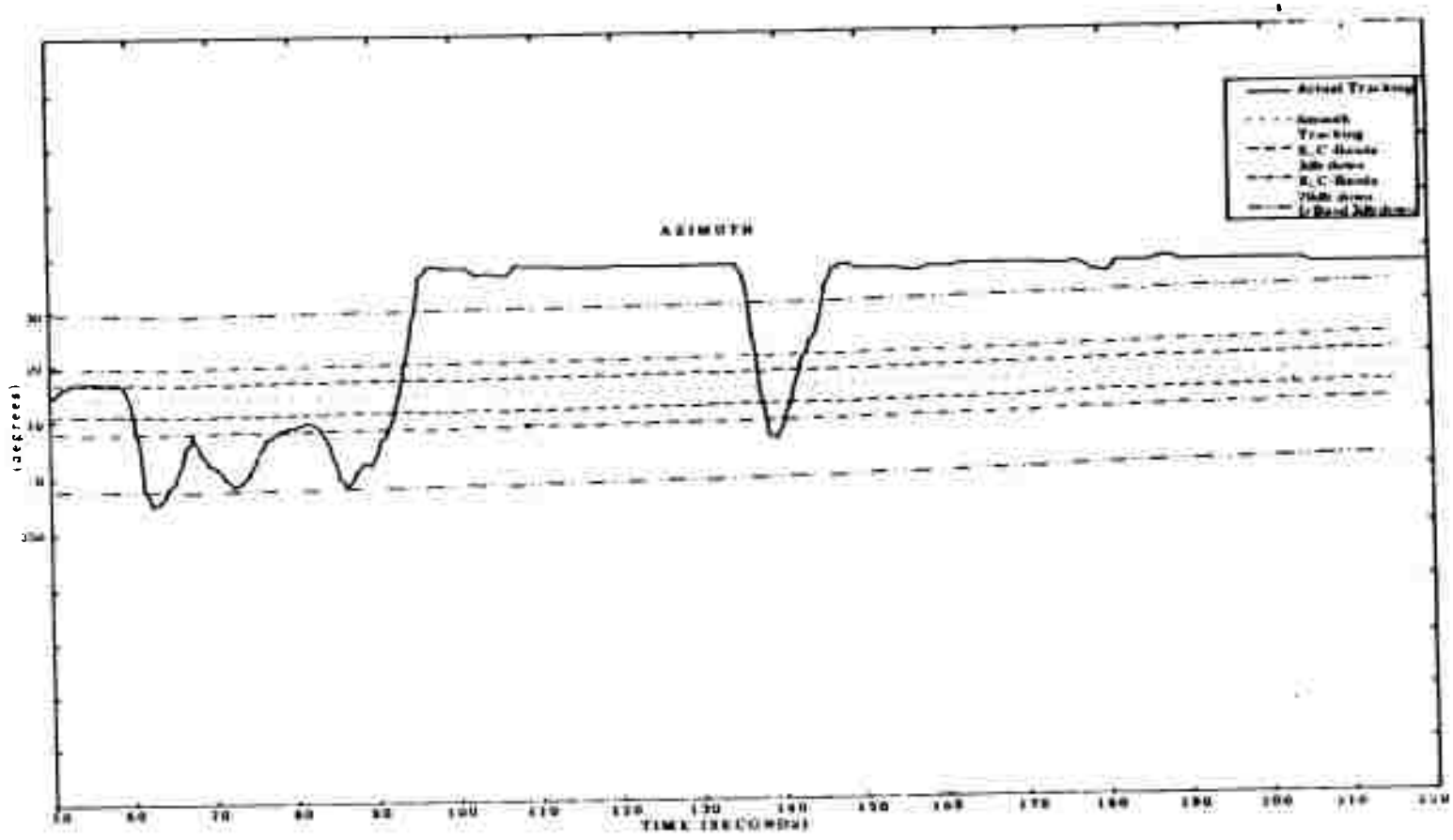

Figure A.2 Azimuth and elevation versus time, Blue Gill, Missile C, Ship 1, H + 50 to H + 220.

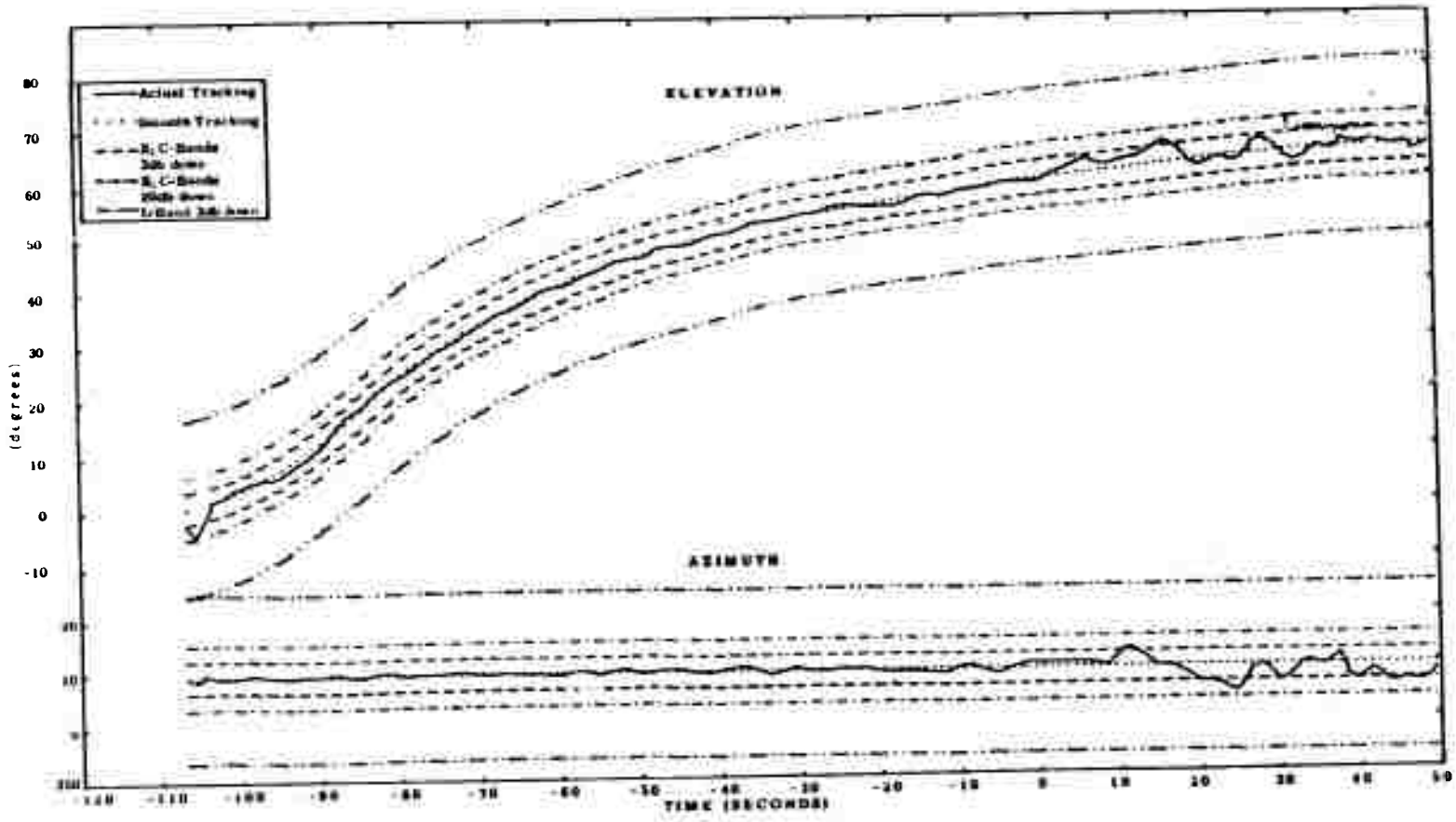

Figure A.3 Azimuth and elevation versus time, Blue Gill, Missile C, Ship 2, H - 120 to H + 50.

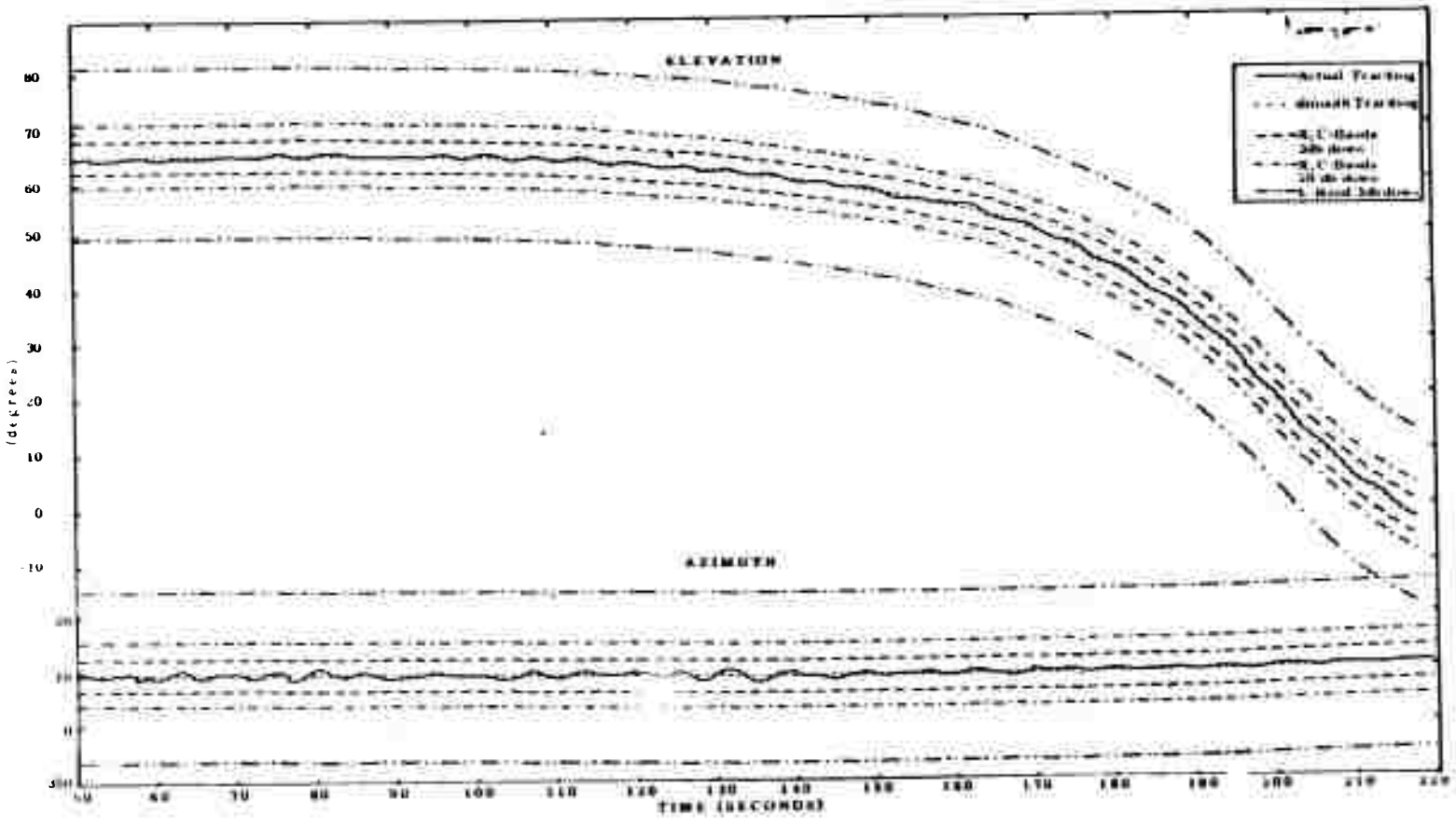

Figure A.4 Azimuth and elevation versus time, Blue Gill, Missile C, Ship 2, H + 50 to H + 220.

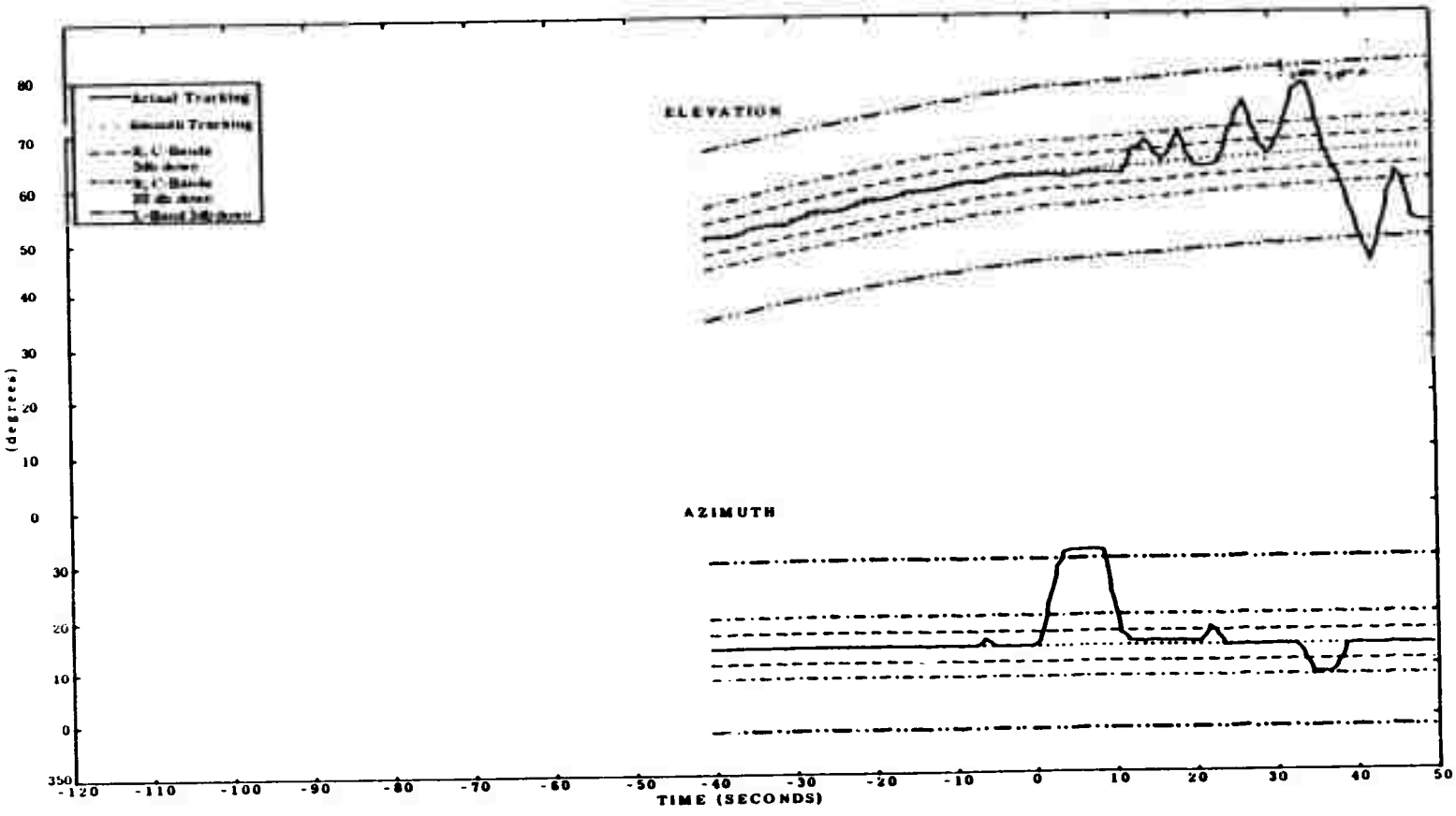

Figure A.5 Azimuth and elevation versus time, Blue Gill, Missile C, Ship 3, H−120 to H+50.

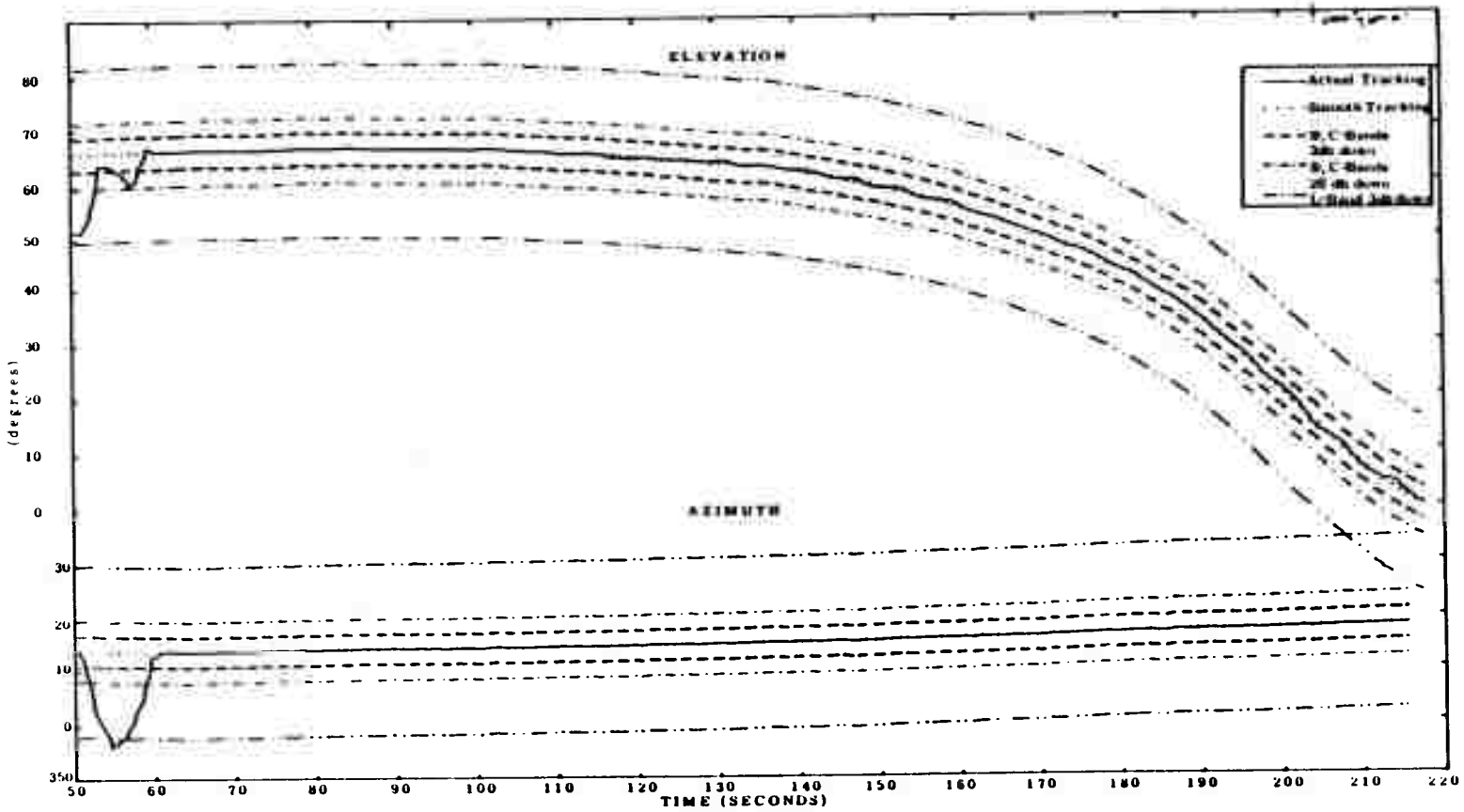

Figure A 6 Azimuth and elevation versus time, Blue Gill, Missile C, Ship 3, H + 50 to H + 220.

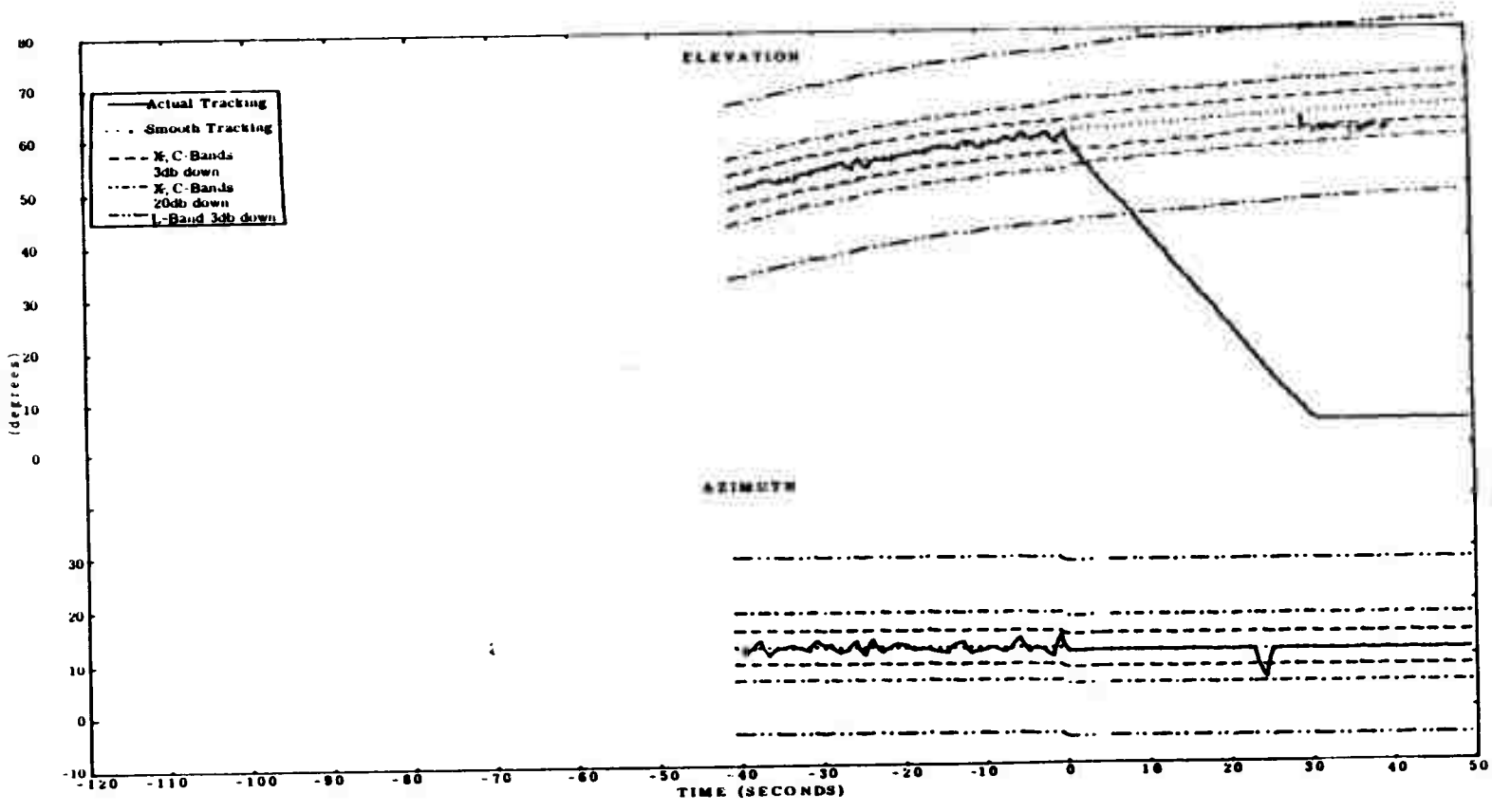

Figure A.7 Azimuth and elevation versus time, Blue Gill, Missile C, Ship 4, H - 120 to H + 50.

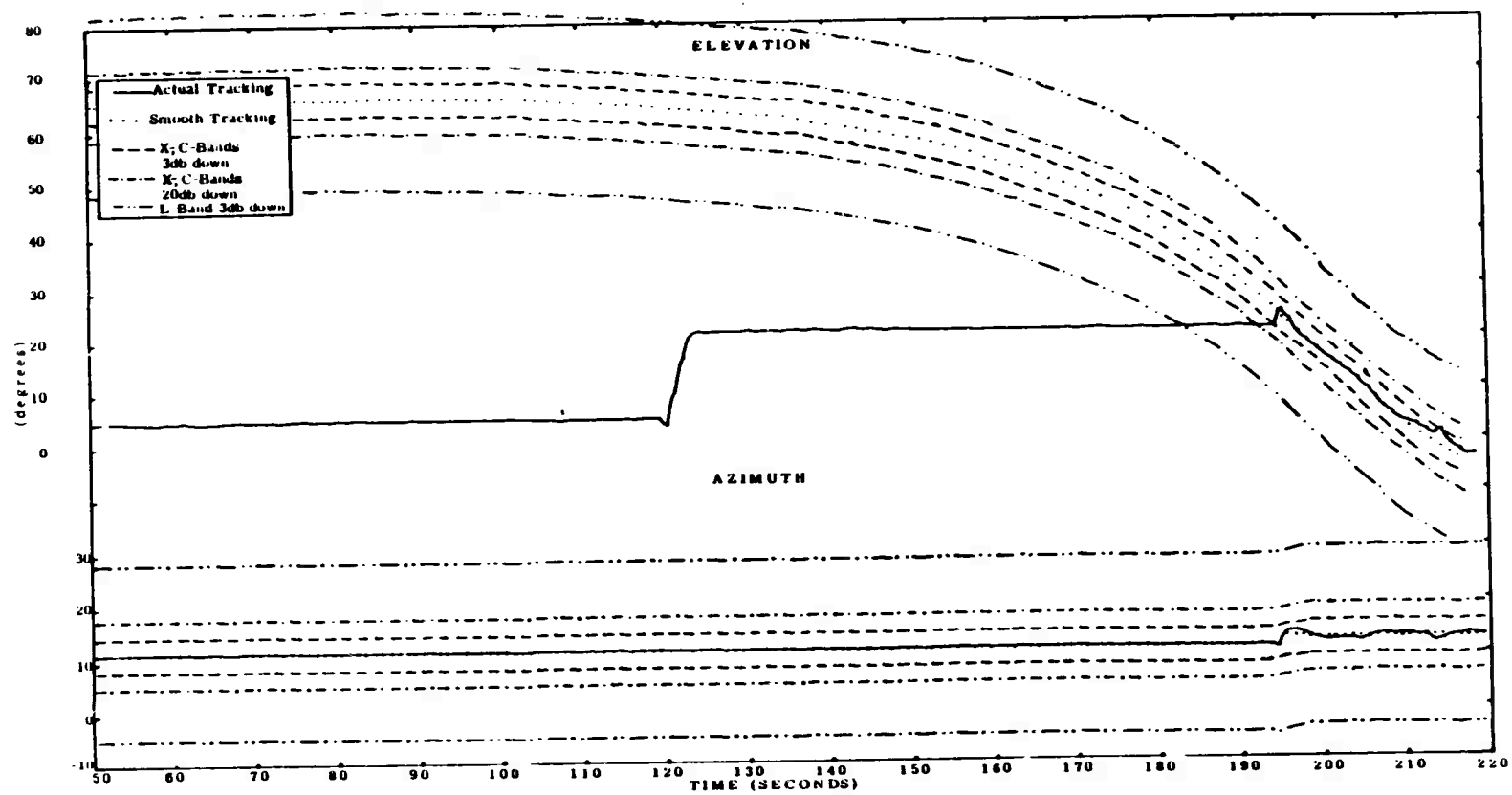

Figure A-8 Azimuth and elevation versus time, Blue Gill, Missile C, Ship 4, H + 50 to H + 220.

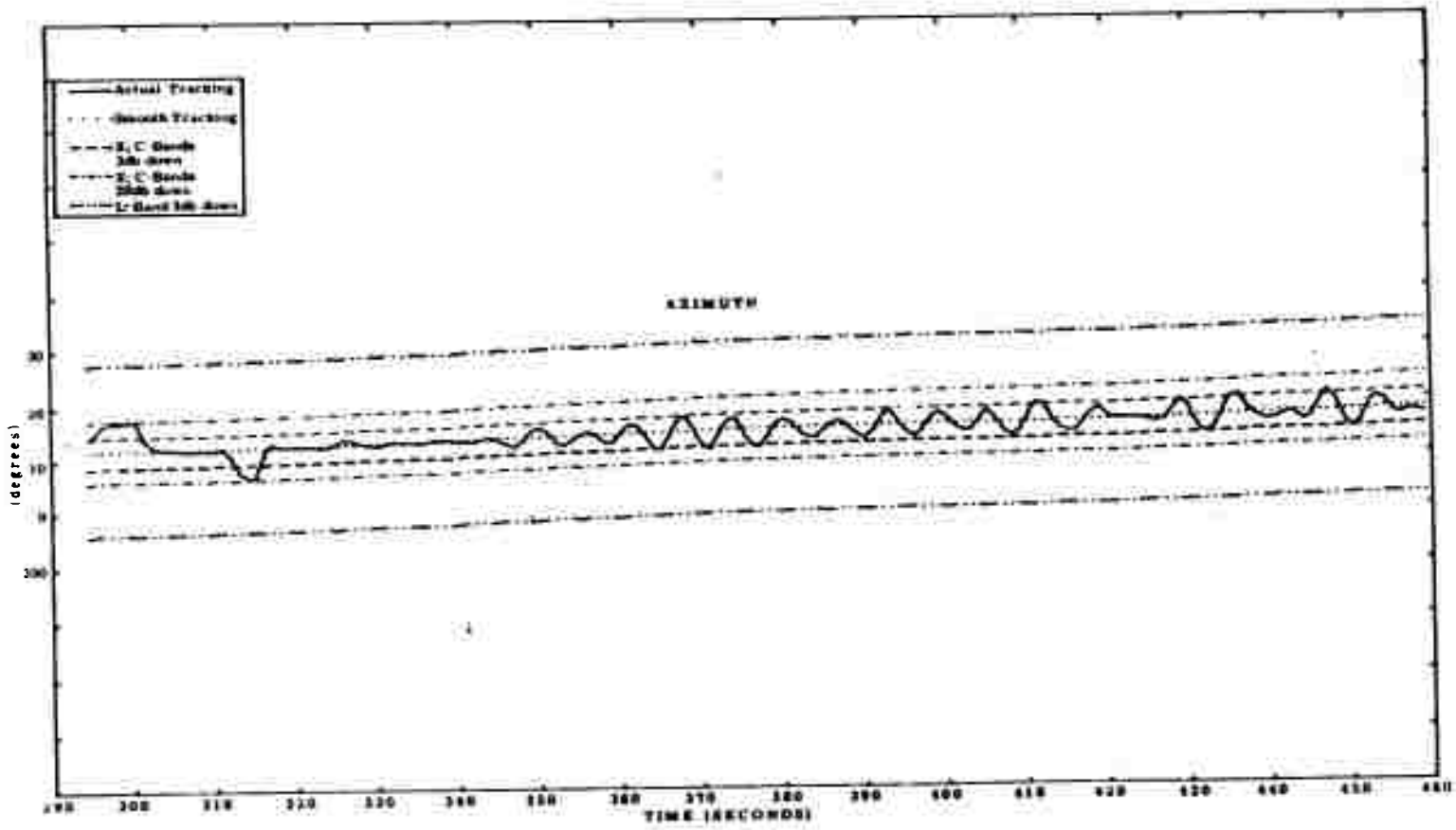

Figure A.9 Azimuth and elevation versus time, Blue Gill, Missile E, Ship 1, H + 290 to H + 460.

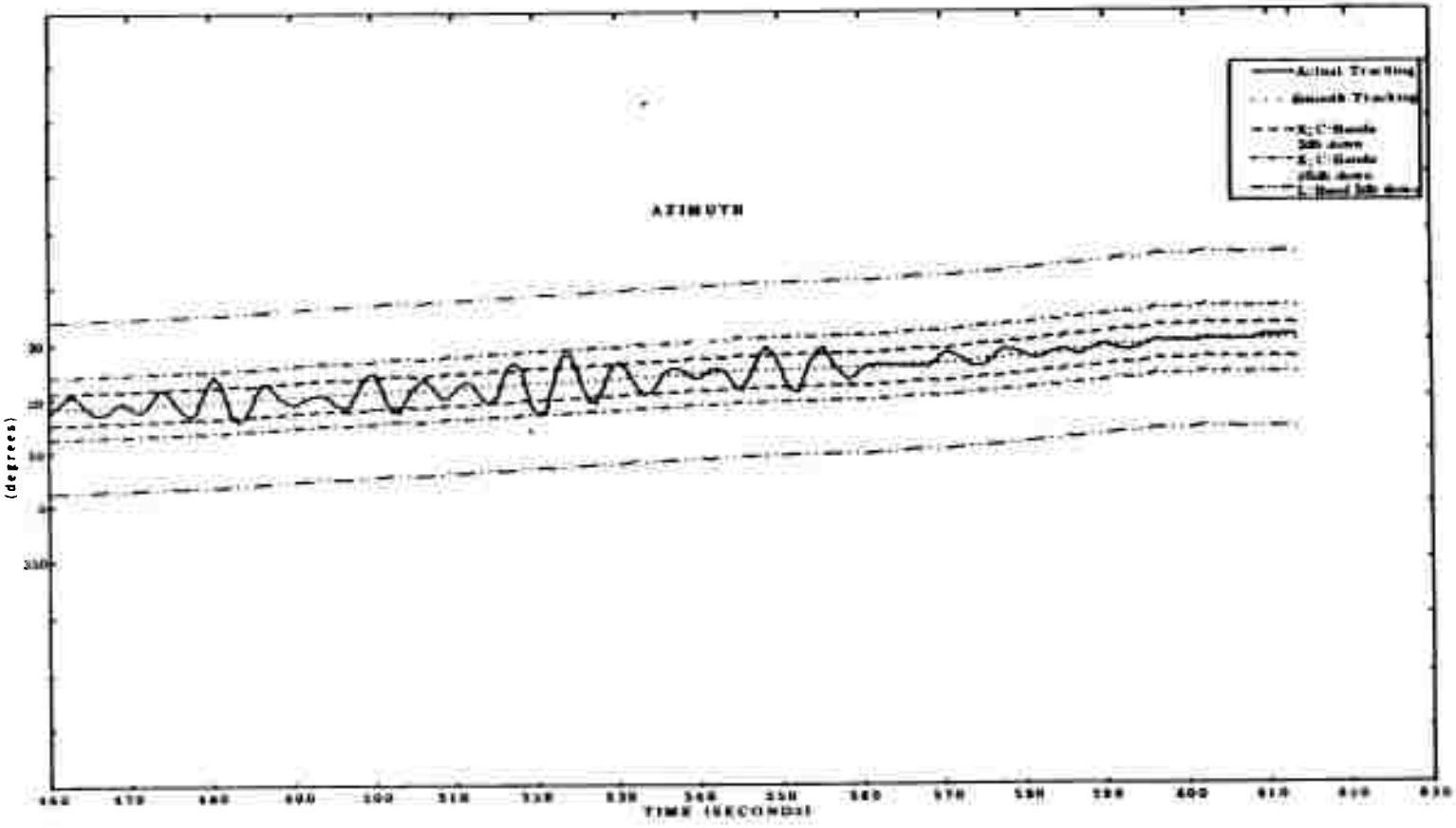

Figure A.10 Azimuth and elevation versus time, Blue Gill, Missile E, Ship 1, H + 460 to H + 630.

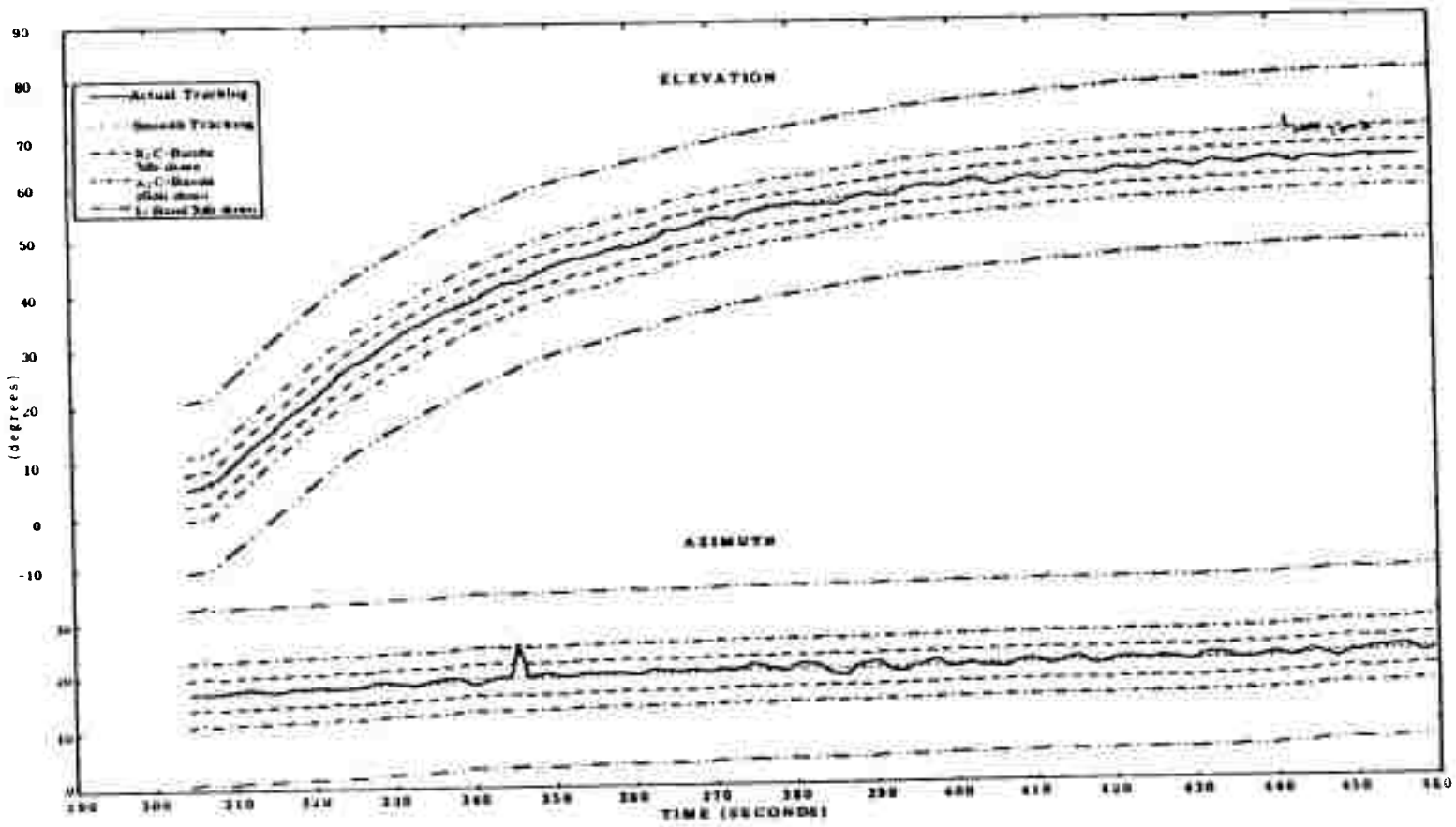

Figure A 11 Azimuth and elevation versus time, Blue Gill, Missile E, Ship 2, H + 290 to H + 460.

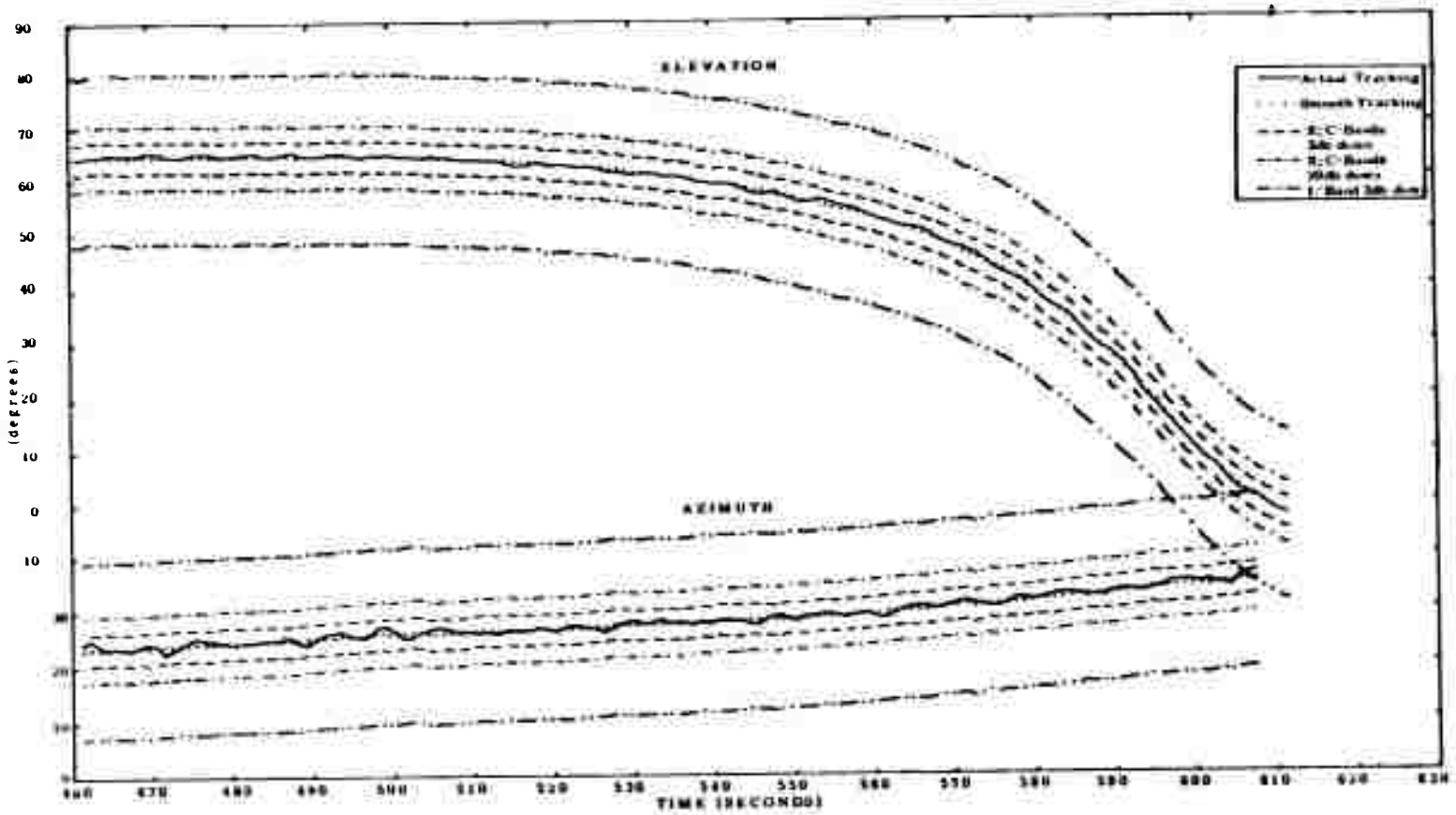

Figure A-12 Azimuth and elevation versus time, Blue Gill, Missile E, Ship 2, H + 460 to H + 630.

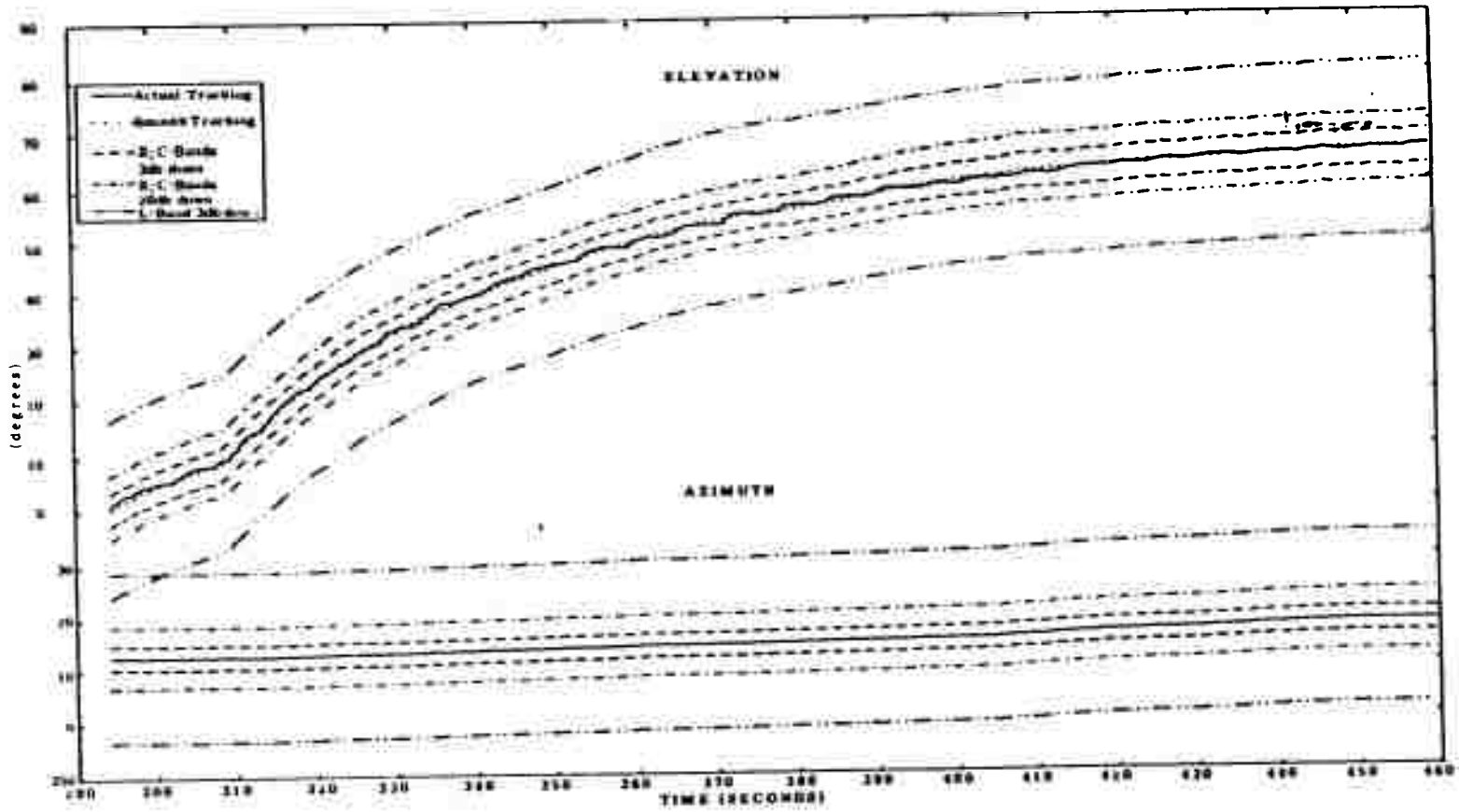

Figure A.13 Azimuth and elevation versus time, Blue Gill, Missile E, Ship 3, H + 290 to H + 460.

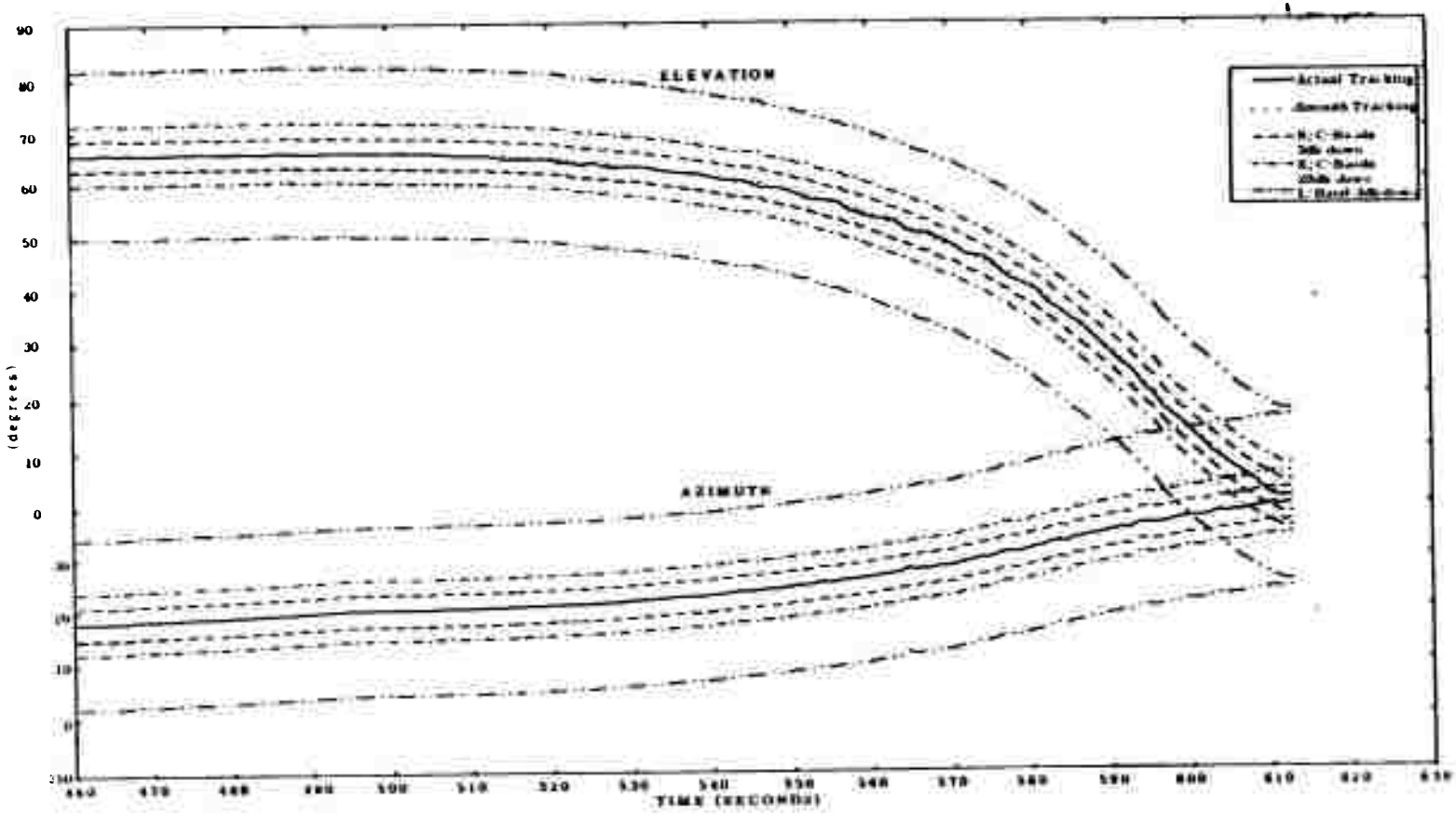

Figure A.14 Azimuth and elevation versus time, Blue Gill, Missile E, Ship 3, H + 460 to H + 630.

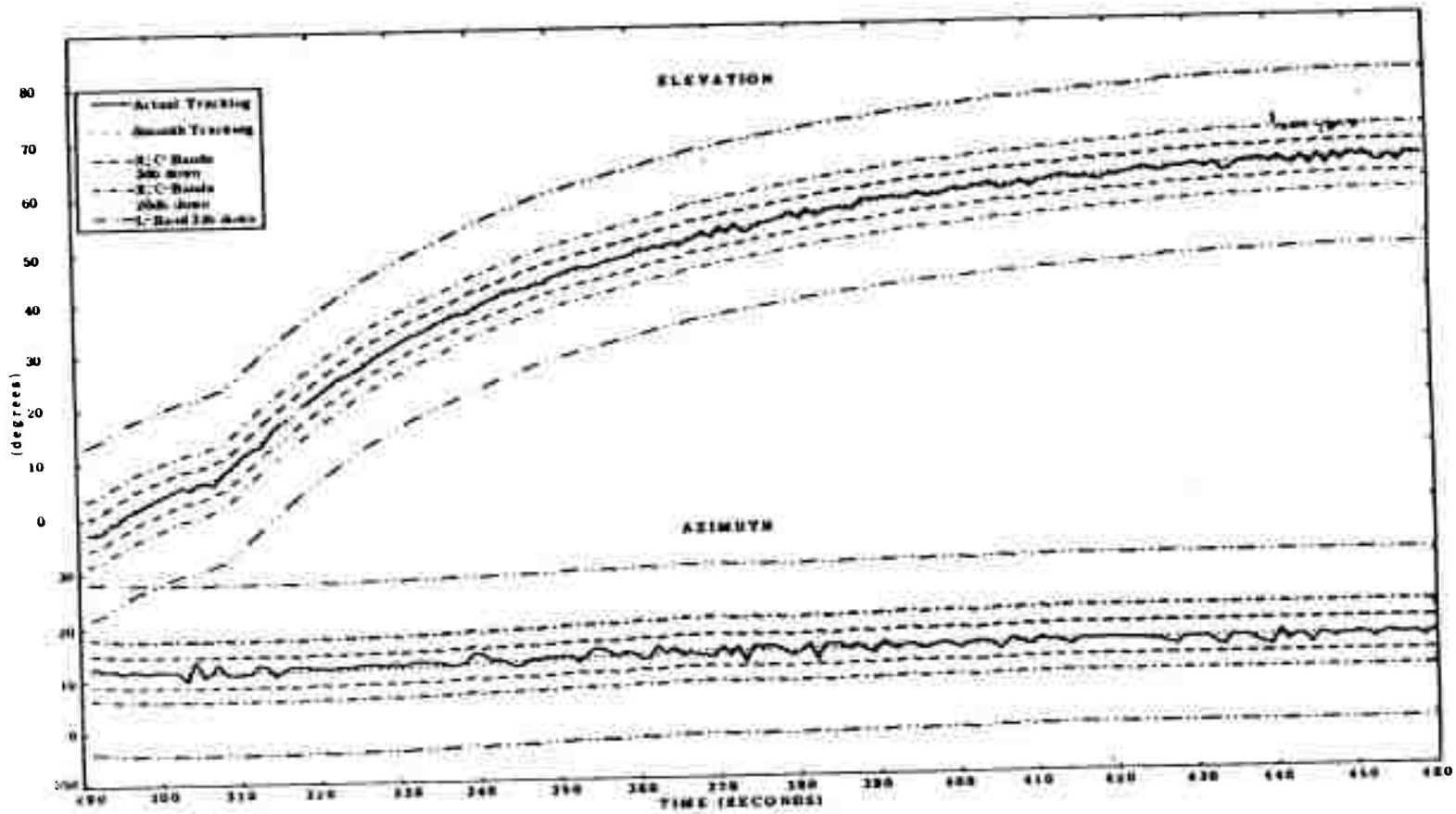

Figure A 15 Azimuth and elevation versus time, Blue Gill, Missile E, Ship 4, H + 290 to H + 460.

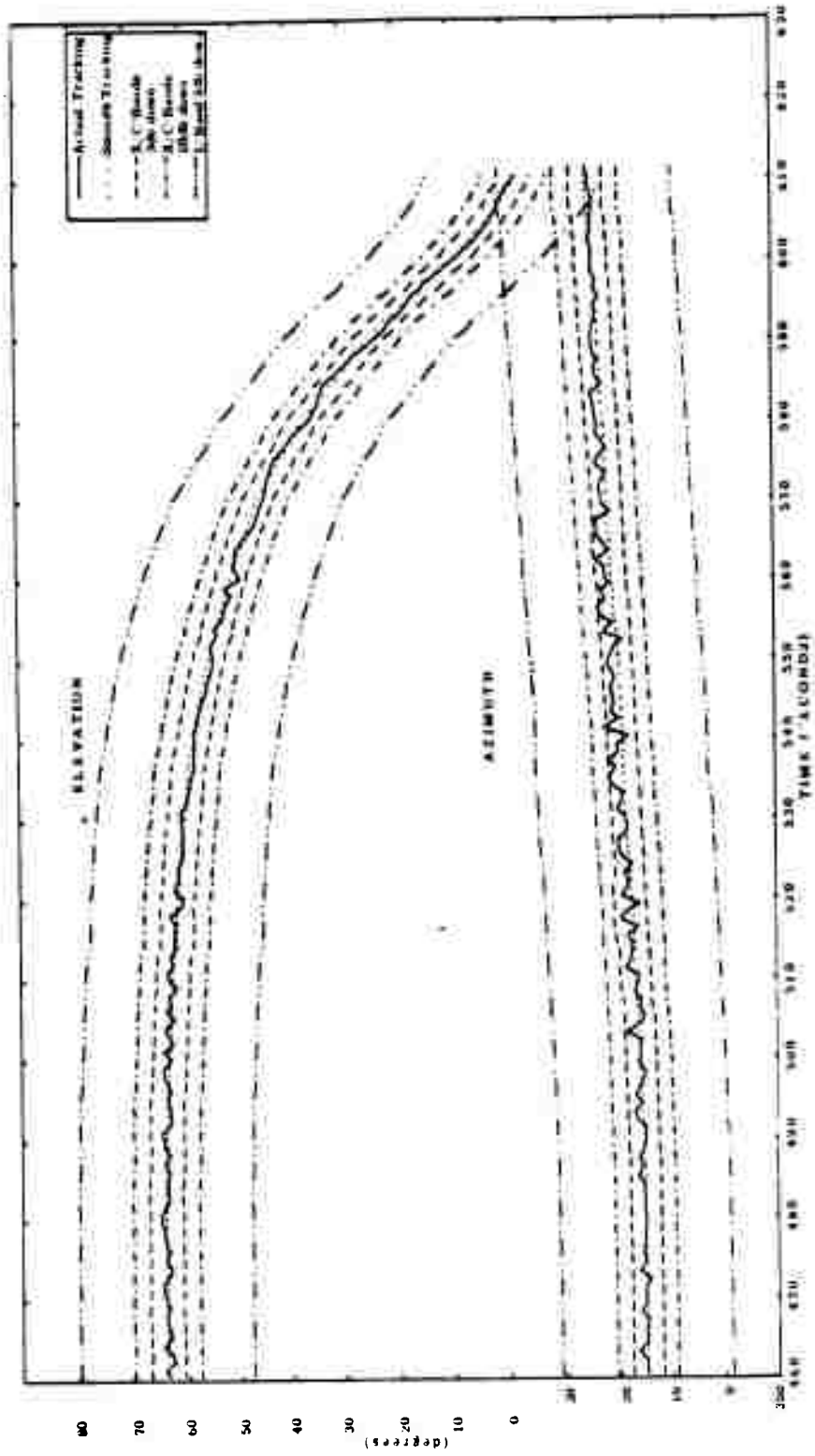

Figure A.16 Azimuth and elevation versus time, Blue Gill, Missile E, Ship 4, H+460 to H+630.

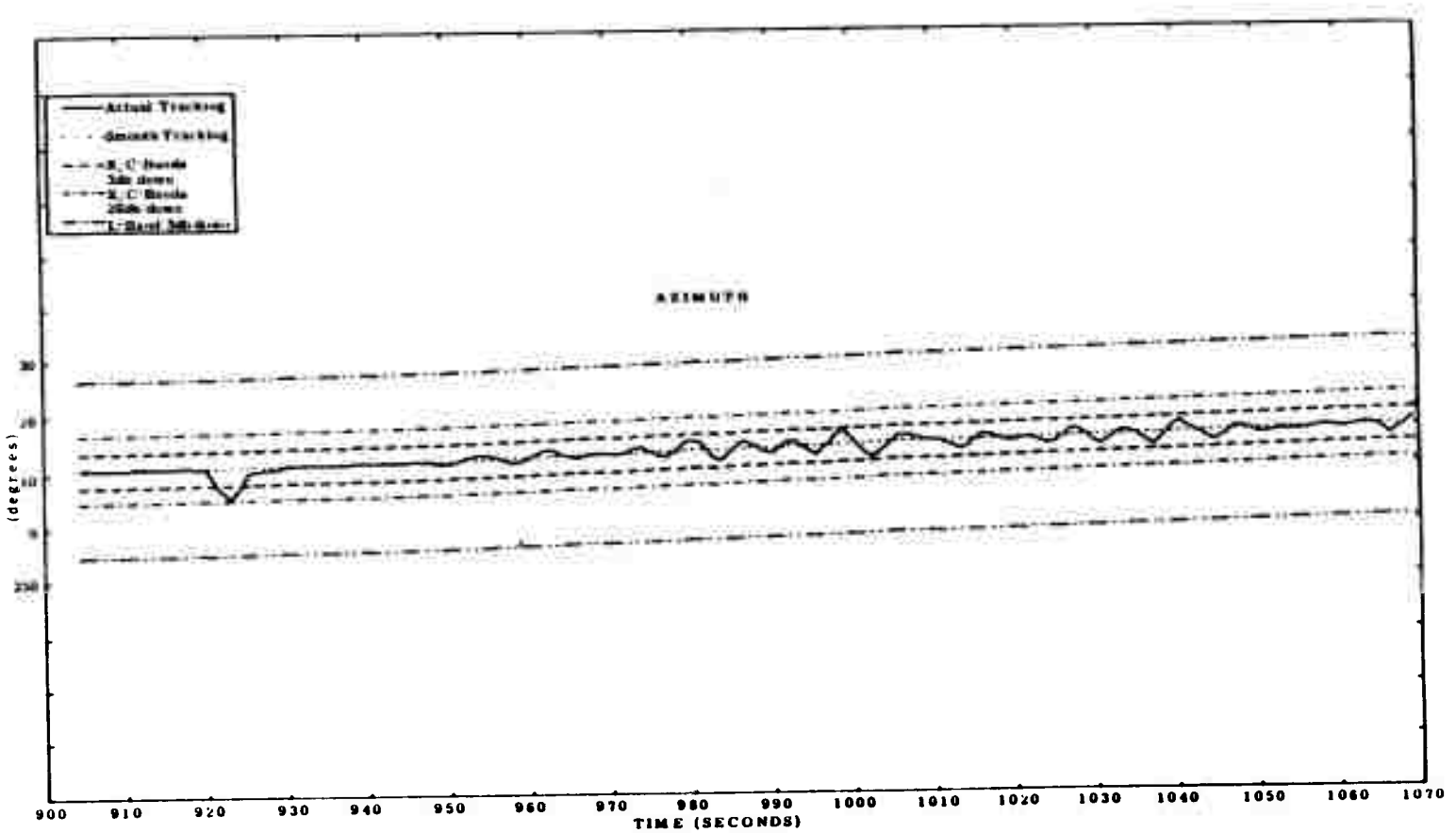

Figure A.17 Azimuth and elevation versus time, Blue Gill, Missile F, Ship 1, H + 900 to H + 1070.

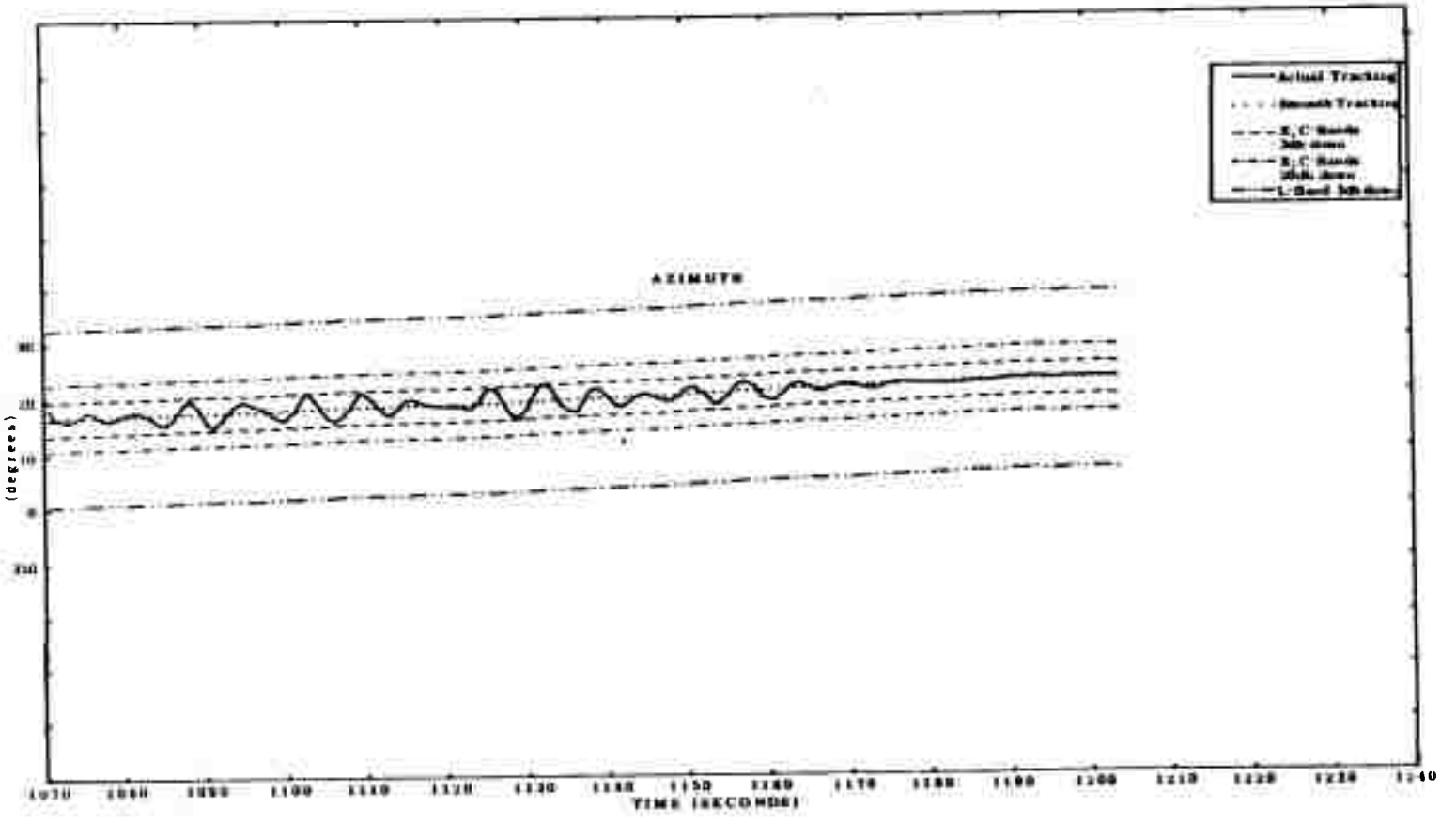

Figure A.18 Azimuth and elevation versus time, Blue Gill, Missile F, Ship 1, H+1070 to H+1240.

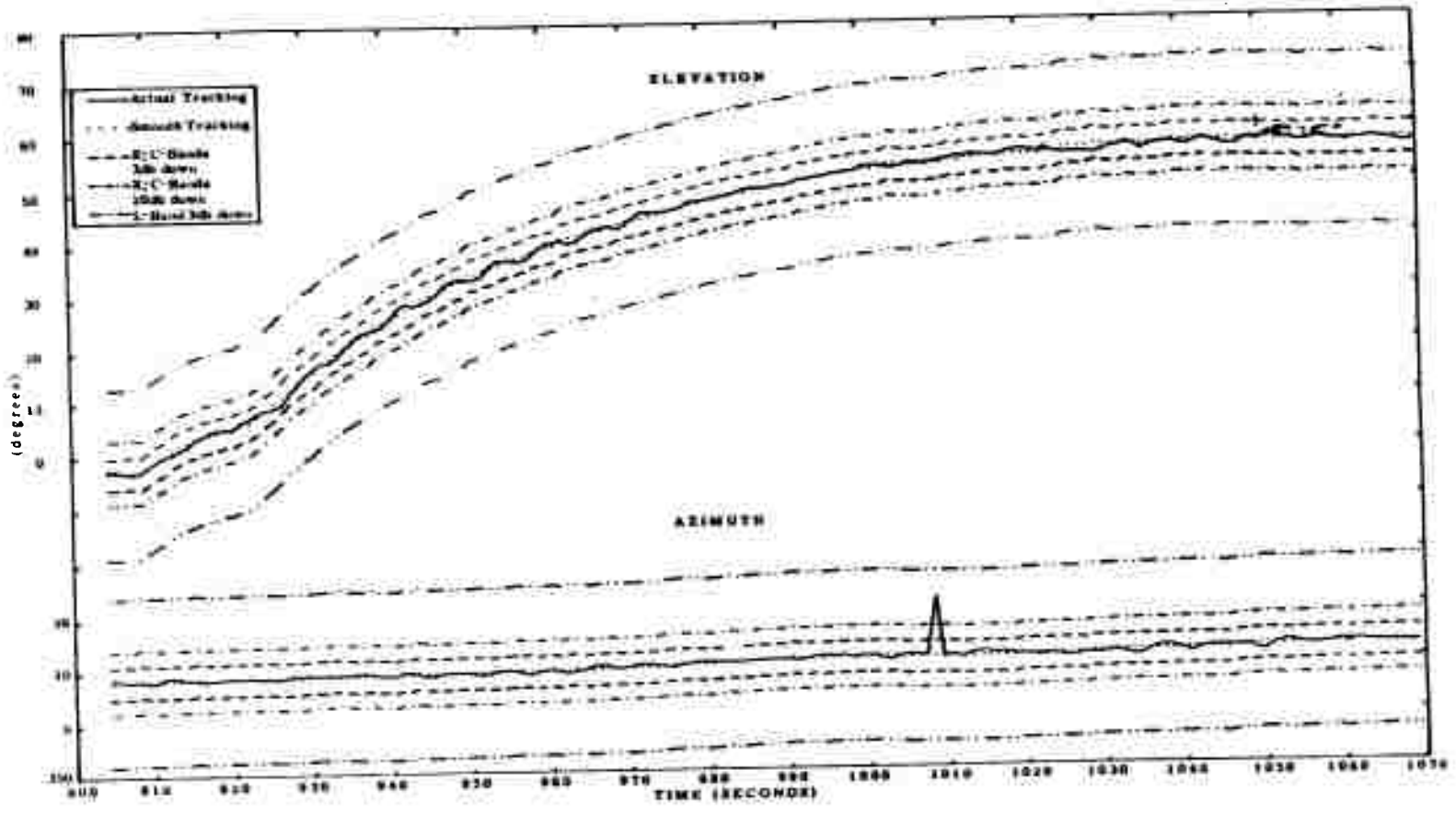

Figure A.19 Azimuth and elevation versus time, Blue Gill, Missile F, Ship 2, H + 900 to H + 1070.

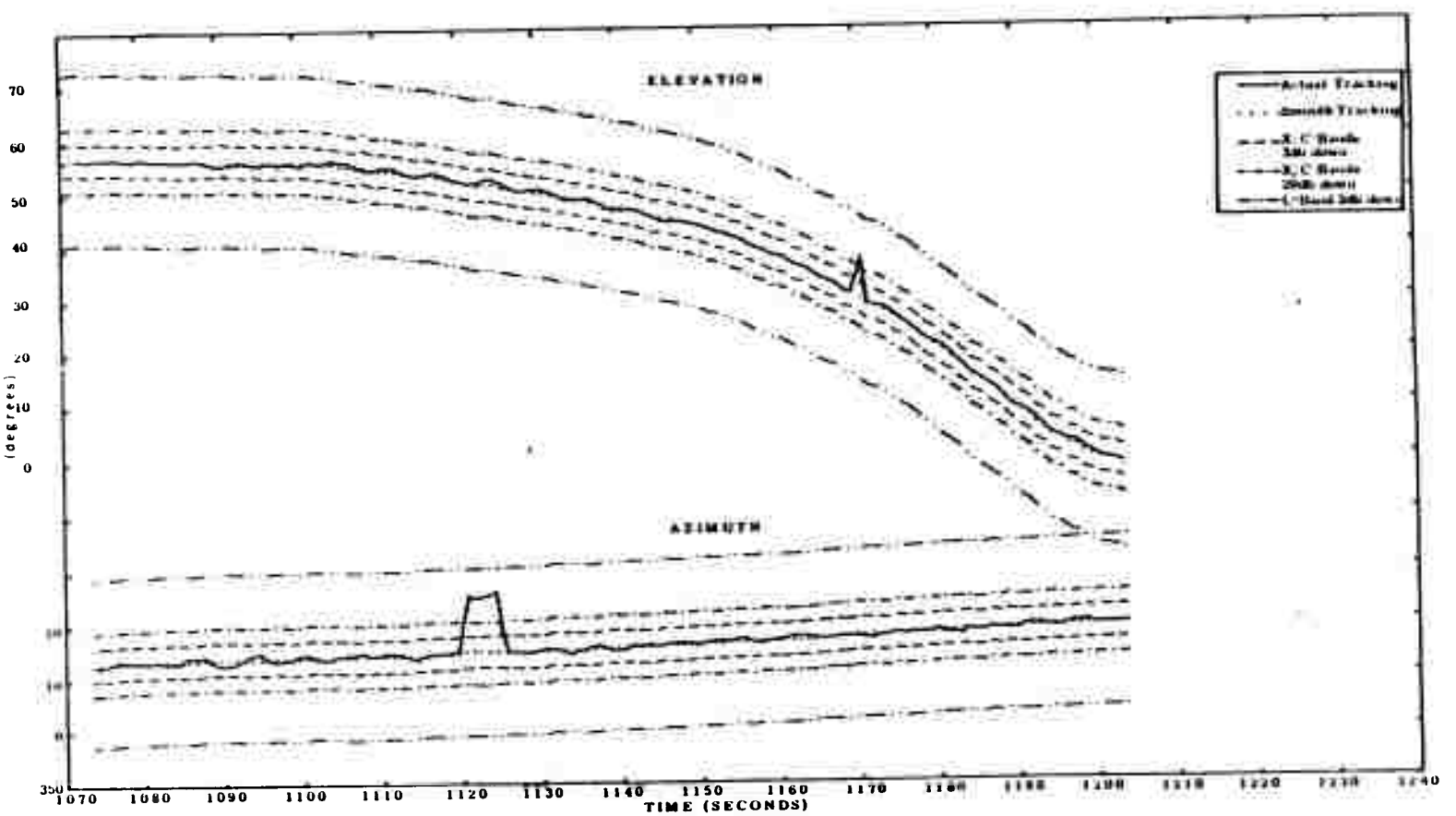

Figure A.20 Azimuth and elevation versus time, Blue Gill, Missile F, Ship 2, H+1070 to H+1240.

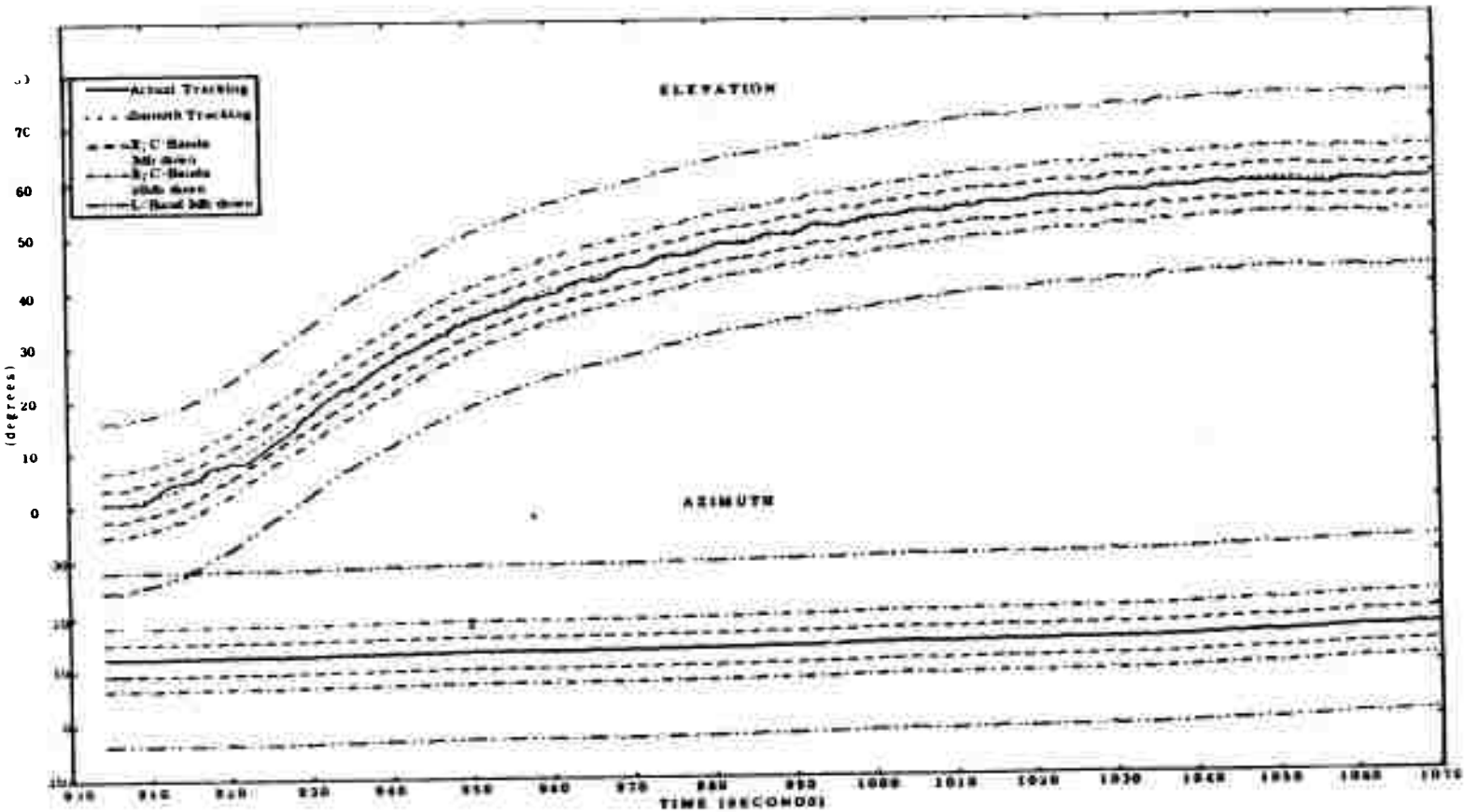

Figure A.21 Azimuth and elevation versus time, Blue Gill, Missile F, Ship 3, H + 900 to H + 1070.

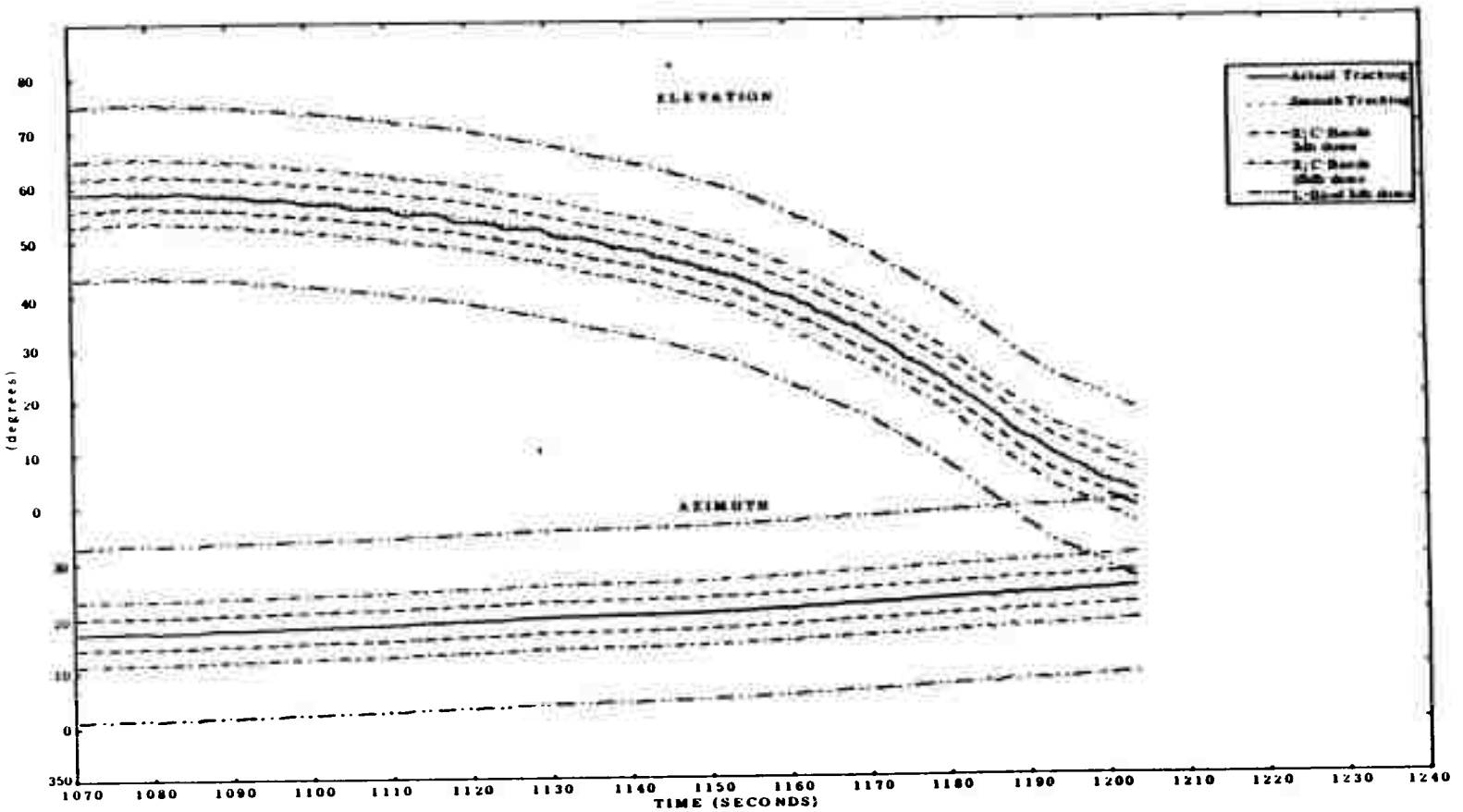

Figure A.22 Azimuth and elevation versus time, Blue Gill, Missile F, Ship 3, H+1070 to H+1240.

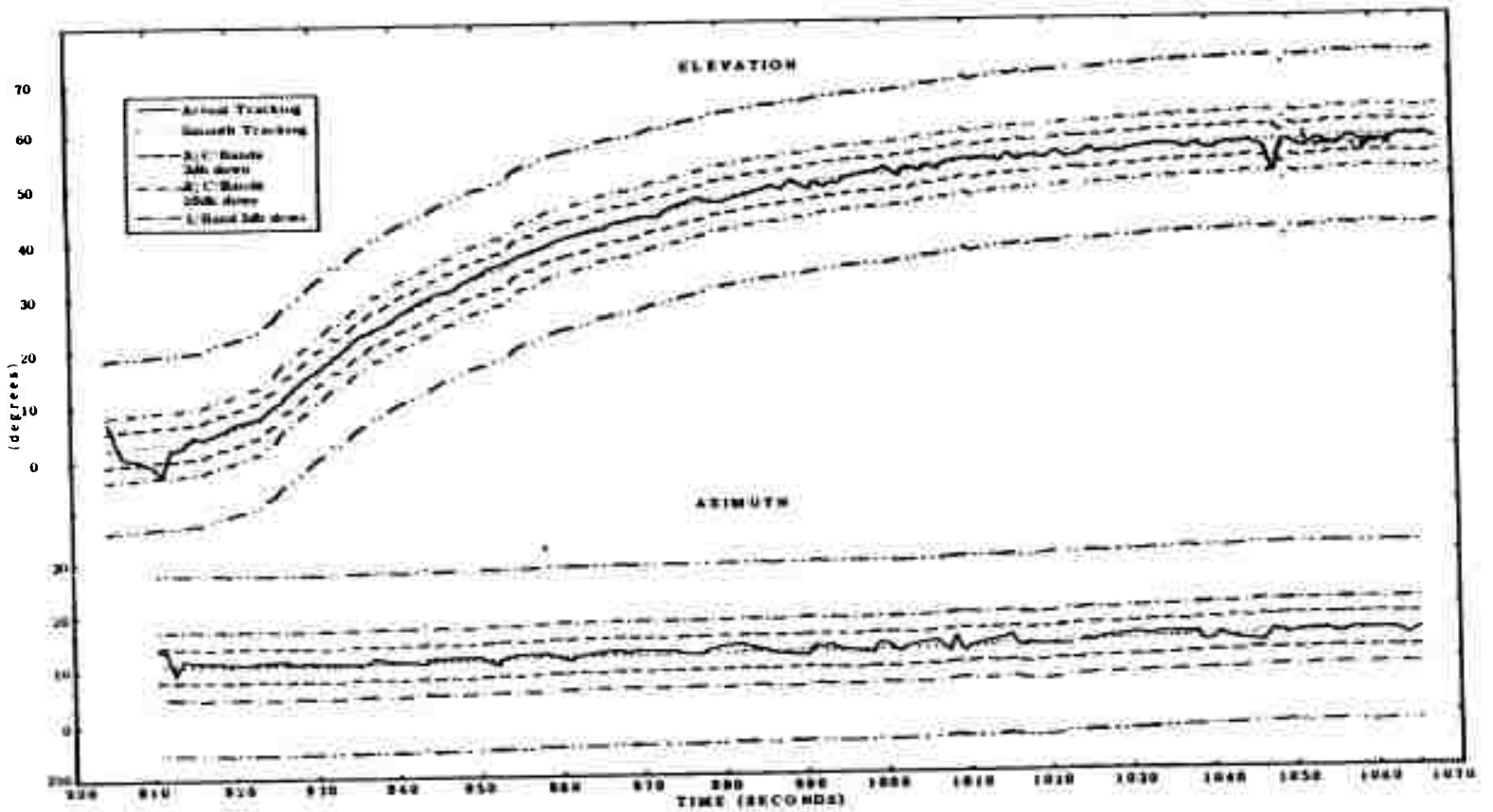

Figure A.23 Azimuth and elevation versus time, Blue Gill, Missile F, Ship 4, H + 900 to H + 1070.

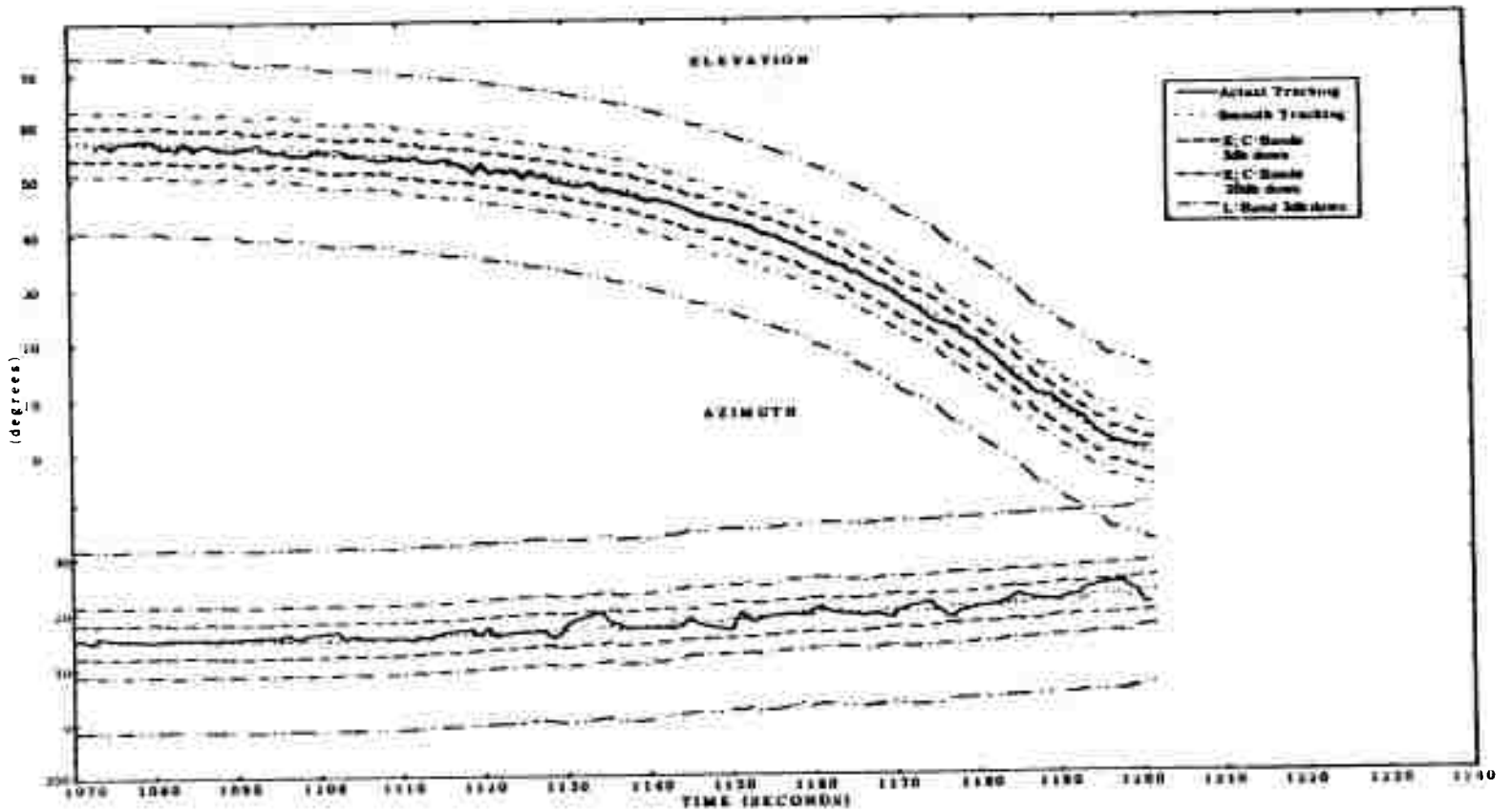

Figure A.24 Azimuth and elevation versus time, Blue Gill, Missile F, Ship 4, H + 1070 to H + 1240.

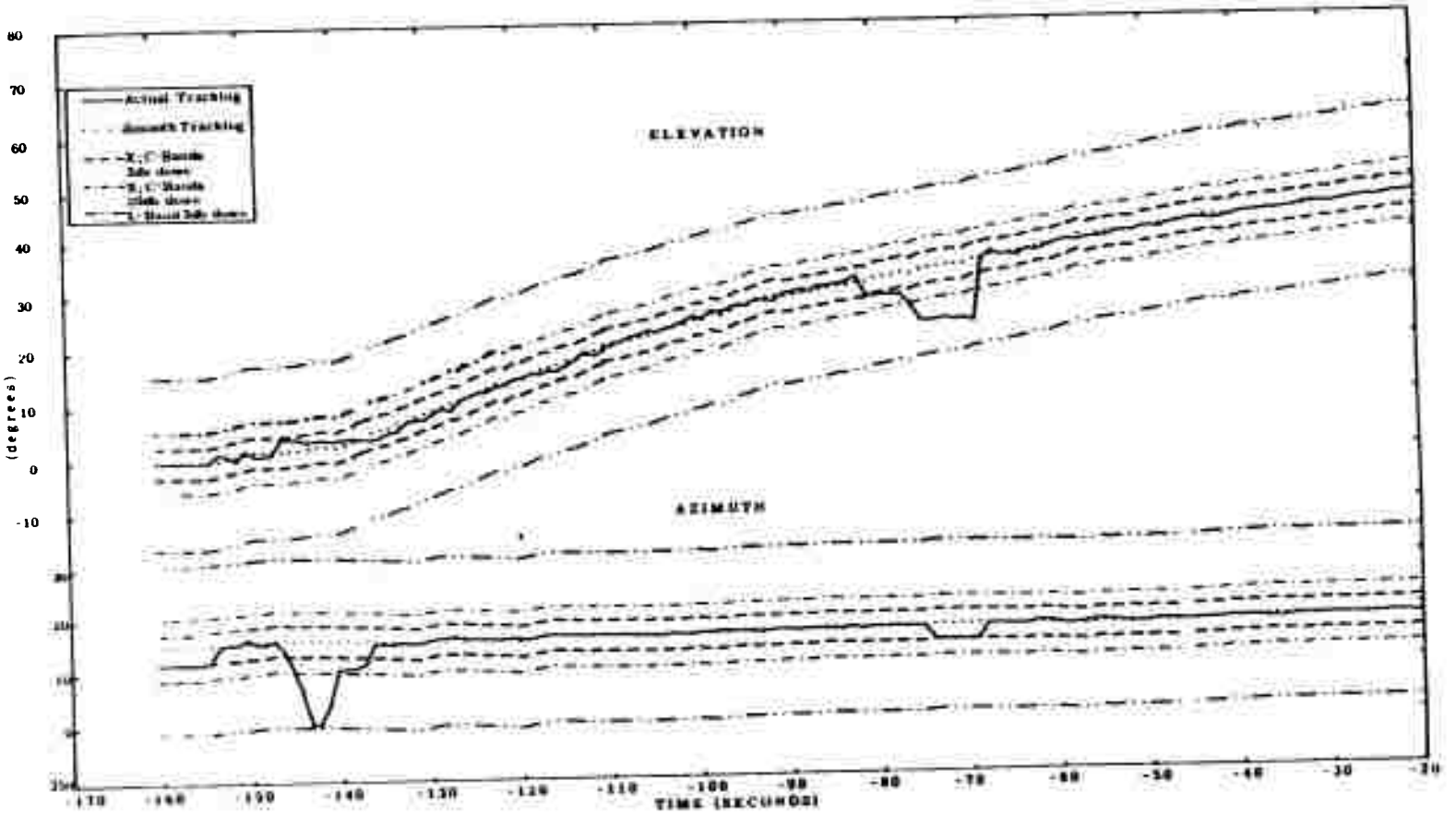

Figure A.25 Azimuth and elevation versus time, King Fish, Missile B, Ship 1, H-170 to H-20.

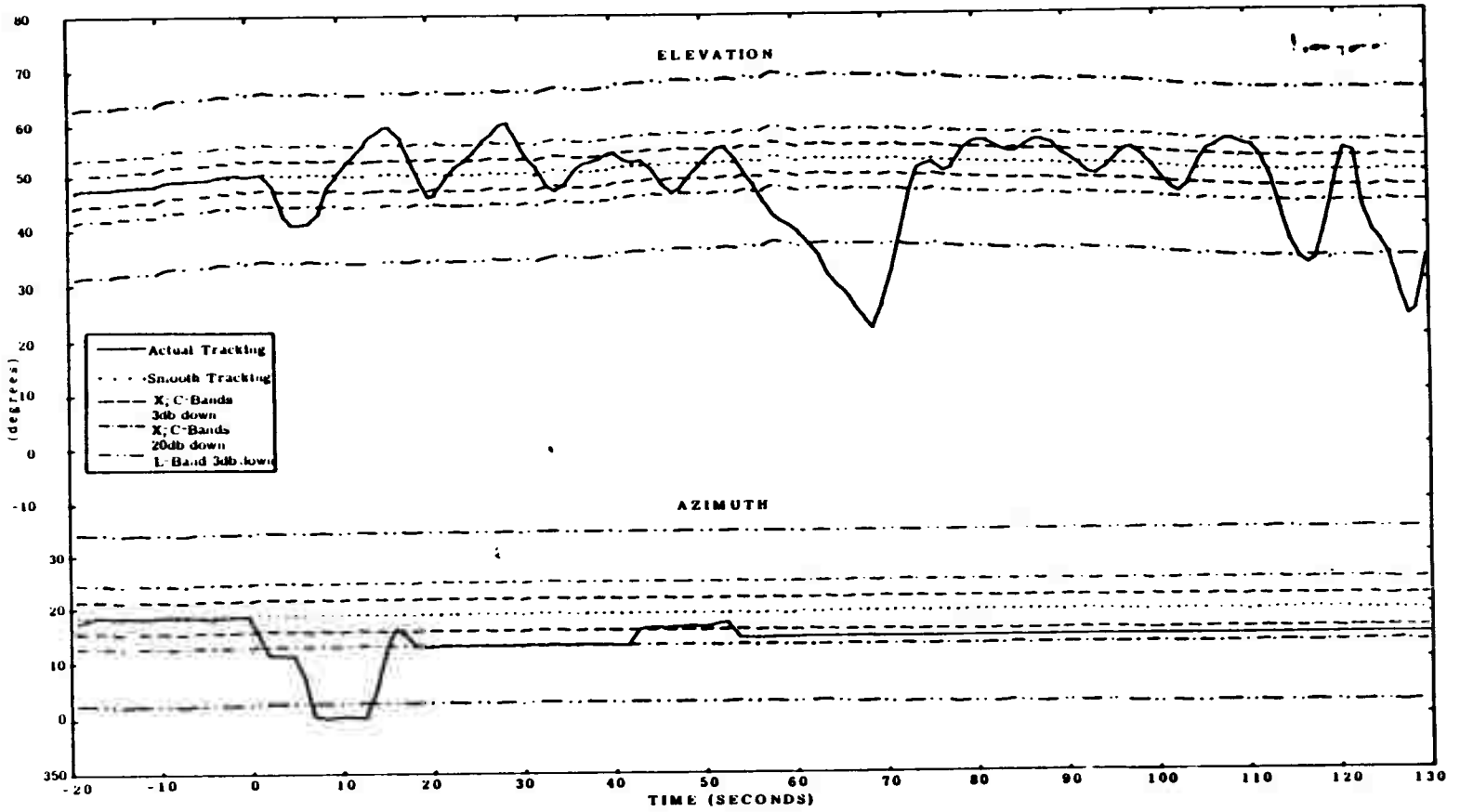

Figure A.26 Azimuth and elevation versus time, King Fish Missile B, Ship 1, H-20 to H+130.

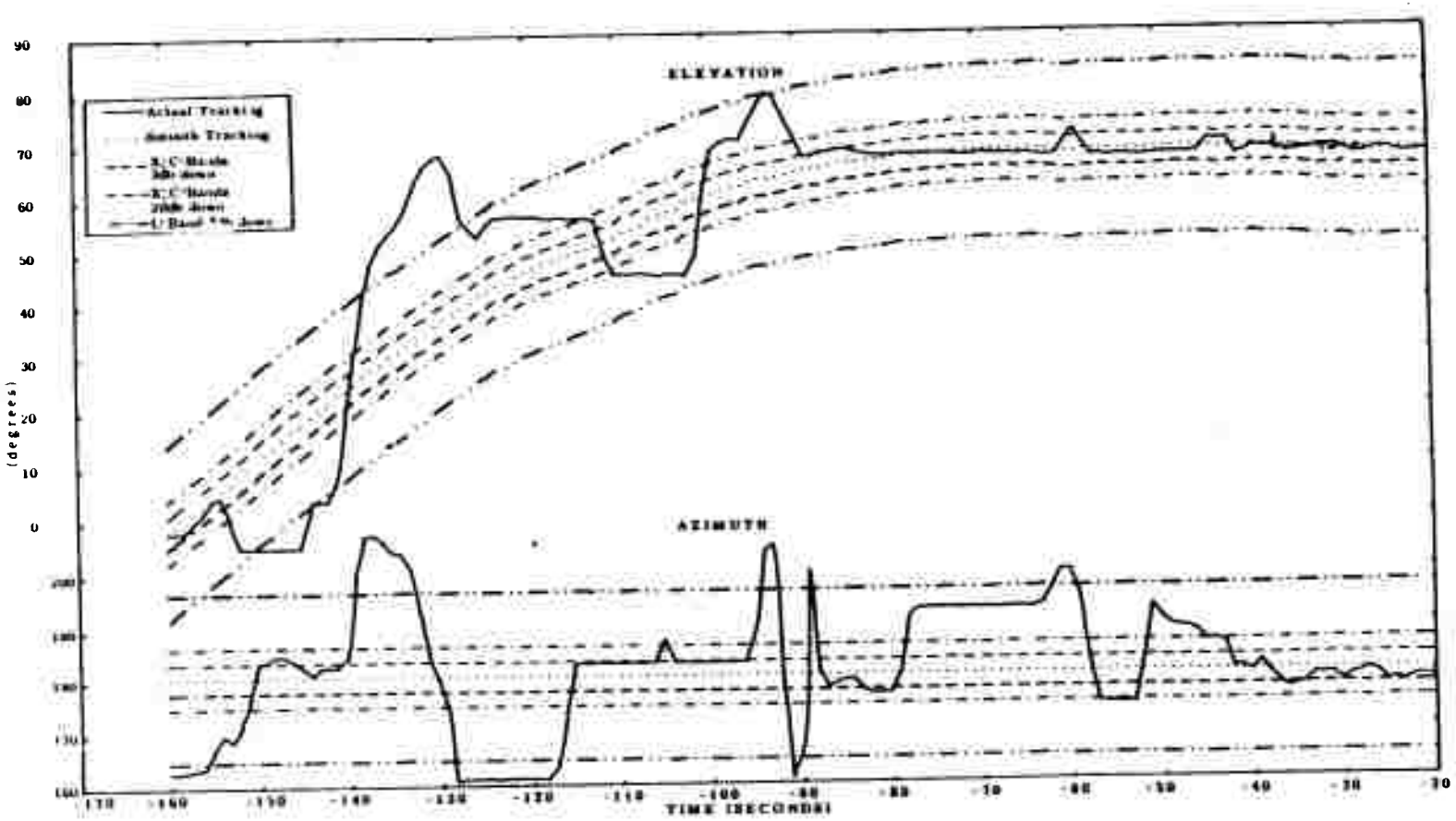

Figure A.27 Azimuth and elevation versus time, King Fish, Missile B, Ship 2, H - 170 to H - 20.

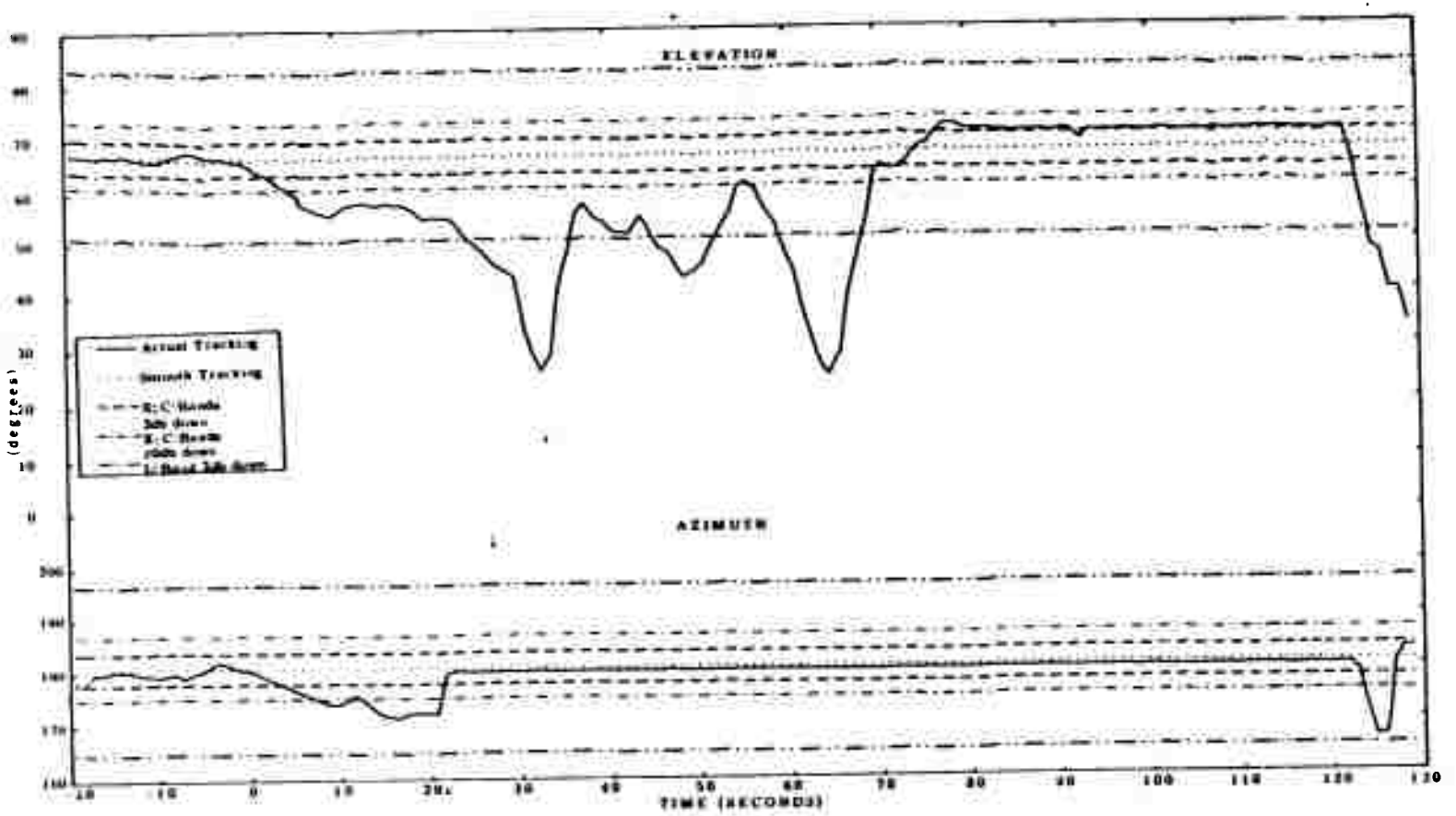

Figure A.28 Azimuth and elevation versus time, King Fish, Missile B, Ship 2, H - 20 to H + 130.

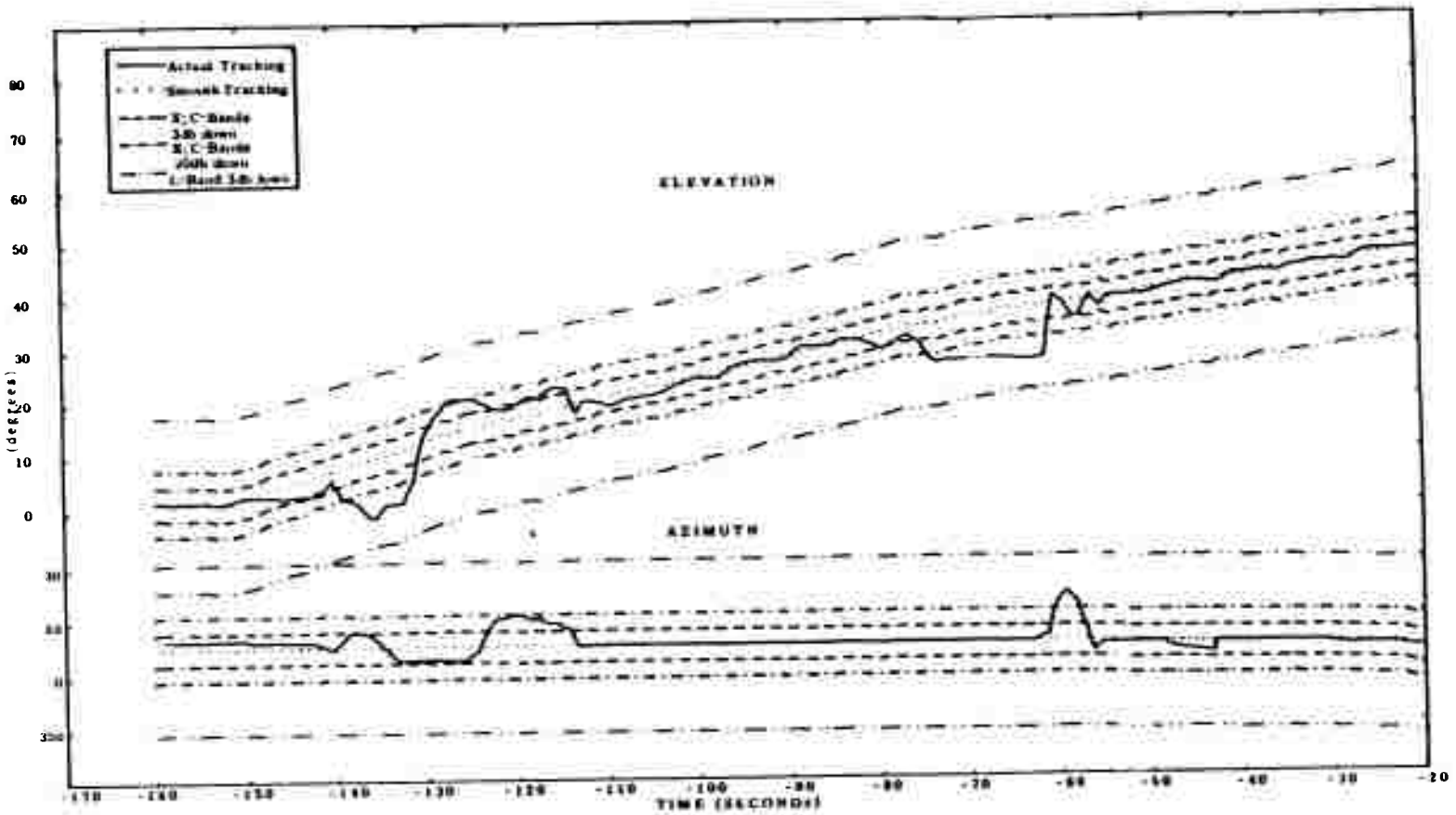

Figure A.29 Azimuth and elevation versus time, King Fish, Missile B, Ship 3, H - 170 to H - 20.

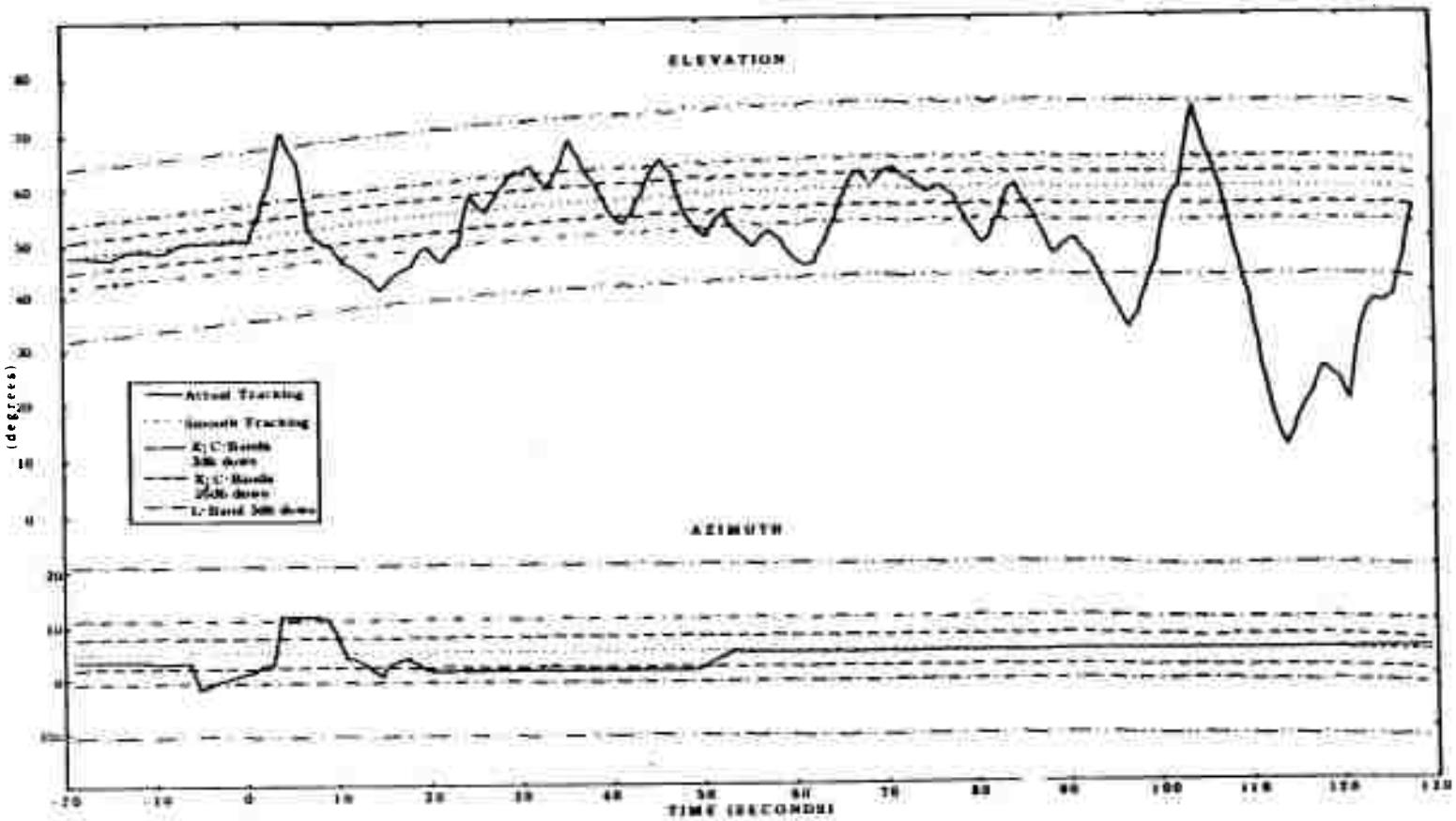

Figure A.30 Azimuth and elevation versus time, King Fish, Missile B, Ship 3, H - 20 to H + 130.

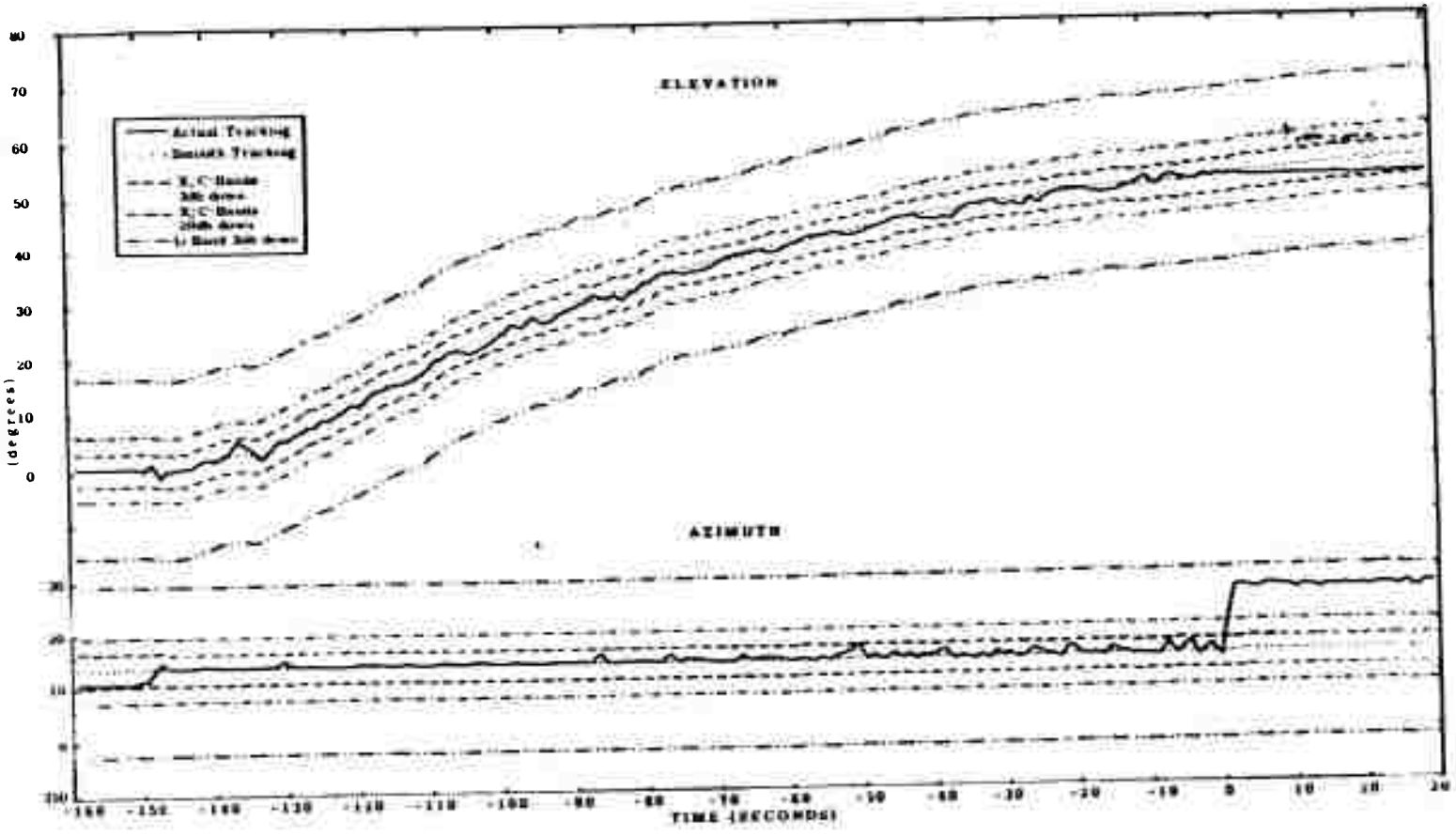

Figure A.31 Azimuth and elevation versus time, King Fish, Missile B, Ship 4, H − 160 to H + 30.

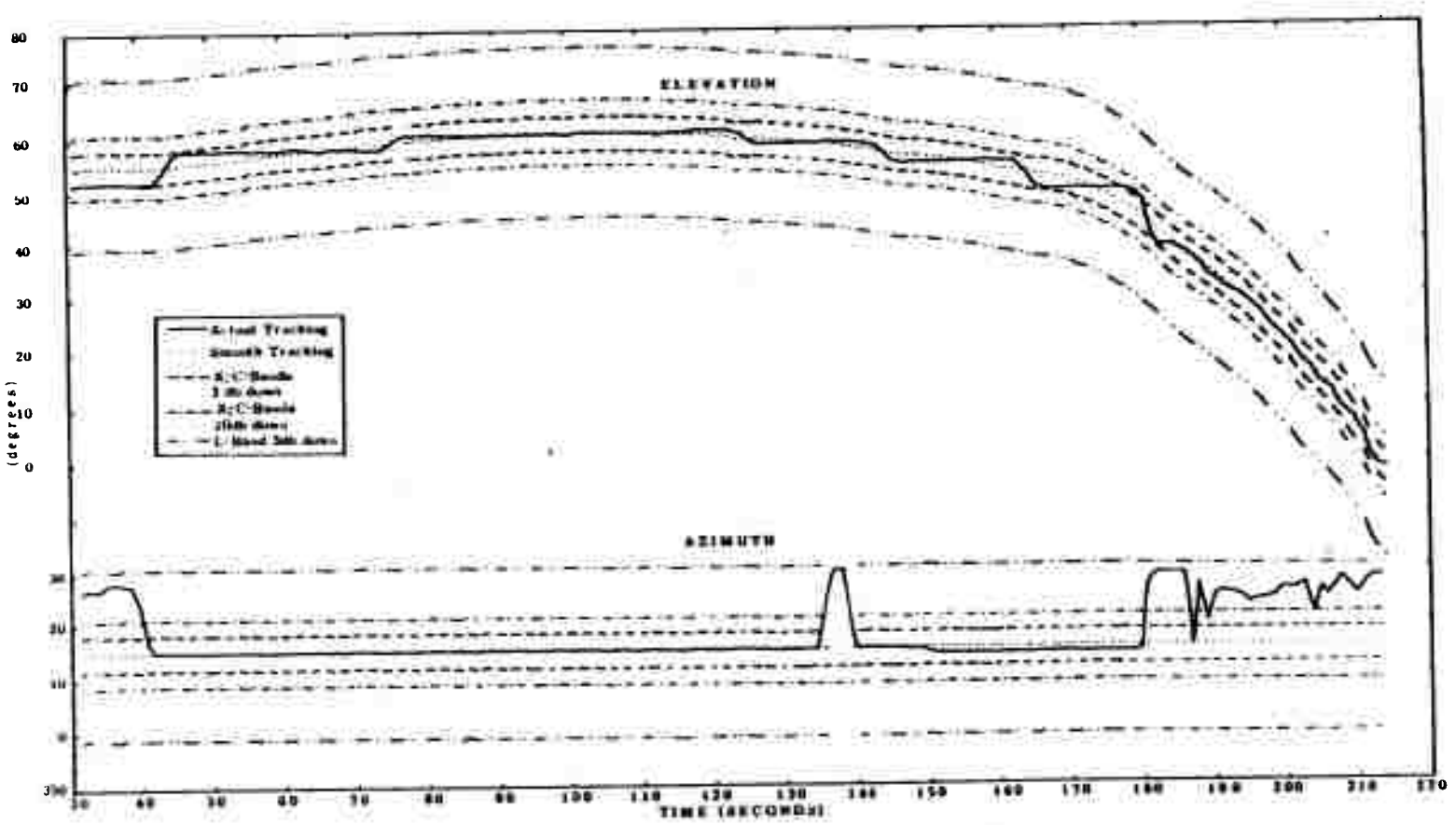

Figure A.32 Azimuth and elevation versus time, King Fish, Missile B, Ship 4, H + 30 to H + 220.

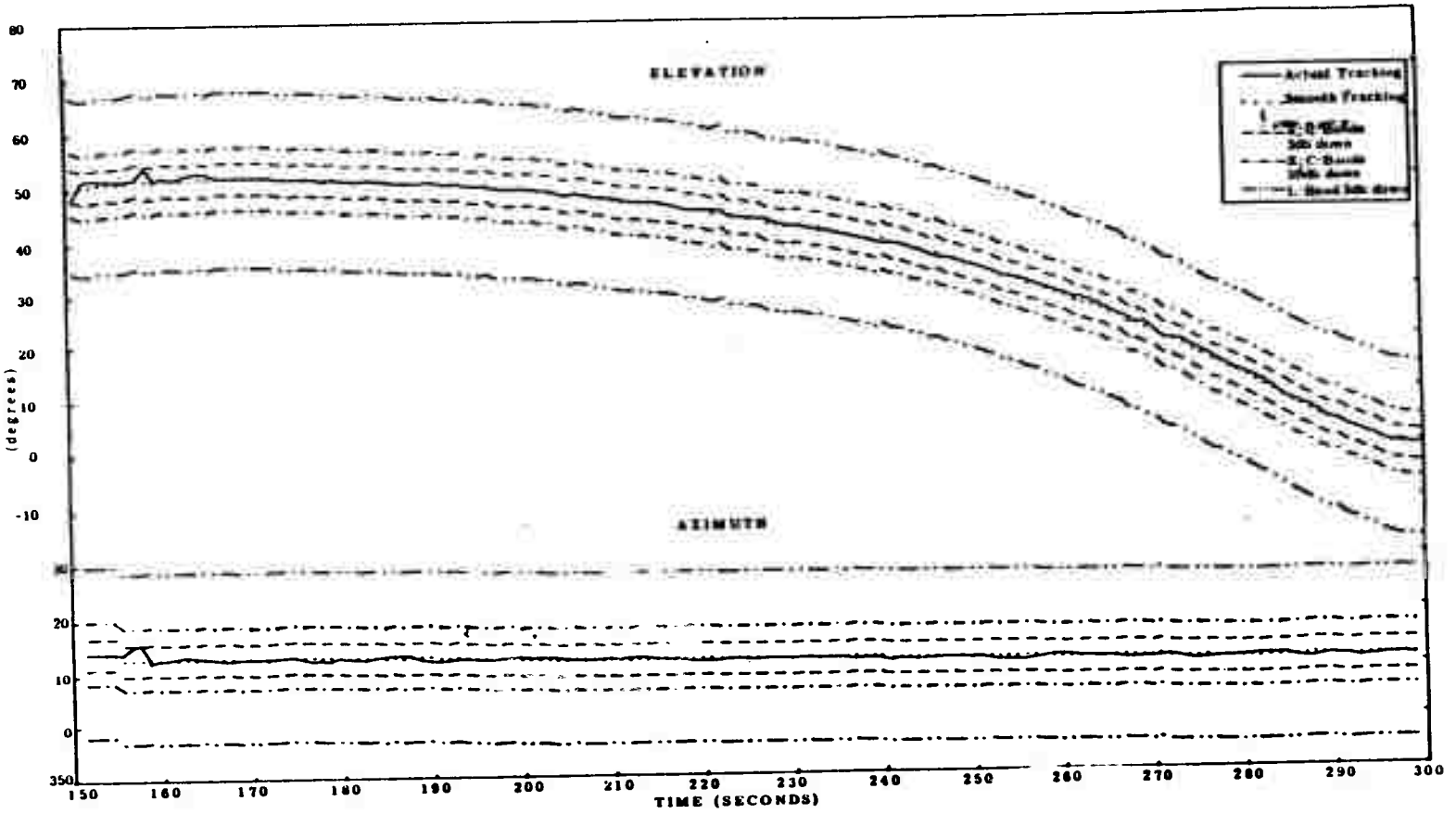

Figure A.33 Azimuth and elevation versus time, King Fish, Missile C, Ship 1, H + 150 to H + 300.

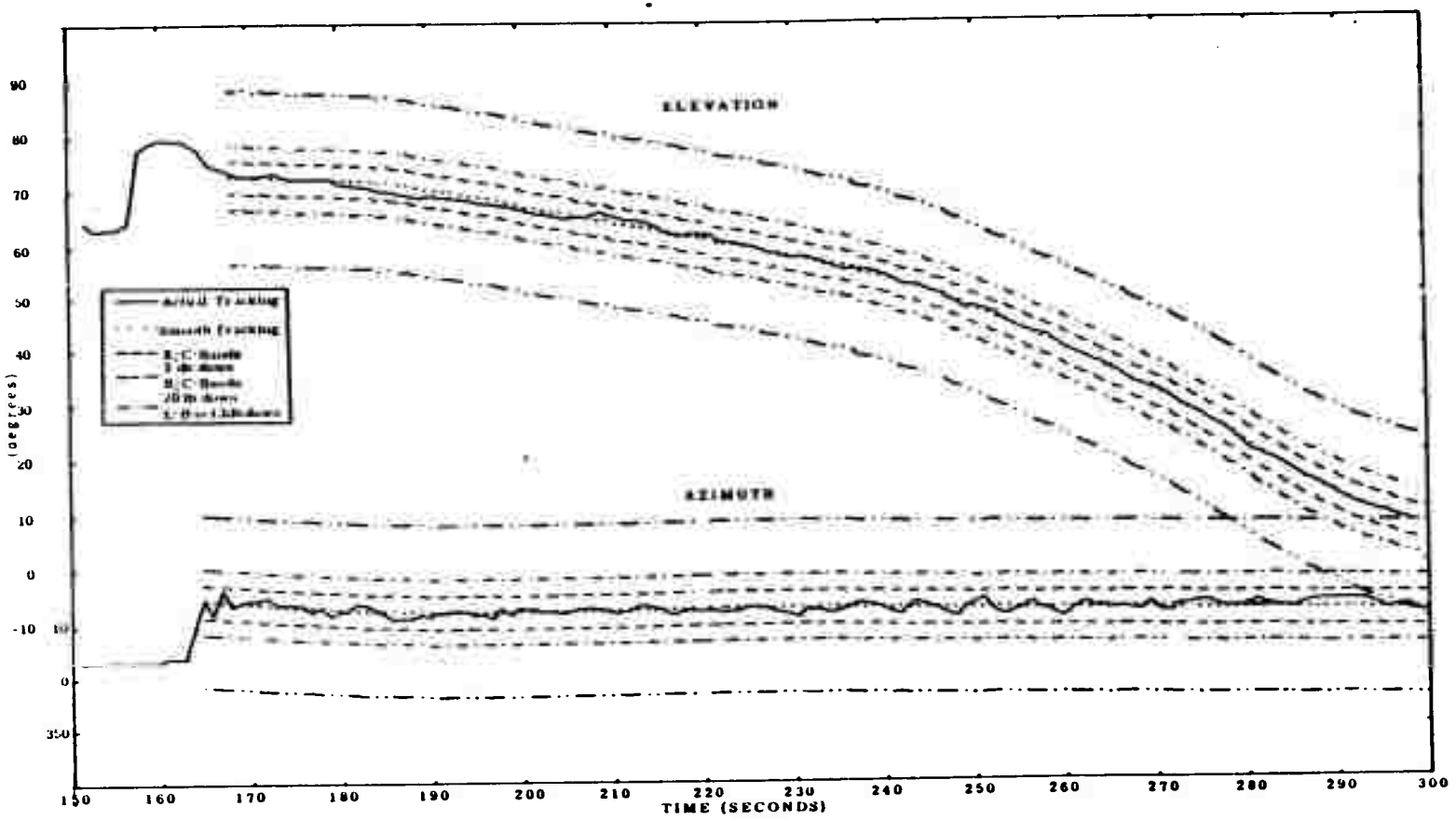

Figure A.34 Azimuth and elevation versus time, King Fish, Missile C, Ship 2, H + 150 to H + 300.

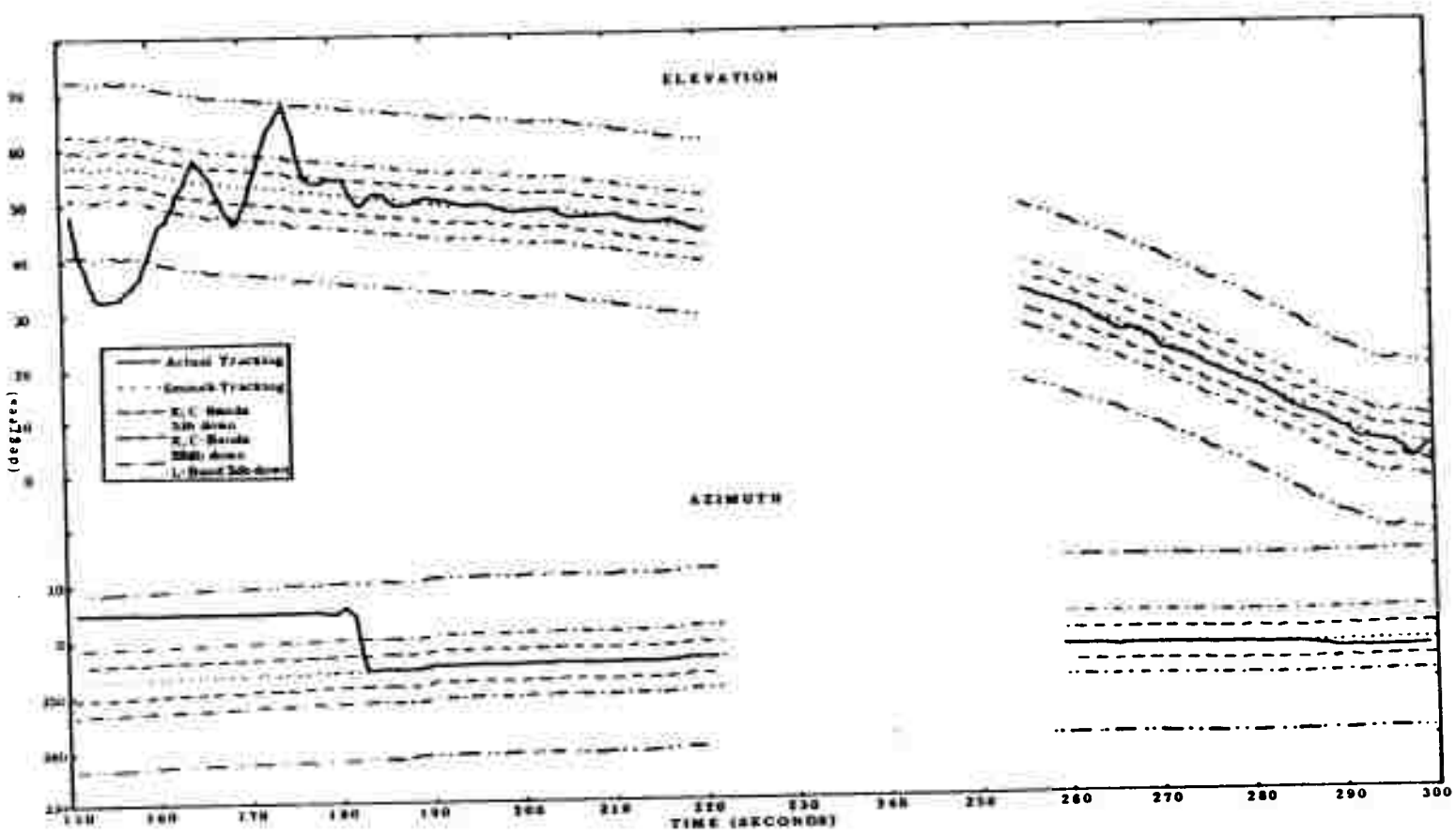

Figure A.35 Azimuth and elevation versus time, King Fish, Missile C, Ship 3, H + 150 to H + 300.

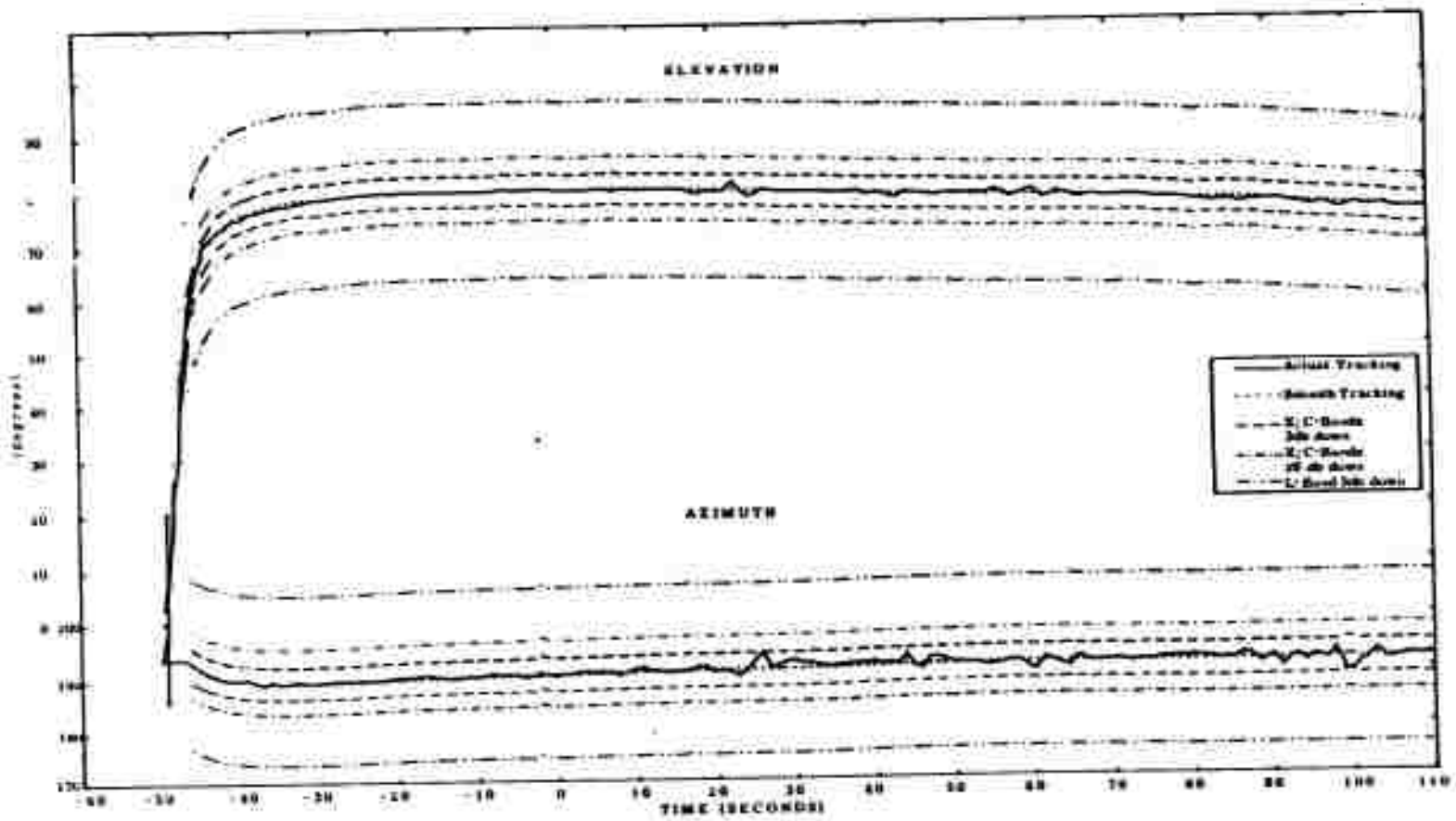

Figure A.36 Azimuth and elevation versus time, Tight Rope, Missile A, Ship 1, H - 60 to H + 110.

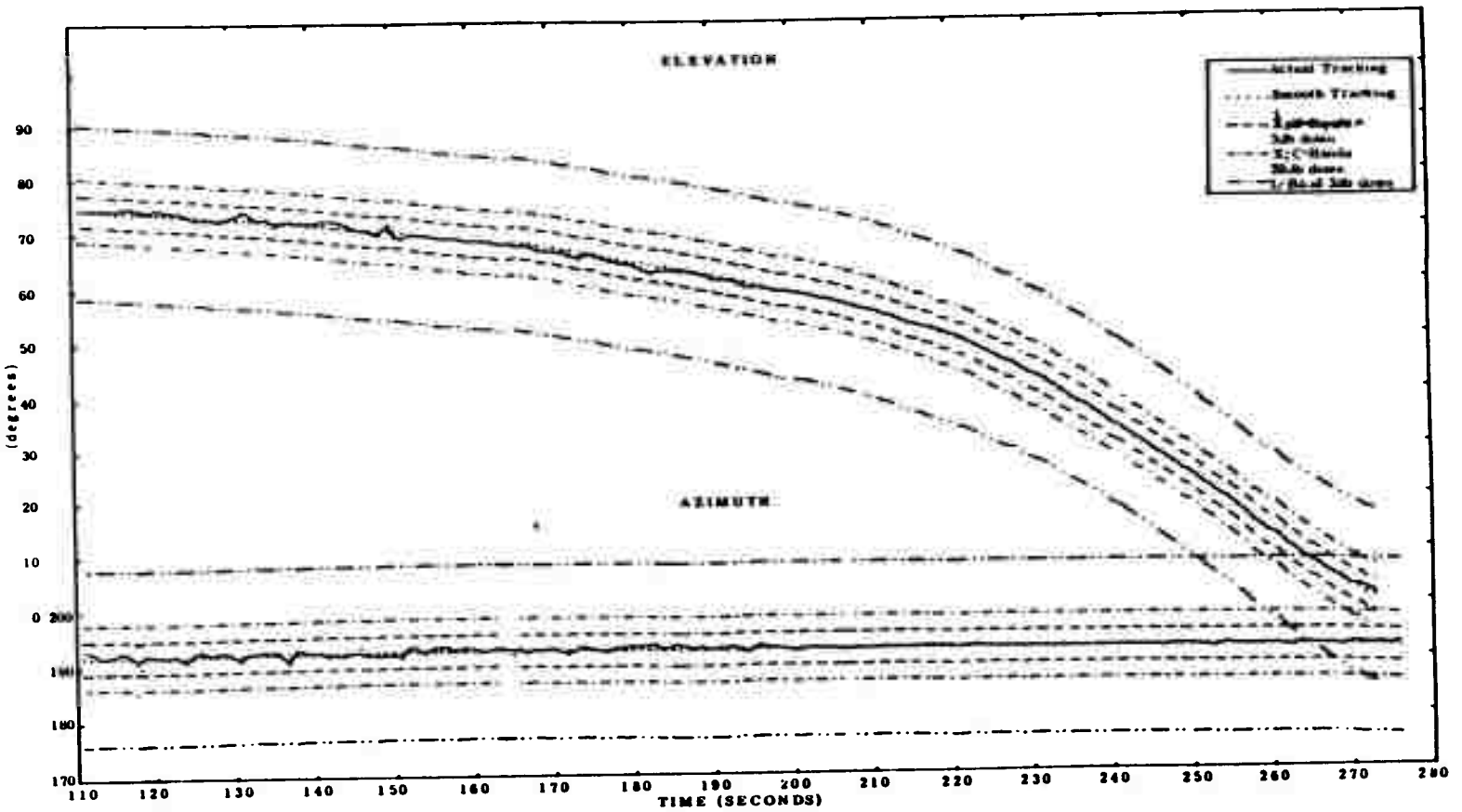

Figure A-37 Azimuth and elevation versus time, Tight Rope, Missile A, Ship 1, H + 110 to H + 280.

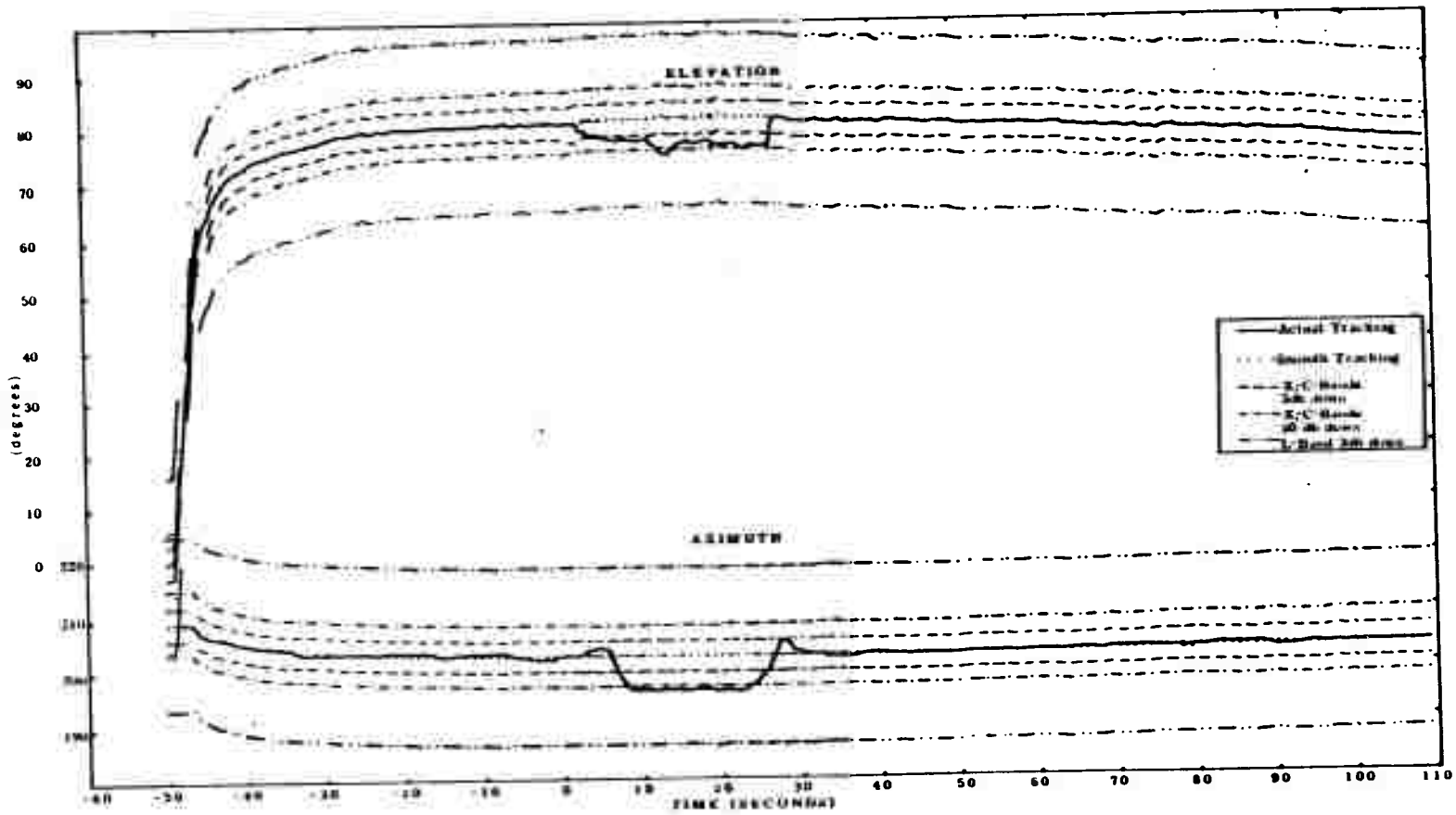

Figure A.38 Azimuth and elevation versus time, Tight Rope, Missile B, Ship 3, H - 60 to H + 110.

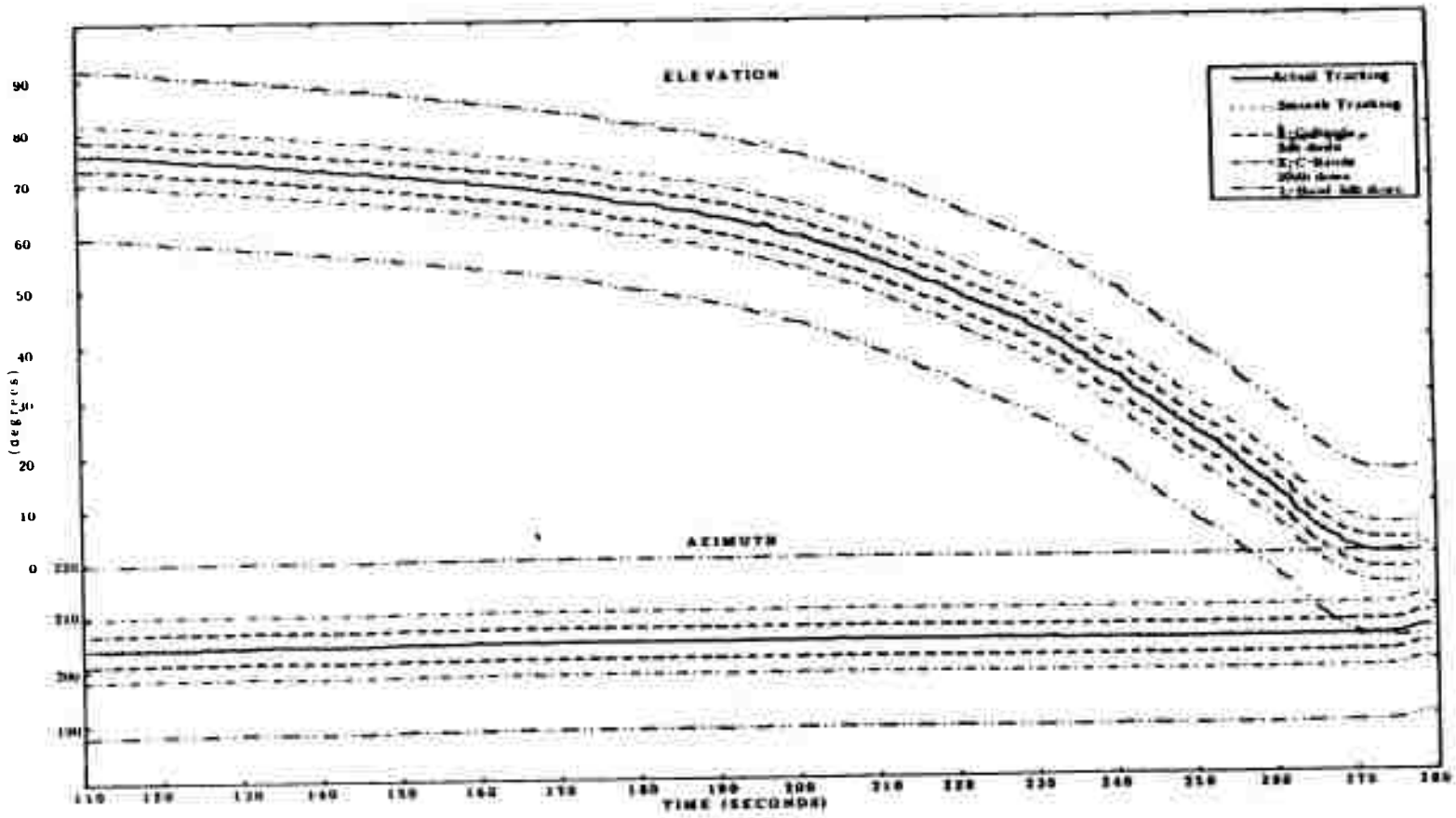

Figure A.39 Azimuth and elevation versus time, Tight Rope, Missile B, Ship 3, H + 110 to H + 280.

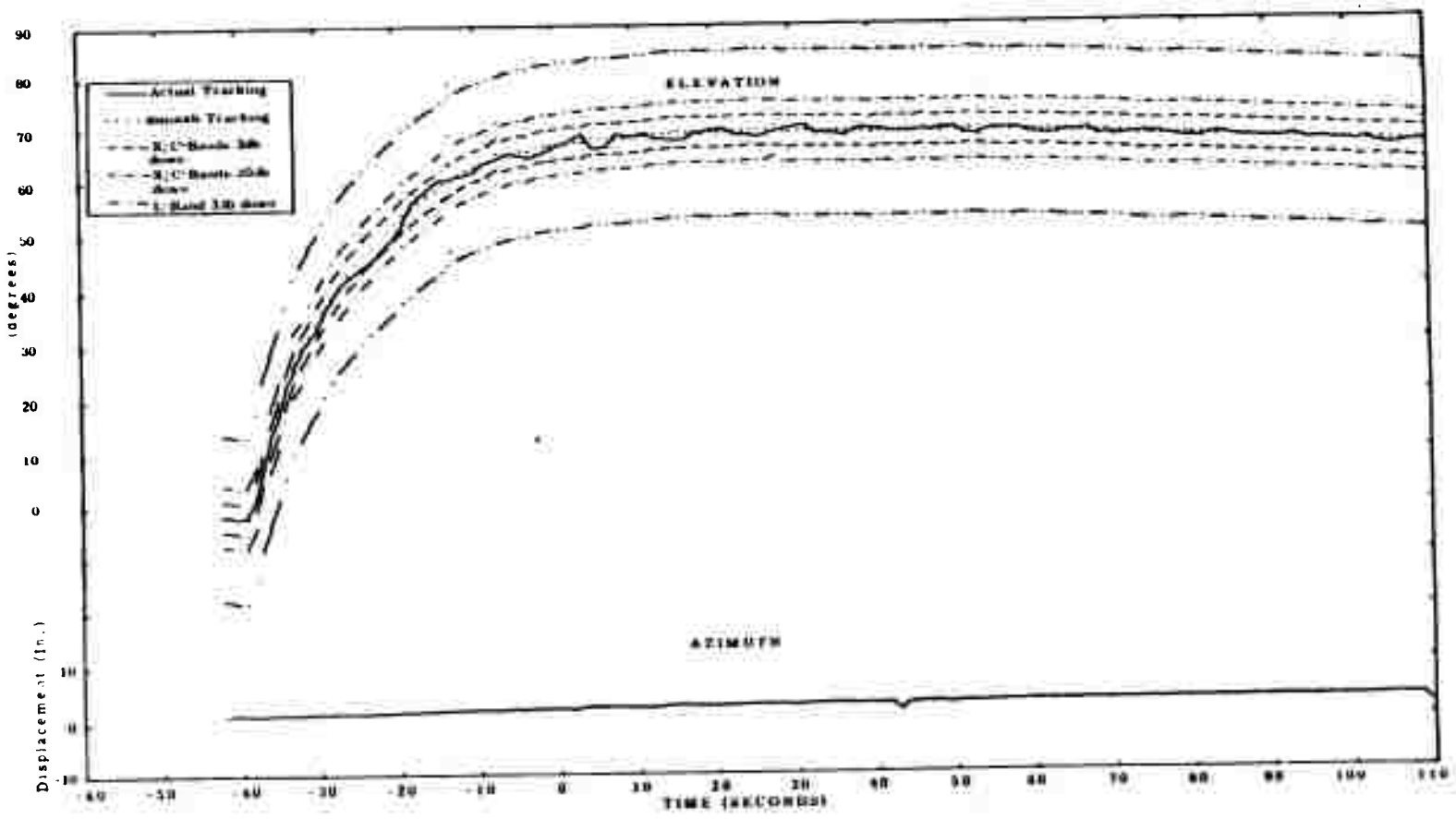

Figure A.40 Azimuth and elevation versus time, Tight Rope, Missile D, Ship 4, H−60 to H+110.

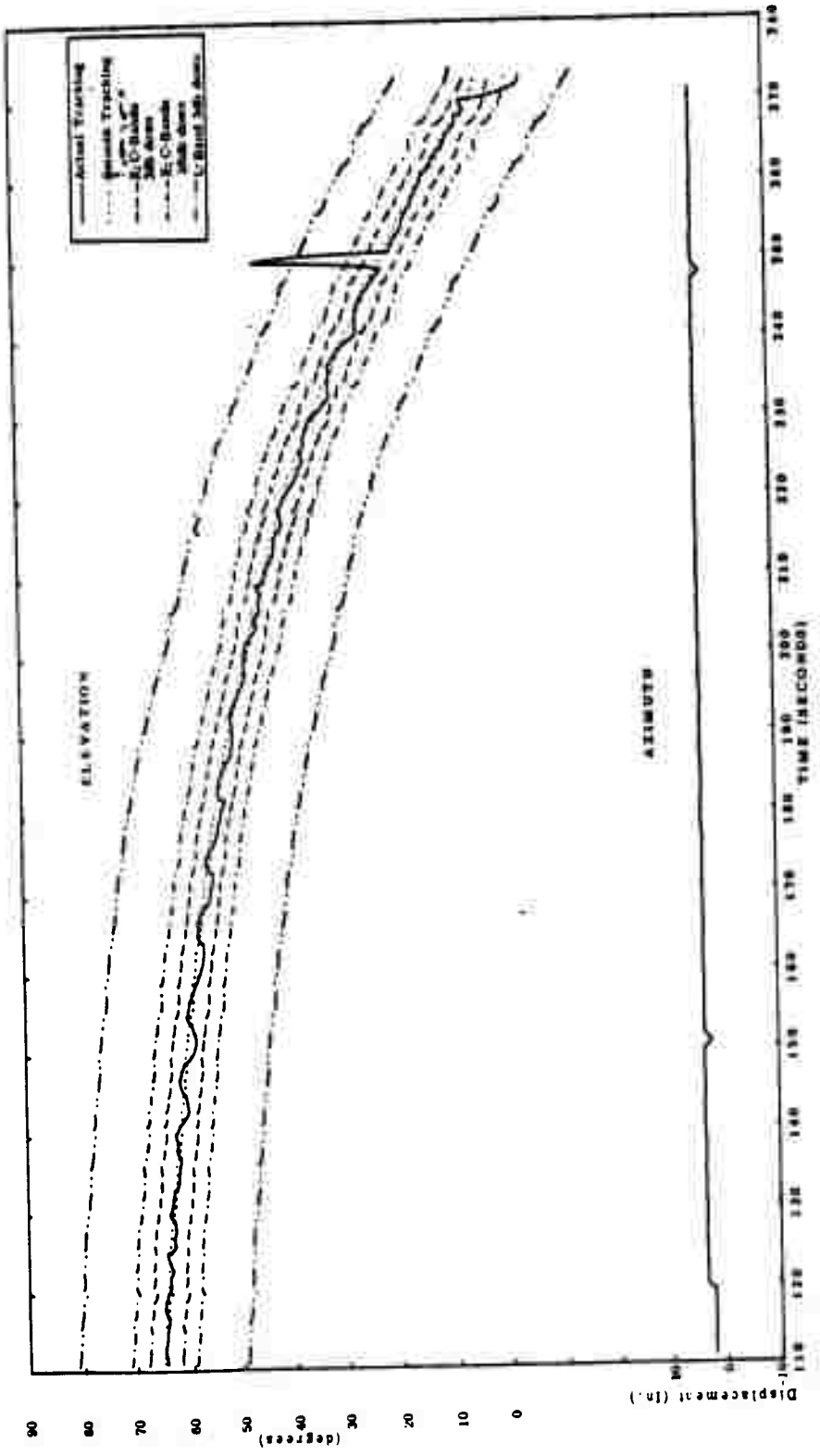

Figure A.41 Azimuth and elevation versus time, Tight Rope, Missile D, Ship 4, M = 110 to M = 280.

APPENDIX B

SUPPORT DATA

Information from supporting activities, which was used to reduce Project 6.1 data, is presented in this appendix. The support data represent the most recent information available from the respective sources. Available data accuracies, quoted by the several support activities, are presented in Table 2.4.

B.1 SHIP POSITION DATA

Data citing the locations of the four ships carrying Project 6.1 tracking systems were furnished by the U. S. Navy. Ship position data for the operational missions in which this project participated appear in Tables B.1 to B.10. The instrumentation employed in the acquisition of position data for each event is referred to in Sections 2.3.4, 3.3.4, and 4.3.4.

B.2 FIREBALL DATA

Data pertaining to fireball positions, dimensions, and rise rates for Blue Gill, King Fish, and Tight Rope were obtained from Edgerton, Germeshausen and Grier, Inc., and are presented in Figures B.1 to B.14 (Reference 7).

Information concerning the locations of the re-entry vehicles at the times of the three events was distributed by Headquarters, Field Command, DASA, and is listed in Tables B.11, B.12, and B.13. The locations of the re-entry vehicles at the times of events are in the various coordinate systems employed during the Fish Bowl operations. The Alpha system employs geographic coordinates in latitude and longitude with altitude calculated above the geoid. The Bravo system employs X and Y distances along a tangent plane calculated from Point John with altitude Z given above the reference plane. The location of Point John is given as:

Latitude:	$16^{\circ}44'03.30"$ N
Longitude:	$169^{\circ}31'41.48"$ W
Elevation:	13.583 ft

B.3 TRAJECTORY TRACKING SYSTEMS AND DATA

B.3.1 Cubic Corporation Missile Tracking Systems. Cubic Corporation was given the responsibility of providing all tracking data for the instrumented sounding rockets utilized in Project 6.1 activities during the Fish Bowl Series. A transponder and three types of ground tracking systems, described below, were employed by Cubic to obtain the required data. The DME system, with its associated

transponder, was used to determine slant range for all missiles fired for Project 6.1 during the test series. The low-accuracy Automatic Gimbaled Antenna Vectoring Equipment (AGAVE) was utilized for azimuth measurements on all but two carriers for this project. Two missiles fired during the Tight Rope experiment were tracked by the higher accuracy Angle Measuring Equipment (AME)-DME combination.

Transponder. A CW-FM transponder provided by Cubic Corporation was used to track the missile. Operating at a frequency of approximately 300 Mc, the transponder utilized the same battery power as the three-frequency transmitter of Project 6.1 and fed its signals to a separate, circularly polarized turnstile antenna located on the payload adapter section at the tail of the signal package. The turnstile was formed by crossed, swept-back dipoles, the circuitry of which was designed to produce right-hand circular polarization when viewed from the back of the missile.

Distance-Measuring Equipment. A CW-FM signal was detected by the transponder which retransmitted the modulations at a different carrier frequency. The total round-trip distance traveled by an energy packet was then

measured in terms of the phase shift of the returned modulation frequency with respect to that of the original modulating source. This system had a stated capability of tracking nine targets simultaneously to a range of 1000 miles with a precision of 10 meters between targets.

Automatic Gimbaled Antenna Vectoring Equipment. This system consisted of four antennas, an azimuth pair and an elevation pair, mounted on a common pedestal. Signals arriving at the AGAVE array from the transponder were combined to provide a sum signal and two difference signals. Each of these three signals was amplified and applied to phase detectors. In this manner, error signals were developed, amplified, and used to drive the corresponding pedestal motor to reduce antenna-pointing errors to zero.

Angle-Measuring Equipment. This system is essentially an angle-measuring interferometer which compared the phase of CW signals transmitted from the tracked vehicle. The measured phase difference was proportional to the difference in length of the two transmission paths. Since antenna separation was small, the path length difference was directly proportional to the direction cosine (with respect to the antenna baseline) of a vector pointing at the target. The

stated accuracy for this system was 0.1 milliradian up to a distance of 1000 miles.

B.3.2 Cubic Corporation Trajectory Data. Tables B.14 to B.24 are tabulations of trajectory data for Project 6.1 rockets tracked by Cubic Corporation tracking systems. The data, in most instances, includes extrapolations of short-time data through times of interest (Reference 8). The spatial coordinates, slant range, horizontal range, and the azimuth and elevation angles of the target are also included.

All data are presented in an East-North-Up coordinate system with the X-axis positive east, Y-axis positive north, and Z normal to the local horizon. Azimuth is measured clockwise from north. Corrections for tropospheric and ionospheric refraction, equipment calibration, scale factor, and parallax in ranging were applied. Range and direction cosine data are edited for ambiguous points, but no smoothing techniques were applied. All data is expressed in feet, seconds, and degrees. Reference point of all processed data is Point John. The Point John reference is given as:

East:	200,000 ft
North:	200,000 ft
Elevation:	13 ft

Tabulated data column headings follow:

24_HR TM:	24-hour clock time in hours, minutes, seconds, and tenths of seconds.
FLT TIM:	Time of flight from assumed time origin in seconds.
SLT RANGE:	Slant range.
HORZ RANGE:	Horizontal range.
EL:	Elevation angle.
AZ:	Azimuth angle.
X COOR:	Spatial coordinate of the target.
Y COOR:	Spatial coordinate of the target.
Z COOR:	Spatial coordinate of the target.
LOT:	Lift-off time.

TABLE B.1 POSITIONS OF SHIPS RELATIVE TO REFERENCE SHIP S-1, BLUE GILL

Station	Bearing, Degrees True	Range, Yards
S-2	100	5400
S-3	200	4500
S-4	141	8000
S-1	Reference ship	

TABLE B.2 POSITIONS OF SHIPS RELATIVE TO JOHNSTON ISLAND, BLUE GILL

Station	Bearing, Degrees True	Range, km
S-1	195	60.15
S-2	190	59.80
S-3	195.3	64.30
S-4	189.7	64.60

TABLE B.3 SHIP BEARING AND SPEED, BLUE GILL

Station	Time Relative to Event, Minutes	Course, Degrees True	Speed, Knots
S-1	H-30 to H+30	080	6
S-2	H-30	080	6
	H-15	080	6
	H	075	6
	H+15	075	6
	H+30	075	6
	Changed course to 075 at H-10		
S-3	H-25	080	6
	H-10	075	6
	H	080	6
	H+5	080	6
	H+30	080	6
S-4	H-30	080	6
	H-20	082	5.5
	H-10	PIR	R
	H	085	6
	H+10	085	6
	H+20	080	6
	H+30	075	6.5

TABLE B.4 POSITIONS OF SHIPS RELATIVE TO GROUND ZERO, BLUE GILL

Station	Bearing, Degrees True	Range, km
S-1	198.0	24.3
S-2	186.0	24.0
S-3	198.3	28.4
S-4	185.8	29.0

TABLE B.5 POSITIONS OF SHIPS RELATIVE TO JOHNSTON ISLAND, KING FISH

Station	Bearing, Degrees True	Range km
S-1	196	146.41
S-2	002	9.27
S-3	187	143.63
S-4	191	134.73

TABLE B.6 POSITIONS OF SHIPS RELATIVE TO GROUND ZERO, KING FISH

Station	Bearing, Degrees True	Range, km
S-1	197	74.1
S-2	012.5	80
S-3	181	72.6
S-4	187.2	63.9

TABLE B.7 SHIP BEARING AND SPEED, KING FISH

Station	Time Relative to Event, Minutes	Course, Degrees True	Speed, Knots
S-1	H-30 to H+30	080	6
S-2	H-30	250	0.3
	H-20	250	0.3
	H-10	250	0.3
	H	250	Stop
	H+10	250	Stop
	H+20	250	0.5
	H+30	250	0.5
S-3	H-30	180	3
	H-20	180	3
	H-10	060	3
	H	070	3
	H+10	085	3
	H+20	090	3
	H+30	090	3
S-4	H-30	015	7
	H-20	015	7
	H-10	060	7
	H+10	090	12
	H+20	090	12
	H+30	090	12

TABLE B.8 POSITIONS OF SHIPS RELATIVE TO JOHNSTON ISLAND AT H-HOUR, TIGHT ROPE

Station	Bearing, Degrees True	Range, km
S-1	359	0.493
S-2	011	7.0
S-3	017	0.72
S-4	023	9.1

TABLE B.9 POSITIONS OF SHIPS RELATIVE TO GROUND ZERO, TIGHT ROPE

Station	Bearing, Degrees True	Range, km
S-1	020	4.6
S-2	020	11.0
S-3	023	4.8
S-4	024	12.4

TABLE B.10 SHIP BEARING AND SPEED, TIGHT ROPE

Station	Time Relative to Event, Minutes	Course, Degrees True	Speed, Knots
S-2	H-30	Unknown	0.3
	H-20	Unknown	1.3
	H-10	067	Stop
	H	067	Stop
	H+10	067	0.5
	H+20	067	1.5
	H+30	067	1.0
S-4	H-30	320	2
	H-15	320	2
	H-10	160	1
	H	180	0.5
	H+15	025	1
	H+30	250	3

TABLE B.11 LOCATION OF REENTRY VEHICLE AT EVENT, BLUE GILL

Designation	Coordinate	Reference System
Latitude (N)	16° 24' 57.03"	Alpha
Longitude (W)	169° 36' 11.15"	
Altitude, km	48.27	
Altitude, feet	158,357	
X, minus feet	26,600 ±60	Bravo
Y, minus feet	116,190 ±60	
Z, plus feet	158,017 ±60	
Azimuth from North	192° 47' 35.79"	From Point John
Elevation angle	52° 55' 24.67"	
Slant range, feet	198,071.1	
Slant range, m	60,372	

TABLE B.12 LOCATION OF REENTRY VEHICLE AT EVENT, KING FISH

Designation	Coordinate	Reference System
Latitude (N)	16° 06' 48.61"	Alpha
Longitude (W)	169° 40' 56.02"	
Altitude, km	97.24	
Altitude, feet	319,038	
X, minus feet	54,887 ±50	Bravo
Y, minus feet	228,802 ±50	
Z, plus feet	317,796	
Azimuth from North	193° 29' 22.92"	From Point John
Elevation angle	53° 29' 17.12"	
Slant range, feet	395,355.2	
Slant range, m	120.504	

TABLE B.13 LOCATION OF REENTRY VEHICLE AT EVENT, TIGHT ROPE

Designation	Coordinate	Reference System
Latitude (N)	16° 42' 26.71"	Alpha
Longitude (W)	169° 32' 32.66"	
Altitude, km	21.03	
Altitude, feet	68,995	
X, minus feet	4,991	Bravo
Y, minus feet	9,774	
Z, plus feet	68,992	
Azimuth from North	207° 03' 02.51"	From Point John
Elevation angle	80° 57' 44.12"	
Slant range, feet	69,846.6	
Slant rahge, m	21,289	

Pages 66 through 117
deleted.

APPENDIX C

SHIPBOARD REFRACTION MEASUREMENTS

Tracking error signals recorded by the four shipboard stations were intended to provide information concerning relative refractive effects sustained between the three microwave frequencies employed by Project 6.1 during the test series. Assuming no functional problems, tracking error data would represent the angle between the pointing direction of an antenna and the arrival direction of a signal.

Two methods that were implemented in an abortive attempt to calibrate tracking error signals generated at the shipboard stations are presented below.

C.1 CALIBRATION METHOD I

Originally, each shipborne tracker was to provide a calibration for its own generated error signals To accomplish this, a low power signal source was placed at some distance to the front and in the near field of the system. With the tracking system in an automatic mode, the antenna providing the track oriented itself toward the beacon and ultimately produced a zero,or nulled, error signal (Figure C.1a).

Placing the system under manual control, the antenna was then rotated laterally until the error signal, properly

monitored, achieved 100 percent modulation. At the first indication of signal distortion, antenna slewing was stopped. The angle through which the antenna had deviated from the signal source was presumed to describe one-half of the principal beamwidth of the antenna (Figure C.1b). The signal levels between these points was assumed linear.

It was expected that a calibration procedure of this sort would provide a gage for measuring apparent relative refraction effects between radiated frequencies.

Attempts to reduce data from early test firings disclosed anomalies in error signals and an inability to reconcile flight data with calibration criteria.

C.2 CALIBRATION METHOD II

An alternate method to calibrate error signals was devised and finally implemented on 13 October 1962. Generally, it consisted of placing the four ships approximately southeast of the island at a nominal 8000-foot range (see Figure C.2). Beacons, radiating atop Nike-Cajun missiles affixed to operational launchers on the island (designated A, B, C, and D), were monitored by the four shipborne tracking systems.

The X- and C-band tracking antennas were sequentially locked automatically to Missile Beacon A while the two

receivers not used for tracking purposes were tuned, in turn, to Missiles A, B, C, and D. An additional elevation calibration for error signals was produced by placing a fifth beacon, designated G, on a tower 55 feet above sea level. The error signal outputs were recorded in standard format on magnetic tape. (As an example: the X-band antenna automatically tracked Missile A while C- and L-band receivers were tuned sequentially to Missiles A, B, C, and D. The next phase of the calibration procedure had the C-band antenna track Missile A while the X- and L-band receivers were tuned to Missiles A, B, C, and D, etc. An outline of the calibration sequence is presented in Table C.1)

The four vessels, steaming against their anchors to maintain directional stability, were monitored from survey points located at the two longitudinal ends of the island. Simultaneous transit readings from both bench mark locations were made of shipboard antenna positions. The positional information so derived was translated to the missile beacon locations so that the angles (Θ_{AB}, Θ_{AC}, Θ_{AD}, Θ_{AG}) generated between the shipboard trackers and the five Johnston Island missile transmitters could be determined (See Figure C.3).

The error signals generated during each calibrated pointing deviation were phase detected and compared with each subtended angle they were purported to represent. Quadrature error amplitudes, observed during any of the calibration modes, varied considerably and did not have any distinct relationship with the computed antenna-to-missile beacon error angles they were suppose to indicate. The cause of these inconsistencies becomes apparent upon further consideration of the geometry of the systems involved in the calibration attempt. Figure C.4 illustrates the parameters incident to the test.

It can be seen that ray paths from the missile transmitter that are reflected from the surface of the ocean will be received within the main lobe pattern of the receiving antenna (as well as in the side lobes). This existent multipath generates a spectrum of arrival angles that introduces erroneous data.

The random nature of tracking error signal data generated during the calibration attempt made it impossible to use such information for angle measurement purposes.

TABLE C.1 CALIBRATION METHOD II, TRACKING SEQUENCE

Antenna Tracking Missile A	Missiles Acquired by Receivers		
	X-Band	C-Band	L-Band
X	A	ABCDG	ABCDG
C	ABCDG	A	ABCDG

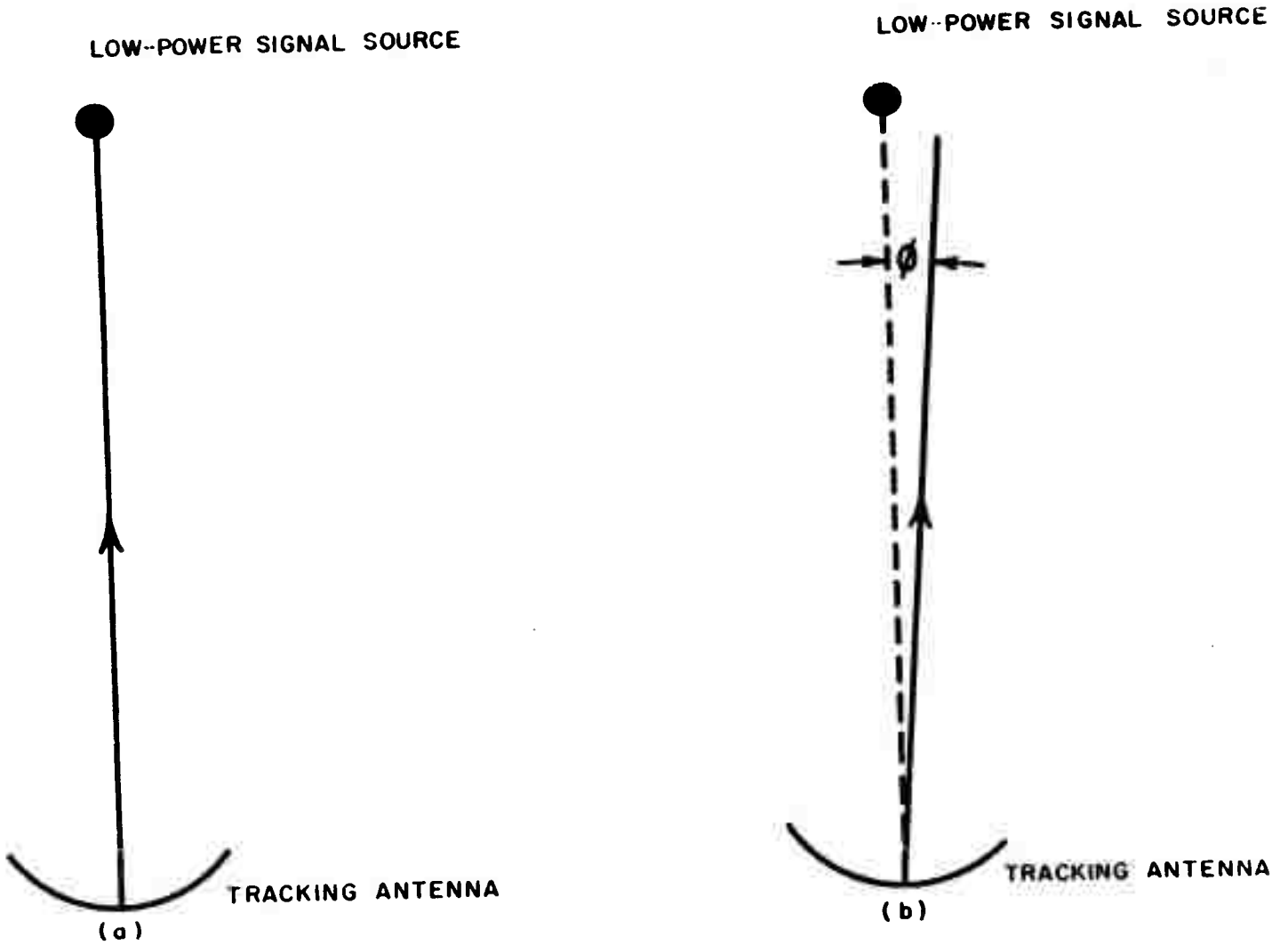

Figure C.1 Calibration Method I, test procedure.

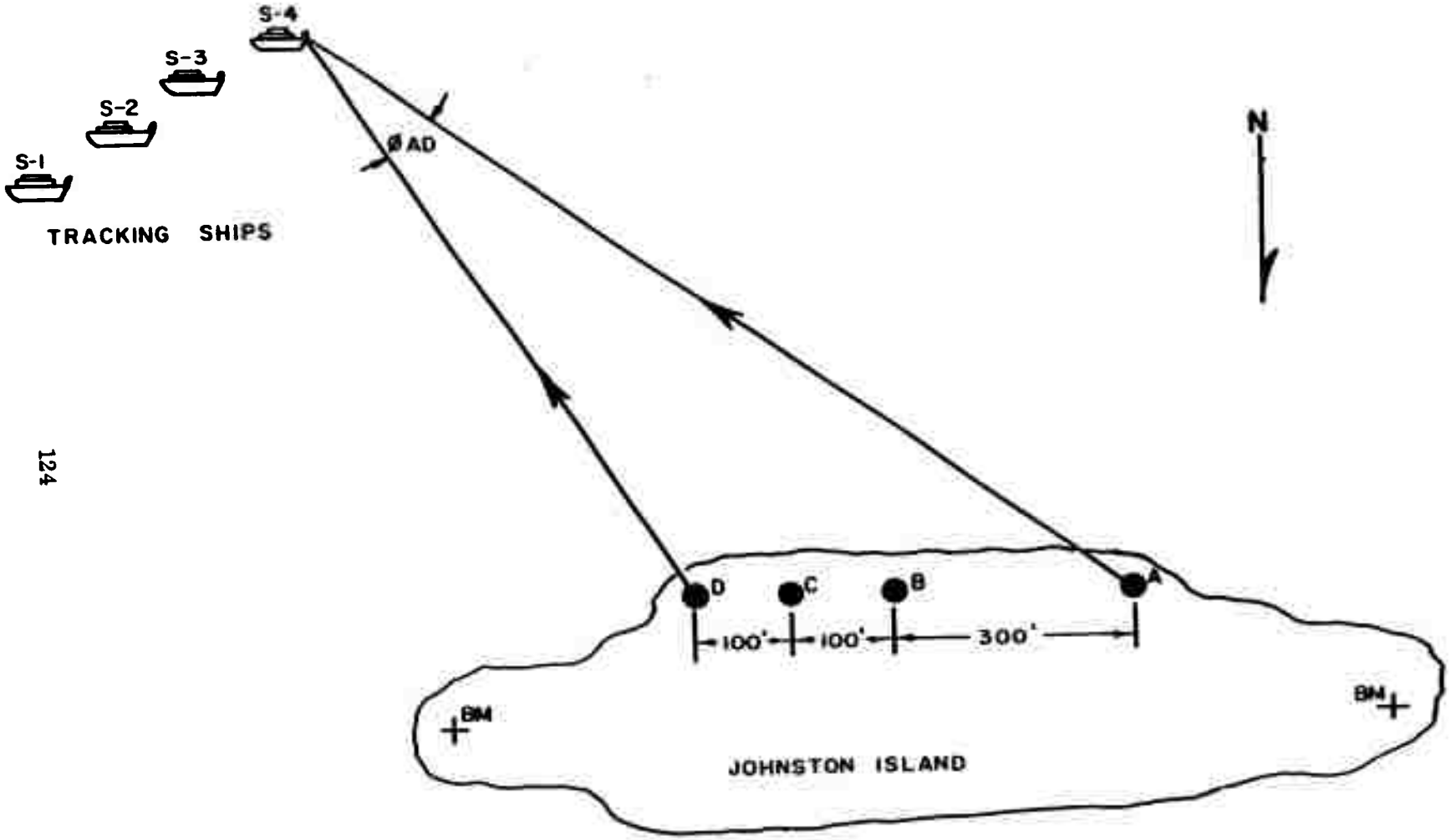

Figure C.2 Calibration Method II, test procedure.

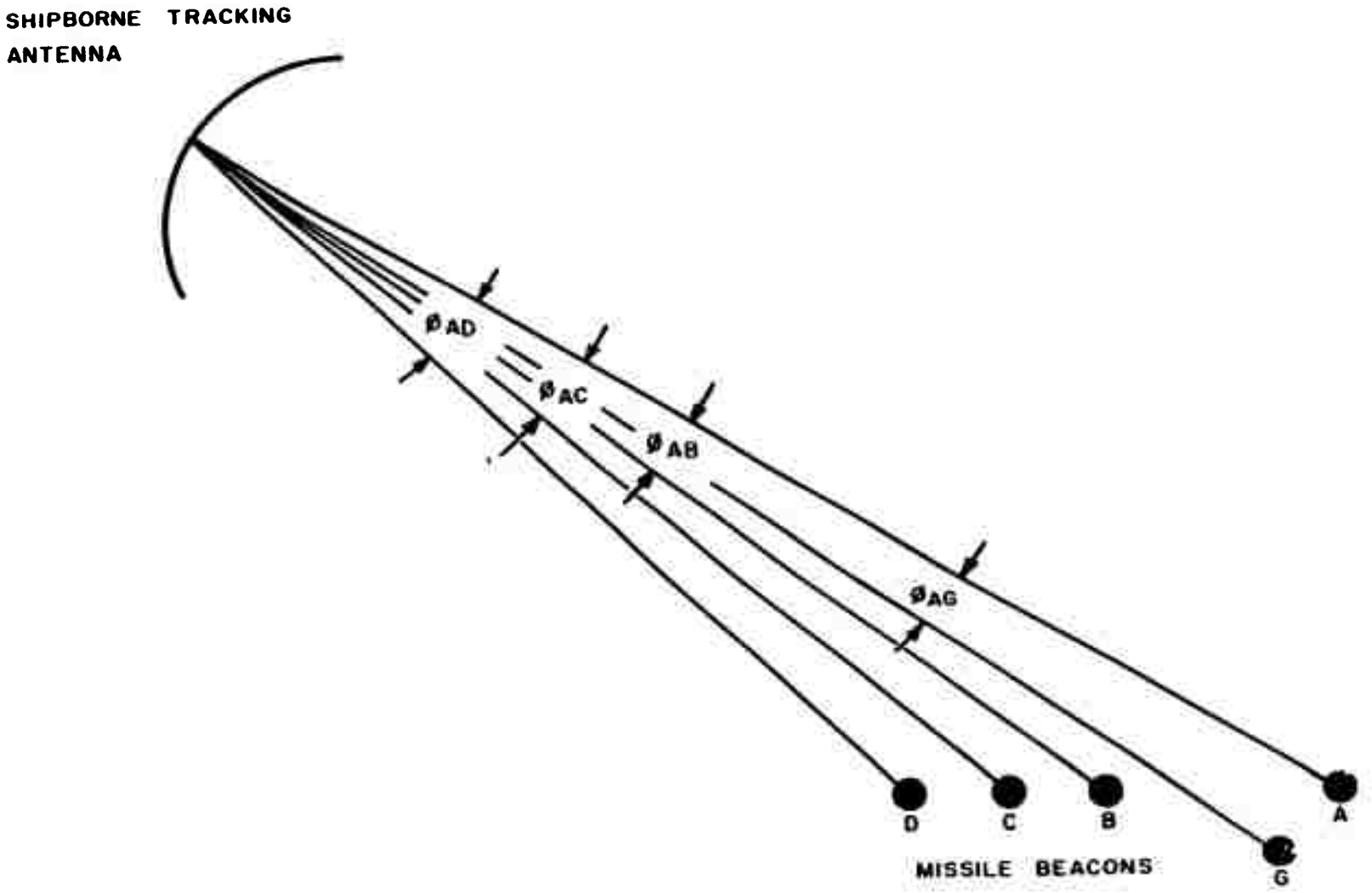

Figure C.3 Calibration Method II, error angles.

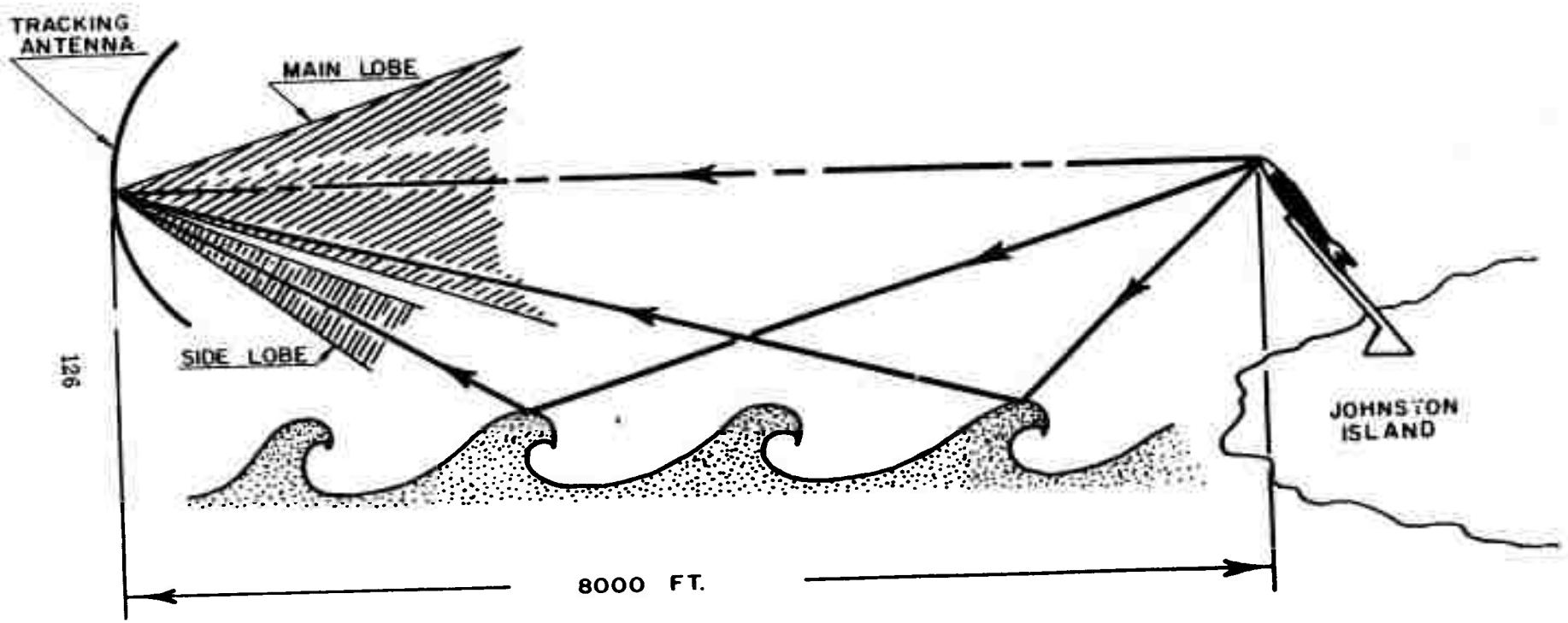

Figure C.4 Calibration Method II, multipath interference.

APPENDIX D

INTERFEROMETER DESCRIPTION

Section D.1 presents a mathematical description of the interferometer, lists beacon frequencies and other necessary constants, and describes the original objectives and final evolved solutions. A discussion of the sources of system error follows in Section D.2.

D.1 DATA REDUCTION

The two original objectives of analyzing the interferometer data were to determine the extent of refraction of electromagnetic waves and the extent of curvature distortion on the incident wavefront. The approach to the problem was to compare the Cubic trajectory with a trajectory determined independently by the interferometer to obtain refraction information, and to compare the solutions of the incident plane wave from different combinations of interferometer antennas to obtain curvature distortion information. The tools available for the first approach were a basic knowledge of an interferometer, Sylvania Electronic Defense Laboratories (EDL) reports on the design and operation of the interferometer, limited Cubic trajectory information, and the interferometer phase recordings.

An independent trajectory solution from the interferometer was desired. A complete trajectory solution was impossible;

hence, a solution was attempted for the direction cosines of the arriving ray. A solution for curvature was suggested by solving for the planes described by the incident wave. These planes could be determined from a knowledge of the direction of the arriving ray (Cubic), and from the phase relation of a combination of three interferometer antennas (phase recordings). A comparison of the planes was to indicate curvature.

This suggested that if the direction of the normal to these incident planes could be determined without using Cubic trajectory, then a comparison of these normals could give the desired curvature. In addition, a comparison of these normals with the trajectory direction could give the refractive information. A method was devised to solve for these normals, a revised version of which is discussed in Section D.1.1.

Since the transmitted frequency of C-band was five times that of L-band, the rate of phase comparisons of the two signals occurred approximately at the same ratio. Although lack of phase-lock between systems precluded a strict phase comparison of L- and C-bands, it was expected that the ratio between their readouts would be sufficiently constant to provide some correlating data between the two frequencies.

Unfortunately, during the entire test series, there were no periods of measurable perturbations during which data from both systems were available simultaneously.

D.1.1 Angular Position Solution. Each interferometer system consists of four receivers with their antennas positioned in any asymmetrical array. The interferometer geometry, shown in Figure D.1, depicts respective antennas located at A, B, C, and D. The coordinate system consists of the horizontal plane of the interferometer (A, B, C, D) and the vertical axis. The origin of the coordinate system is at the point in the horizontal plane where the sum of the squares of the distances from the origin to the antennas is minimum. The vectors A, B, C, and D describe the antenna positions with respect to the origin.

The baseline between each pair of antennas is a leg of the interferometer. For the six interferometer legs, the following vectors define each baseline:

$$\vec{r}_1 = \vec{A} - \vec{B}$$
$$\vec{r}_2 = \vec{C} - \vec{B}$$
$$\vec{r}_3 = \vec{A} - \vec{C}$$
$$\vec{r}_4 = \vec{D} - \vec{A}$$
$$\vec{r}_5 = \vec{D} - \vec{B}$$
$$\vec{r}_6 = \vec{D} - \vec{C}$$

The respective unit vectors for each baseline are

$$\hat{u}_i = \frac{\vec{r}_i}{|\vec{r}_i|} \text{ for } i = 1, \ldots\ldots, 6$$

The signal which the interferometer detects from the missile is considered a plane wave. The normal to the wave front is the ray path, and the observed ray paths at each receiver are assumed to be parallel. For any given pair of receivers, geometry can be constructed as shown in Figure D.2.

The parallel rays are traveling from the missile. Ray (2) travels a greater distance, AC, than Ray (1) resulting in a phase difference between A and B.

From the geometry

$$\cos \theta_i = \frac{\text{distance AC}}{\text{distance AB}}$$

Describing the distance AB in wavelengths d_i, and the distance AC in wavelenghts ℓ_i,

then

$$\cos \theta_i = \frac{\ell_i}{d_i}$$

The value of ℓ_i is called a lobe number and represents the integral and partial number of wavelengths in the distance AC.

When ℓ_i is exactly an integral number of wavelengths, the electrical phase difference is zero. The interval between two adjacent integral values of ℓ_i is 360 electrical degrees.

The space angles (θ_i) at which the phase zeroes occur for each leg of the interferometer are shown in Figures D.3 to D.8. The interferometer leg lengths in wavelengths, d_i, are presented for each missile in Tables D.1 to D.3.

Defining a unit normal vector N_I to be in the direction the ray paths are approaching, then the dot product of this unit normal and the baseline unit vector gives the cosine of the spacial angle θ_i.

Thus, $$\hat{N}_I \cdot \hat{U}_i = \cos \theta_i = \ell_i/d_i$$

Knowing d_i and reading ℓ_i from the interferometer records, the components of N_I can be determined by the above relation and the Pythagorean Theorem. Specifically, for legs 1 and 2

$$N_I^x U_1^x + N_I^y U_1^y + N_I^z \cdot 0 = \ell_1/d_1 = \cos \theta_1$$

$$N_I^x U_2^x + N_I^y U_2^y + N_I^z \cdot 0 = \ell_2/d_2 = \cos \theta_2$$

These equations can be solved for N_I^x and N_I^y.

$$N_I^x = \frac{U_2^y \cos \theta_1 - U_1^y \cos \theta_2}{U_1^x U_2^y - U_1^y U_2^x}$$

and

$$N_I^y = \frac{U_1^x \cos \theta_2 - U_2^x \cos \theta_1}{U_1^x U_2^y - U_1^y U_2^x}$$

Then $$N_I^z = [1 - (N_I^x)^2 - (N_I^y)^2]^{1/2}$$

and the unit normal vector is

$$\hat{N}_I = N_I^x \hat{1}_x + N_I^y \hat{1}_y + N_I^z \hat{1}_z$$

Two interferometer legs and their respective phase information are required then to solve for the unit normal. The unit normal components N_I^x, N_I^y, and N_I^z are the direction cosines of the trajectory vector.

If separate trajectory information is available and translated to the coordinate system of the interferometer, its direction cosines are comparable to the ones determined from the interferometer. For the trajectory vector $\vec{R}$, the direction cosines are:

$$N_T^x = X/R$$

$$N_T^y = Y/R$$

$$N_T^z = Z/R$$

The comparison can be made by dotting or crossing the two unit vectors so that

$$\hat{N}_I \cdot \hat{N}_T = \cos \phi$$

or

$$\hat{N}_I \times \hat{N}_T = \sin \phi$$

the component expressions are

$$\phi = \cos^{-1} \left[N_I^x N_T^x + N_I^y N_T^y + N_I^z N_T^z \right]$$

and

$$\phi = \sin^{-1} \left[(N_I^y N_T^z - N_T^y N_I^z)^2 + (N_T^x N_I^z - N_I^x N_T^z)^2 + (N_I^x N_T^y - N_T^x N_I^y)^2 \right]^{1/2}$$

The two normals N_1 and N_2 were solved by using legs 4 and 6, and 1 and 3, respectively. These combinations, along with two more (legs 4 and 5 to give normal N_3 and legs 5 and 6 to give normal N_4) were chosen because the two legs used to determine the normal had a common antenna. In addition, comparison of N_1 and N_2 provided one dimension of curvature and N_3 and N_4 provided another. The ability to solve for these normals led to the development of the Refraction and Angular Wavefront Curvature (RAWC) computer program. Using the interferometer phase information and other trajectory information, this program computed the angular differences between the trajectory vector and the normals N_1 and N_2. The angular difference between the unit normals N_1 and N_2 and between N_3 and N_4 were also computed. The interferometer input data consisted of lobe numbers, which are the number of wavelengths representing the phase difference between two antennas. The integral ramps, or lobes, were counted, and the partial lobe amplitudes were read from each phase comparison at one-second intervals. This reading interval was believed to be sufficient to detect significant refraction and curvature changes. The trajectory data was time correlated

to the interferometer data.

D.1.2 White Sands Missile Range Firing Data. In addition to the actual Dominic test data (Blue Gill, Tight Rope and King Fish), interferometer and radar data were available from a WSMR firing. These data were read and computed to determine if the method of solution was sufficiently accurate to serve its purpose. The results of the RAWC computation for the WSMR data showed that the refractive and curvature angular differences were much greater than the expected values, indicating a gross error. In order to have another perspective of the indicated discrepancies between the WSMR interferometer data and the radar (AN/FPS-16) trajectories, simulated lobe counts derived from the radar trajectory were compared with counts taken from the actual phasemeter data. These comparisons are shown in Figures D.9 to D.14. Also, a comparison of interferometer and radar vectors for each interferometer combination was made. These comparisons are presented in Figures D.15 to D.28. However, since the difference values were consistently large, it was believed that a relative refractive and curvature angle might be determined. Thus, the Dominic data was evaluated with the available trajectory to determine the changes in the refractive and curvature angular values.

D.1.3 Dominic Data Problems. A problem existed in

establishing a reference point for the lobe counting of Dominic phase data. This reference point was found by using the available trajectory information to compute the respective lobe numbers for each interferometer leg. These computed lobe numbers were then time-correlated with the lobe readings that had been counted from an arbitrary reference point. Through this matching, the actual lobe reading was obtained by correcting the integral portion of the lobe values for each leg to that of the computed integral lobe value.

Since most of the raw Cubic trajectory was not usable, trajectory simulation was attempted by employing existing Nike-Cajun computer simulation programs. These simulated trajectories, and later a new usable Cubic trajectory, were all run on the RAWC program for the Dominic tests. No obvious results of refractive or curvature angular changes were obtained. Also, it was concluded that curvature could not really be determined at the trajectory ranges under consideration. However, different computed normals should be nearly identical.

Although the angular differences between the trajectory vector and the interferometer normals were large, the large differences between the normals indicated that there was a possible mismatch of lobes when establishing the reference point. Various search techniques were tried to correct the

combination of lobe numbers to reduce the angular difference of the computed normals. A workable technique, which would correct simple but not complex errors, was finally obtained. However, the results indicated that even if the technique could not find the correct combination it would not cause divergence of the computed normals.

It was found that the combinations of interferometer legs need not have a common antenna to solve for the normal, since the incident plane wave would not change significantly. Of the 14 usable lobe combinations, 15 combinations are possible, but one involves parallel legs; those used in the search technique were:

Legs AB and BC

Legs AB and AD

Legs BC and CD

Legs AD and CD

Legs AC and BD

Five normals were computed from the above combinations. An average normal was determined and used to recompute the respective lobes. The computed and actual lobes were compared; the lobe with the greatest deviation was corrected toward the average. With this new lobe a new average was determined, and the iterative process was continued.

For Blue Gill, the new Cubic trajectory seemed to be the best obtainable as indicated by the results of the RAWC program and the search technique.

D.1.4 Least-Squares Solution. Ideally, all the 14 normals should have the same values (assuming a plane wave-front). The previously described programs indicated a wide dispersion in vectors computed from data recorded during unperturbed times. A least-squares solution program was prepared in an effort to compute a single meaningful vector to replace the 14 individual solutions. The solution, which is detailed below, was first used on the WSMR data and compared to the radar data. A plot of the comparison is shown in Figure D.29.

The interferometer trajectory angle solution involves the solution of six equations in two unknowns.

$$\cos \theta_i = \hat{N} \cdot \hat{U}_i \quad \text{for } i = 1, 2, \ldots, 6$$

where

$$\cos \theta = \frac{\text{lobe number of } i^{th} \text{ leg}}{\text{length of } i^{th} \text{ leg in wavelengths}}$$

$\hat{N}$ = unknown trajectory unit vector

$\hat{U}_i$ = interferometer geometry vectors or unit vectors in direction of leg baseline

This over-determined system of linear equations is not usually compatible. The method of least squares, however, makes it possible to adjust an arbitrarily over-determined and incompatible set of equations.

Let $U = \begin{vmatrix} U_{11}, U_{12} \\ U_{21}, U_{22} \\ \cdot \quad \cdot \\ \cdot \quad \cdot \\ \cdot \quad \cdot \\ U_{61}, U_{62} \end{vmatrix}$ matrix of geometry

6 x 2

$N = \begin{vmatrix} N^x \\ N^y \end{vmatrix}$ matrix of unit vector N
2 x 1

$C = \begin{vmatrix} \cos \theta_1 \\ \cdot \\ \cdot \\ \cdot \\ \cos \theta_6 \end{vmatrix}$ matrix of slant plane direction cosines

6 x 1

$$U \cdot N = C$$

Due to errors in measurement, the equations are not mathematically compatible. Defining a residue vector R

$$U N - C = R,$$

these vector components cannot all be zero. But there is a best solution available under the given circumstances.

Taking the square of the length of the residue vector, one can determine N by the condition that R^2 shall become a minimum. The minimizing of $(U N - C)^2$ has a definite solution no matter how incompatible the given system is.

The least-squares solution of U N = C is

$$\tilde{U} U N = \tilde{U} C$$

where $\tilde{U}$ = transpose of U

Substituting back into U N = C, the compatibility of the best solution N can be demonstrated.

D.1.5 Short-Term Refraction. The initial prospects of obtaining refraction measurements assumed the availability of good trajectory data from launch to event time. For long-term refraction, a sufficient period of accurate pre-event trajectory is necessary as a control factor to test compatibility between the phase data and the furnished trajectory. Direction angles generated by interferometer data must be shown either to agree with the missile trajectory or to evidence a relationship whereby the two sets of data can be predictably reconciled. If a good agreement or a definitive relationship between the two systems cannot be assessed during this early period, then any differences noted between them after event cannot be evaluated.

When a significant degree of signal refraction takes place almost instantaneously, such as at the time of detonation, relative measurements of the extent and duration of the perturbation may be possible for a short time interval. In the absence of precise trajectory information, refraction measurements are limited to periods in which angular deviation rates of change are sufficient to be noticeable and differentiated from nonperturbed data. This limitation is dependent

upon the rate of change of missile motion and consequently will vary between different channels of phase data. Within a short time frame (about one second), it is feasible to extrapolate from pre-event data for purposes of comparison with actual post-event phase deviations. The change in missile position during the brief measurement period is considered negligible.

For the Dominic series, there were no trajectories available which were adequate for long-term refraction measurements. Therefore all measurements, for which data is presented, are of short-time refraction.

One of the most critical problems encountered in the reduction of phase data for the three operational missions was the need to distinguish between phasemeter noise and legitimate refraction data at times of interest. As discussed in Section 1.6.5, the characteristics of phasemeters employed by this project were such that low signal-to-noise inputs yielded outputs of noisy data, or random oscillations. As the threshold levels for phasemeter performance were nebulous and varied with equipment, it was necessary to examine all recorded excursions critically, even those produced by low signal inputs, for the possibility of extracting valid refraction measurements. Although the nature of phase deviations for short time

intervals (notably at events) may not be totally predictable, certain aspects of their behavior were tested for compatibility with established theoretical refraction behavior.

Differential equations were developed for the expected change in phase for each leg of the interferometer system as a function of the change in azimuth and elevation angles of the incident ray. The coefficients of these equations are functions of the relative geometry of the ray path and baselines at the moment of interest. These equations were used to determine if the recorded phase perturbations were compatible with those expected from an actual refraction or whether they might be attributed to system noise.

At H = 0, during Blue Gill, the unperturbed ray path was incident to the interferometer array with an elevation angle of approximately 68 degrees and an azimuth angle of approximately 7 degrees from the BD axis.

The equation for the differential change of phase for leg BD is derived below (see Figure D.30). The phase difference is given by

$$\phi_p = 360 \left(\frac{L}{\lambda} - n\right)$$

where ϕ_p is the phase difference in degrees, λ is the wavelength, and n is an integral number which, for small changes,

can be considered constant. Differentiating ϕ_p:

$$d\phi_p = \frac{360}{\lambda} dL.$$

However, since

$$L = S \cos \theta,$$

$$d\phi_p = \frac{-360\ S}{\lambda} \sin \theta\ d\theta.$$

From Figure D.30,

$$\cos \theta = \cos Az \cos El$$

and

$$\sin \theta\ d\theta = \cos Az \sin El\ dEl + \sin Az \cos El\ dAz,$$

therefore, $d\theta_p = \frac{360\ S}{\lambda} (\cos Az \sin El\ dEl + \sin Az \cos El\ dAz).$

For leg BD at C-band frequencies,

$$\frac{S}{\lambda} \approx 450.$$

Using the unperturbed values, Az = 7° and El = 68°,

$$d\phi_p = -360\ (450)\ (\cos 7^\circ \sin 68^\circ\ dEl + \sin 7^\circ \cos 68^\circ\ dAz)$$

or

$$d\phi_p = -148\ dEl - 7.36\ dAz,$$

where dEl and dAz are in milliradians.

Similar calculations for the other legs yield the following sets of equations:

AB: $d\phi_p = 7.3\ dAz + 48.5\ dEl$

AC: $d\phi_p = 15.0\ dAz - 4.7\ dEl$

AD: $d\phi_p = -103\ dEl$

BC: $d\phi_p = 7.45\ dAz - 53.0\ dEl$

CD: $d\phi_p = -14.2\ dAz - 96\ dEl$

At H = 0, during King Fish, the azimuth angles, although opposite in sense, were approximately the same as those for Blue Gill, but the elevation angle was about 84 degrees. The resulting equations from this geometry are:

AB: $d\phi_p = 53.5\ dEl + 2.0\ dAz$

AC: $d\phi_p = -3.5\ dEl + 4.4\ dAz$

AD: $d\phi_p = -108\ dEl$

BC: $d\phi_p = -55\ dEl + 2.4\ dAz$

BD: $d\phi_p = -161\ dEl - 1.5\ dAz$

CD: $d\phi_p = -104\ dEl - 3.9\ dAz$

The apparent deviations in azimuth and elevation for the 14 interferometer combinations were calculated from the six independent equations above. Results are presented in Tables D.4 and D.5 for some representative times. The dispersion of the Blue Gill results in the azimuth plane as a function of time is shown in Figure D.31. (Virtually all deviations appear in azimuth-sensitive phase comparisons.) Both directional components derived from recorded phase data are compared for consistency with azimuth and elevation directions deduced from the relative geometries. Additional presentations of

Blue Gill and King Fish dispersion factors are given in Figures 2.82, 3.47, and 3.48.

It is evident that refraction was not observed in Blue Gill data, but was observed for that of King Fish.

D.2 SOURCES OF SYSTEM ERROR

There are several possible sources of error inherent to interferometer systems. The system errors contributed by the various sources will vary in extent from the imperceptible to those that are highly detrimental to precision phase measurements. Errors will cause anomalies in certain phase relationships which are inherent to the interferometer system. These relationships involve the summation of phase differences about a closed loop of antennas (see Figure D.1; the directional designation for each phase comparison is strictly a convention for simplifying calculations). For any one frequency, at any time, the algebraic sum of phase difference in a loop must equal zero. Hence,

$$\phi_{AB} + \phi_{BC} + \phi_{CA} = 0,$$

$$\phi_{CA} + \phi_{AD} + \phi_{DC} = 0, \text{ etc.}$$

An examination of data from the operational missions and preceding test firings indicates the existence of phase-loop summation, or closure, errors. Errors of closure varied

with time and between loop combinations. A mean, representative measure of closure error is 30 electrical degrees. The various types of error sources are discussed in terms of their relative application to the interferometer system and its associated geometries used in the Dominic experiments.

D.2.1 Lead-In Cables. Inequality in the lengths of cable between any antenna pair and the interferometer van will result in a phase error

$$\Delta\phi_c = 360 \frac{\Delta L}{\lambda_c} \text{ electrical degrees}$$

where ΔL is the difference in cable lengths and λ is the wavelength of the frequency under consideration. As an example, a cable length difference of one centimeter in the C-band system will result in a phase shift of 60 electrical degrees. Since there are six antenna pair combinations in each interferometer system, it is conceivable to be subject to different phase shifts in all 12 phase-data channels. No information concerning the precision of, or methods used in, the measurements of cables is available for an analysis of probable error.

Cables between the antenna array and the interferometer van are subject to physical bruising by pedestrian and vehicular traffic if they are not set in covered troughs or otherwise protected. Physical bruising can change the electrical

length of a cable or its characteristic impedance at the point of bruise. Interferometer cabling on Johnston Island was exposed on the surface of the ground for short distances.

Unless shielded from the elements to aid temperature stabilization, cable lengths will change from day to night or during significant changes in the weather. As all cables should have identical expansion rates, the effects of temperature variations in the applicable environment are considered negligible.

D.2.2 Doppler Shift. The doppler effect created by the movement of the missile beacon relative to the interferometer array will introduce some varying phase shift error in phase data. For the worst case (which is actually prohibited by launch geometry and trajectory), the doppler-generated phase shift between antennas is:

$$\phi_D = \frac{(360)\, V_m}{c} \quad \text{electrical degrees}$$

where V_m is the maximum radial velocity of the missile. For a maximum missile velocity of 2 km/sec (slightly higher than Project 6.1 rockets),

$$\phi_D = 2.4 \times 10^{-3} \text{ electrical degrees}$$

During actual missile flights, phase shift caused by relative missile motion is considerably less than this negligible amount.

D.2.3 Atmospheric Refraction. Atmospheric refraction effects on interferometer data were negligible during Dominic due to the high slant plane angles involved during times of interest.

D.2.4 Antenna Misalignment. Errors in geodetic location surveys of the four interferometer antennas can introduce significant inaccuracies in phase data reduction. Types of possible alignment errors include: (1) bearing errors involving the two cross-axes of the interferometer antenna array, (2) antennas not lying in a horizontal plane, and (3) incorrect spacing between receiver antennas. Survey accuracies for the Johnston Island interferometer array are given as ±1/8 inch in horizontal and vertical position.

D.2.5 Phase Shift Between Receivers. Phase shift generated between a pair of interferometer receivers can significantly degrade phase data. A test of phase error introduced by various receiver combinations was performed some time after the completion of the Dominic series. With a common signal source providing the input to each receiver pair, the input frequency was varied from the nominal (5 kMc) frequency in steps of 0, ±20, ±40, and ±60 kc. The output of each receiver pair was examined for phase shift. In the worst case, a phase shift of 10 electrical degrees was observed.

D.2.6 Multipath. The reception of multipath signals due to ground reflections can introduce perturbations into phase data. Since slant plane elevation angles to the missile are high after launch, it is expected that signal reflections from ground contours would be in the low-gain side lobes of the receiving antennas and generally beyond the dynamic range of the system.

TABLE D.1 EQUIVALENT WAVELENGTHS OF INTERFEROMETER LEGS, BLUE GILL, MISSILE A, H - 195 SEC

Frequency Bands	Beacon Frequency Wavelength, cm	Interferometer Leg Lengths, Wavelengths					
		AB	BC	AC	AD	BD	CD
C	6.310996	163.3308	177.1559	118.8402	319.3727	475.3608	326.6600
L	31.554978	32.6662	35.4312	23.7680	63.8745	95.0722	65.3320

TABLE D.2 EQUIVALENT WAVELENGTHS OF INTERFEROMETER LEGS, KING FISH, MISSILE C, H - 85 SEC

Frequency Band	Beacon Frequency Wavelength, cm	Interferometer Leg Lengths, Wavelengths					
		AB	BC	AC	AD	BD	CD
C	6.3112546	163.3241	177.1486	118.8353	319.3596	475.3413	326.6466
L	31.556273	32.6648	35.4297	23.7671	63.8719	95.0683	65.3293

TABLE D.3 EQUIVALENT WAVELENGTHS OF INTERFEROMETER LEGS, TIGHT ROPE, MISSILE A, H - 50 SEC

Frequency Band	Beacon Frequency Wavelength, cm	Interferometer Leg Lengths, Wavelengths					
		AB	BC	AC	AD	BD	CD
C	6.311979	163.3054	177.1283	118.8217	319.3230	475.2868	326.6091
L	31.559894	32.6611	35.4257	23.7643	63.8646	95.0573	65.3218

TABLE D.4 DISPERSION OF SAMPLE RECORDED DEVIATIONS FOR THE FOURTEEN SYSTEM COMBINATIONS, BLUE GILL

System Combinations	0.005 Sec dAZ	dEL	0.050 Sec dAZ	dEL
AB-AC	-9.4	1.5	-5.3	0.8
AB-AD	1.6	2.6	-6.7	1.1
AB-BC	20.8	-1.6	0.3	0.0
AB-BD	24.4	0.5	1.0	0.0
AC-AD	-9.9	2.6	-5.2	1.1
AC-BC	-12.3	-1.5	-5.8	-0.8
AC-BD	-10.5	0.3	-5.5	0.0
AC-CD	-9.7	1.7	-5.3	0.0
AD-BC	41.5	2.6	7.9	1.1
AD-BD	-44.6	0.0	-22.5	0.0
AD-CD	-4.9	0.0	-7.5	0.0
BC-BD	18.9	0.2	0.0	0.0
BC-CD	17.6	0.9	0.0	0.0
BD-CD	15.1	-0.9	0.0	0.0
Mean	2.8	0.65	-3.9	0.24
Dispersion	21.3	1.46	6.9	0.58
Ratio, db	-8.8	-3.5	-4.9	-3.5

TABLE D.5 DISPERSION OF SAMPLE RECORDED DEVIATIONS FOR THE FOURTEEN SYSTEM COMBINATIONS, KING FISH

System Combinations	0.084 Sec dAZ	dEL	1.008 Sec dAZ	dEL
AB-AC	-21.6	-0.125	-8.2	-0.103
AB-AD	-21.8	-0.164	-11.7	-0.032
AB-BC	-23.8	-0.125	-8.1	-0.105
AB-BD	-23.8	-0.125	-12.2	-0.023
AC-AD	-21.6	-0.160	-8.3	0.035
AC-BC	-21.7	0.010	-8.2	-0.108
AC-BD	-21.6	-0.109	-8.2	0.005
AC-CD	-21.7	0.049	-8.3	0.048
AD-BC	-25.6	-0.239	-4.9	0.101
AD-BD	-17.5	-0.078	-10.7	-0.013
AD-CD	-16.3	-0.055	-8.0	0.041
BC-BD	-23.8	-0.125	-6.2	0.020
BC-CD	-21.3	0.040	-6.3	0.010
BD-CD	-15.7	-0.065	-6.7	0.016
Mean	-21.3	-0.094	-8.3	-0.007
Dispersion	2.9	0.083	2.1	0.062
Ratio, db	8.7	0.5	6.0	-9.5

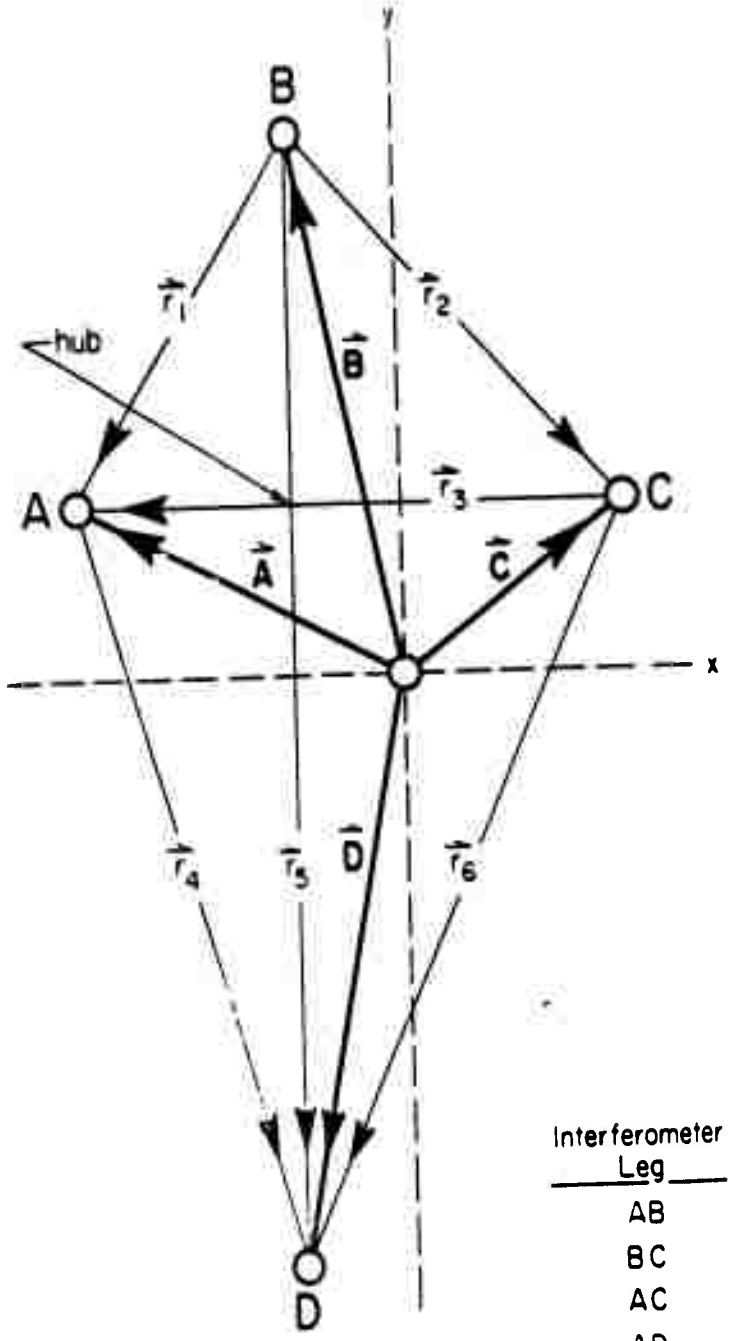

Interferometer Leg	Leg Length Meters
AB	10.3078
BC	11.1803
AC	7.5000
AD	20.1556
BD	30.0000
CD	20.6155

Figure D.1 Interferometer geometry.

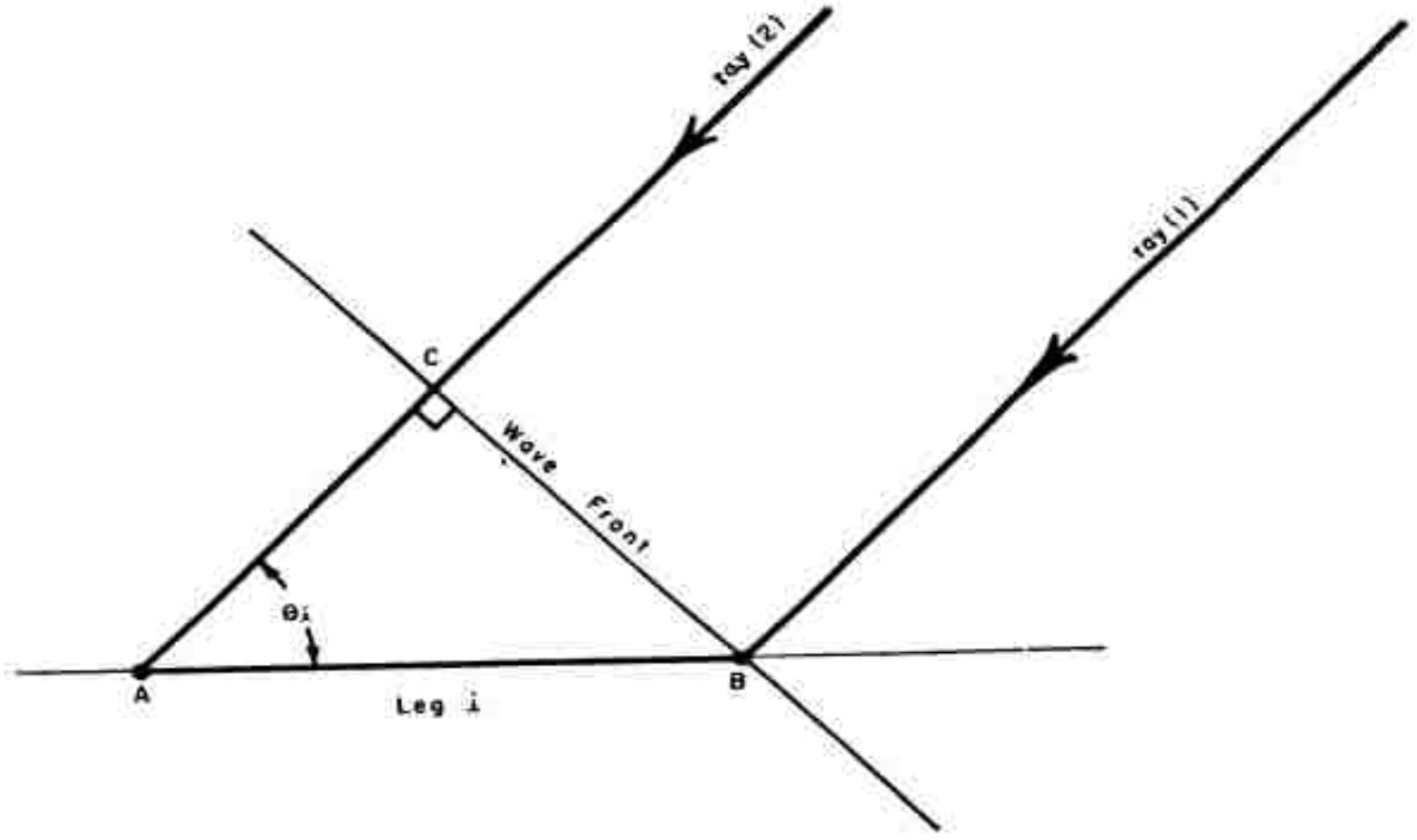

Figure D.2 Wave front incident to an interferometer antenna pair.

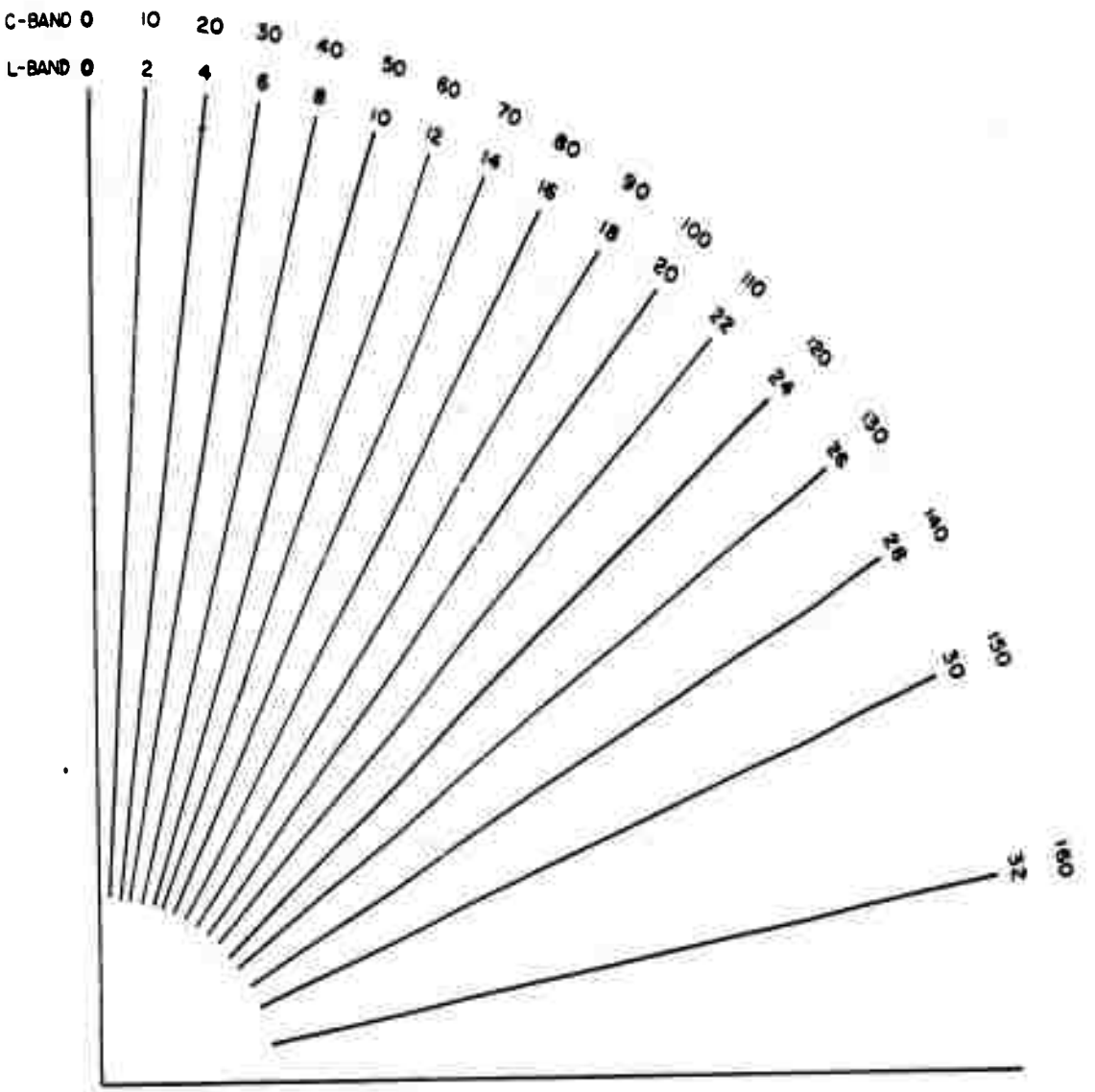

Figure D.3 Slant plane lobe diagram, interferometer, Leg AB.

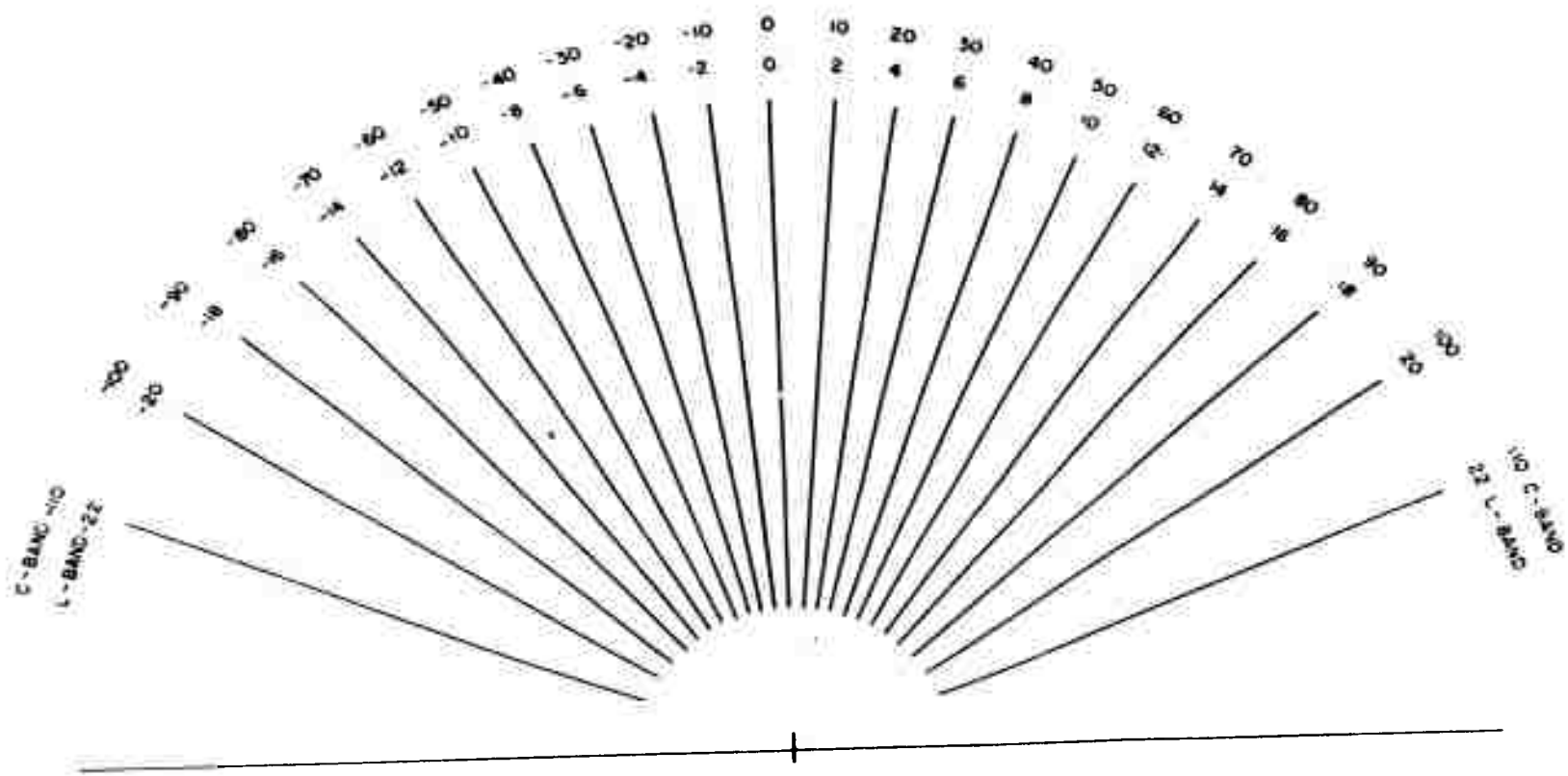

Figure D.4 Slant plane lobe diagram, interferometer, Leg AC.

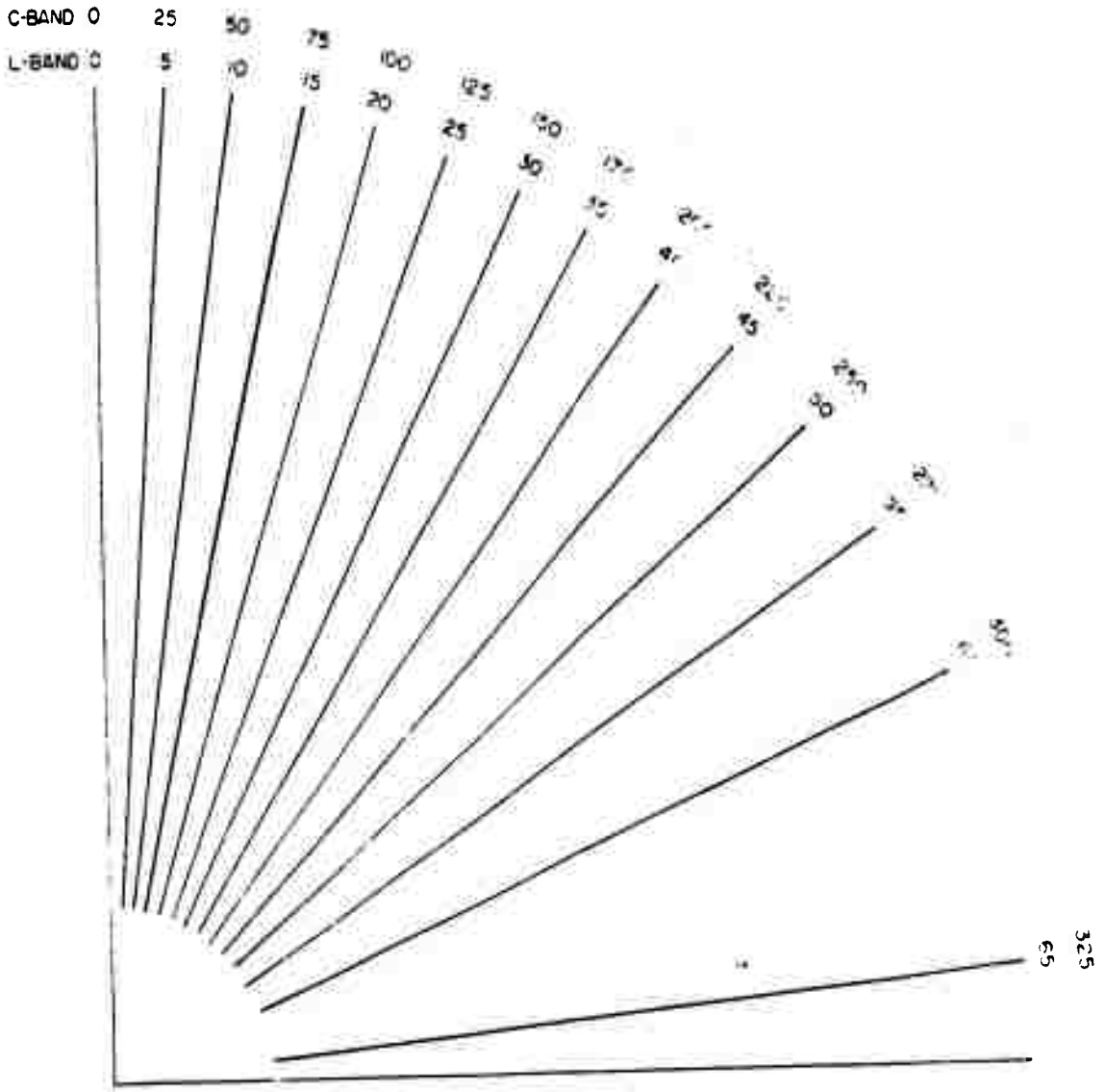

Figure D.5 Slant plane lobe diagram, interferometer, Leg CD.

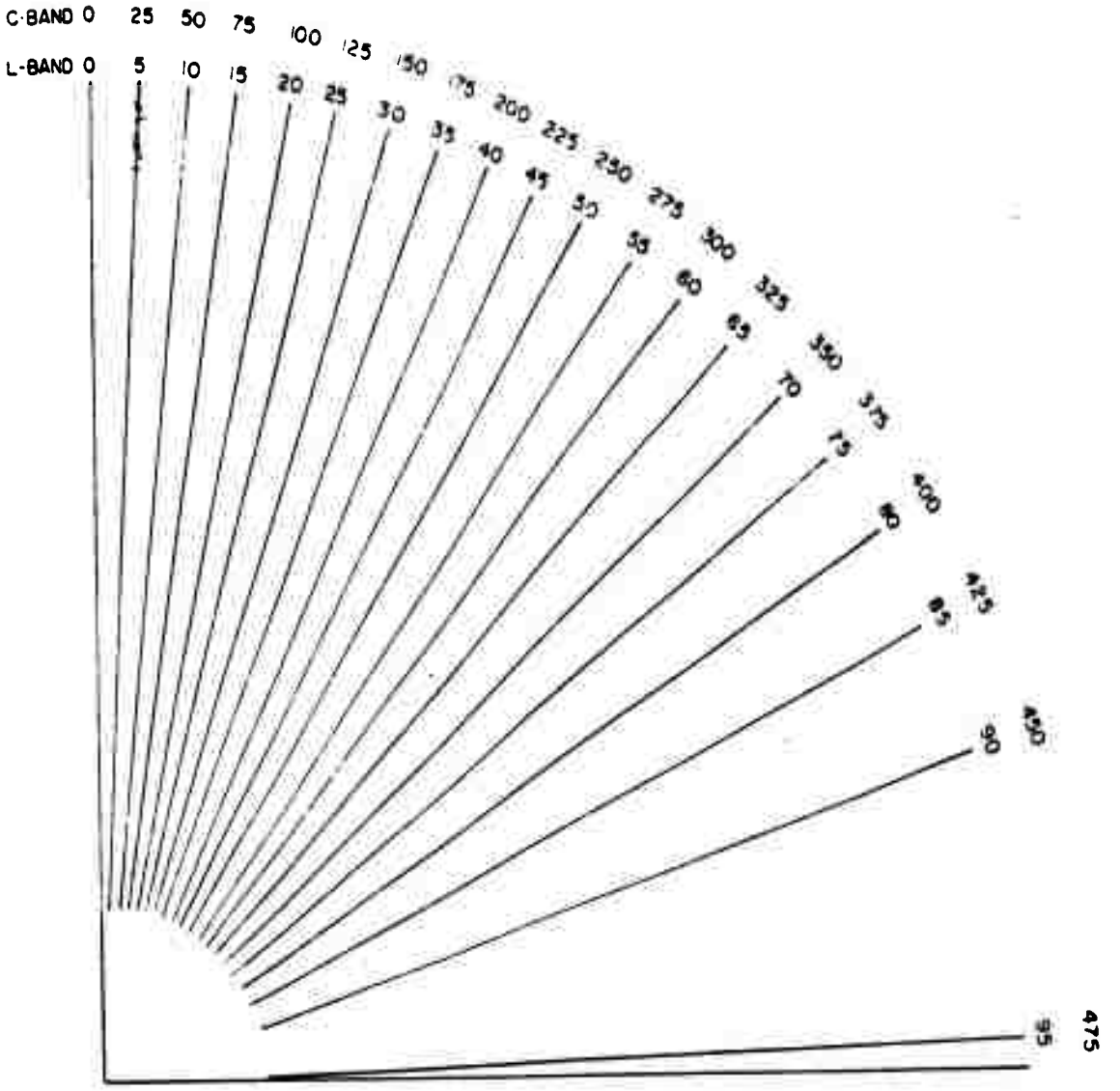

Figure D.6 Slant plane lobe diagram, interferometer, Leg BD.

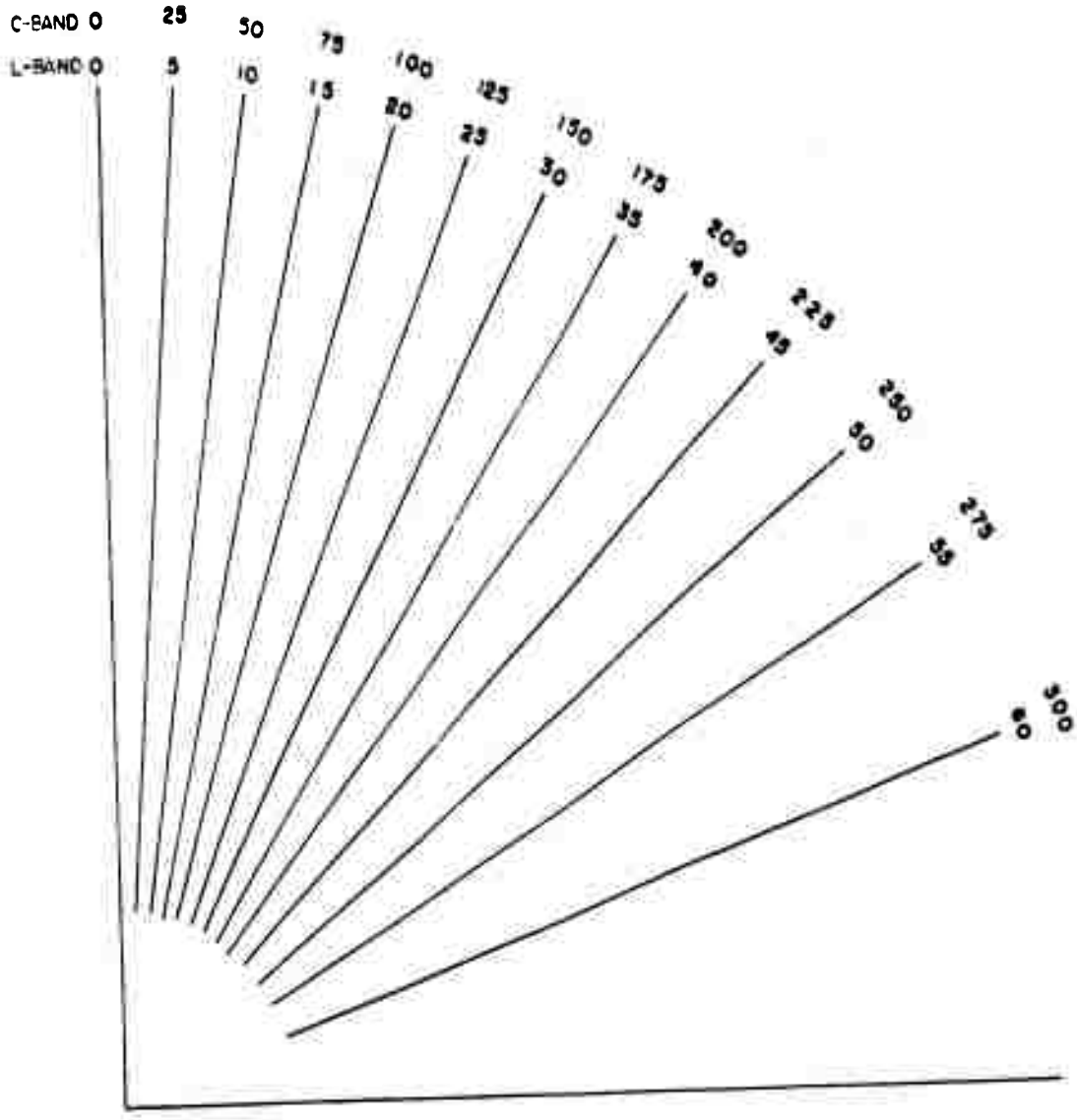

Figure D.7 Slant plane lobe diagram, interferometer, Leg AD.

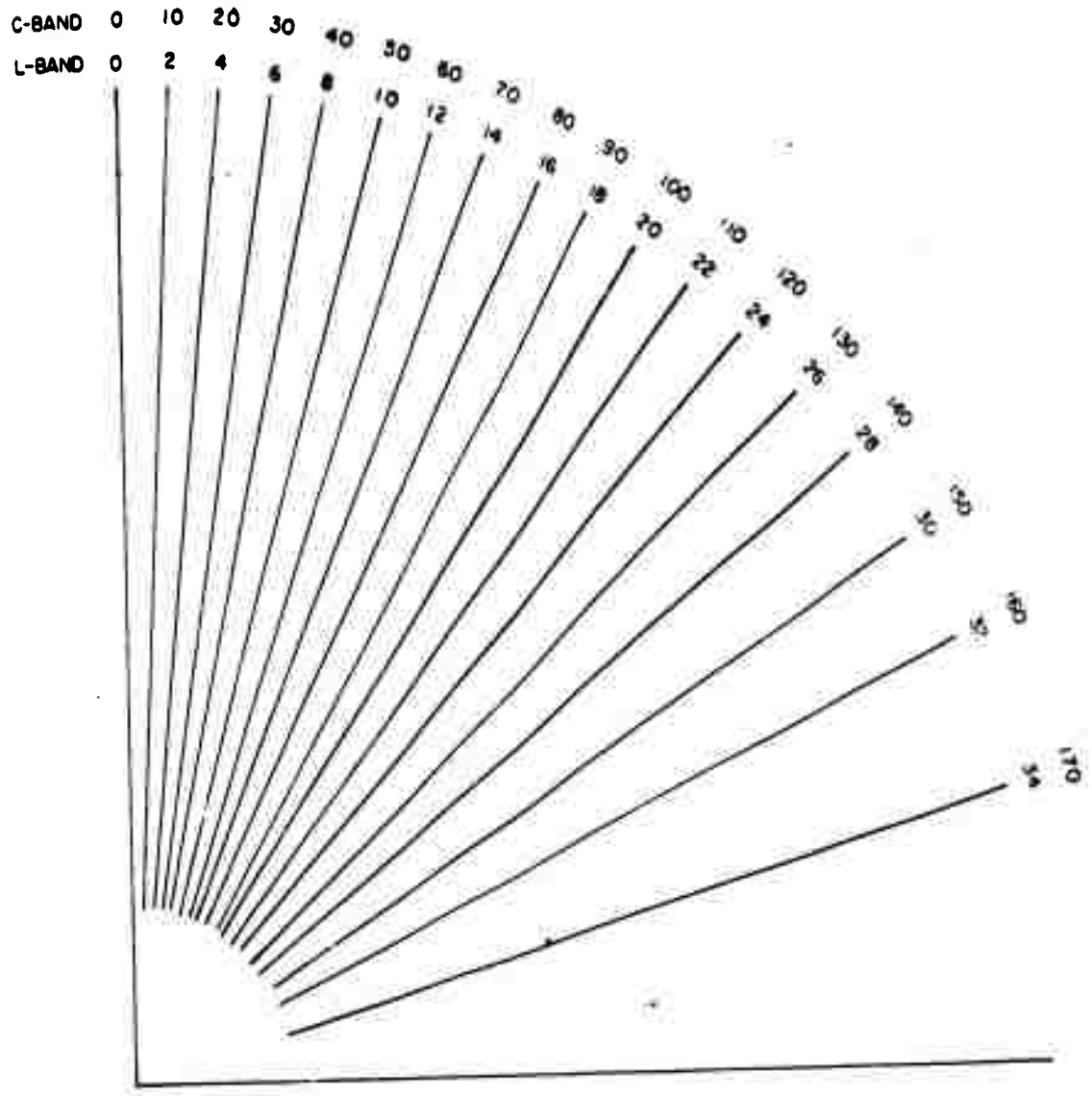

Figure D.8 Slant plane lobe diagram, interferometer, Leg BC.

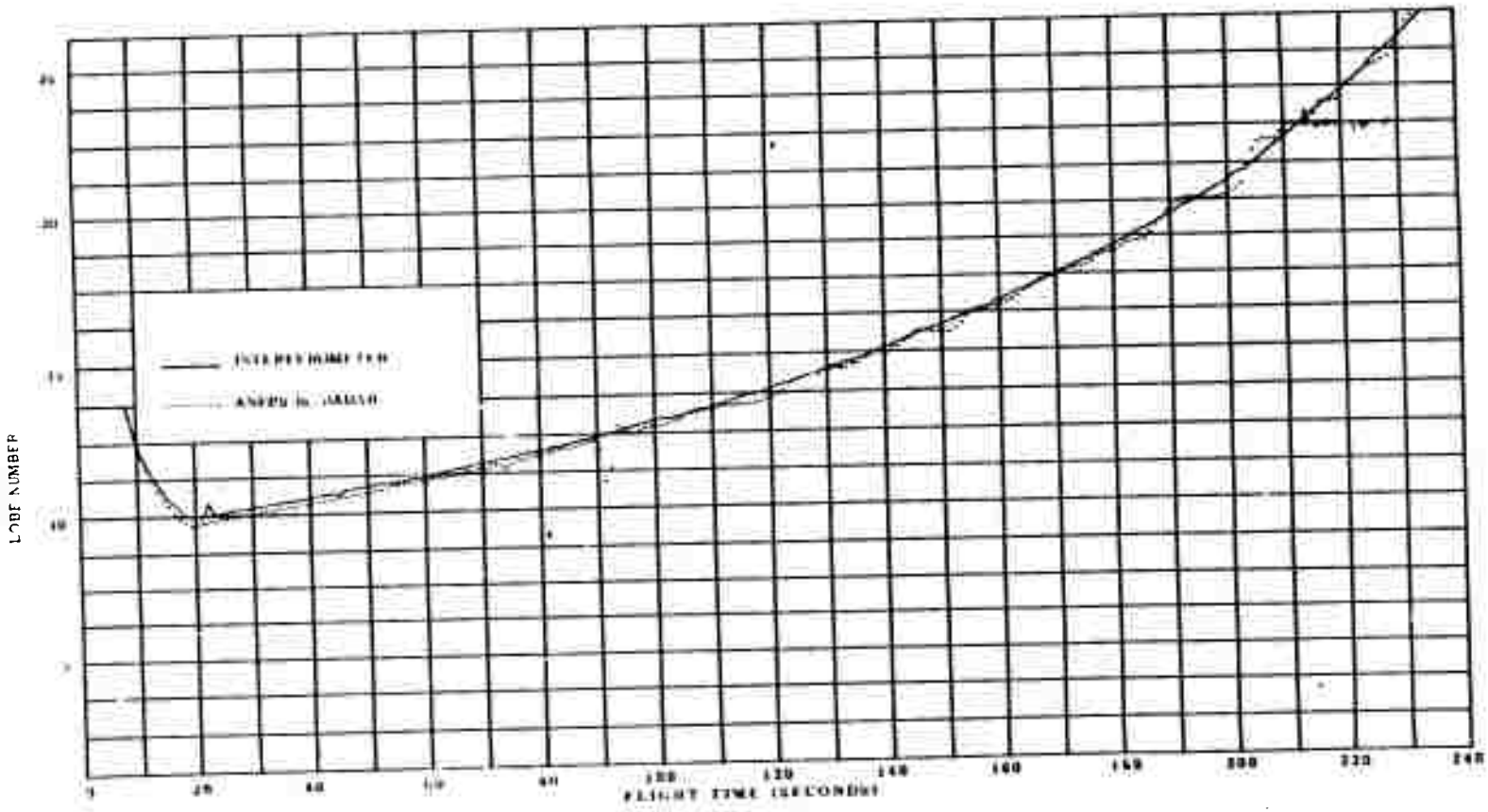

Figure D.9 Trajectory and interferometer lobe numbers, WSMR test, Leg AB.

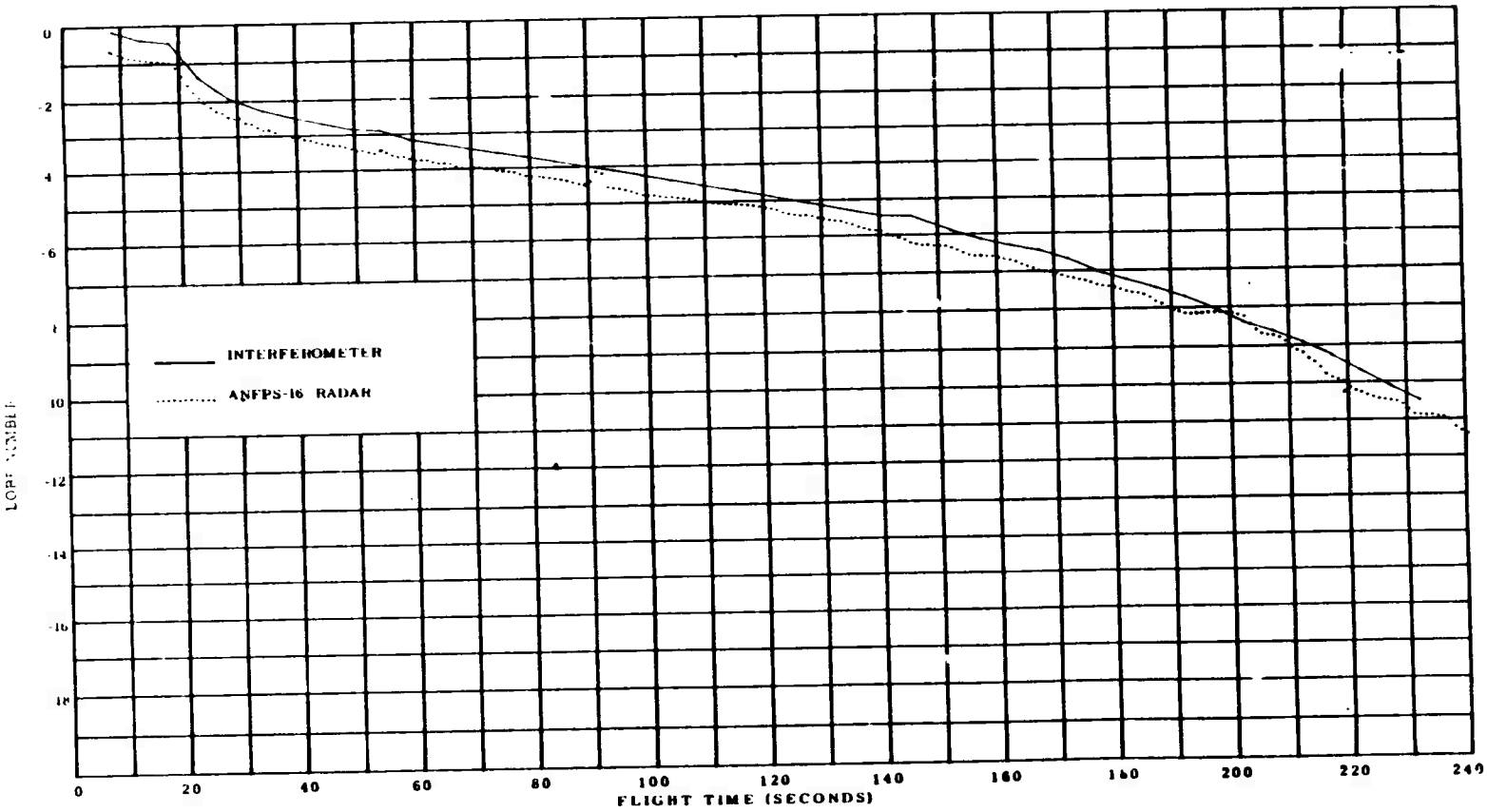

Figure D.10 Trajectory and interferometer lobe numbers, WSMR test, Leg AC.

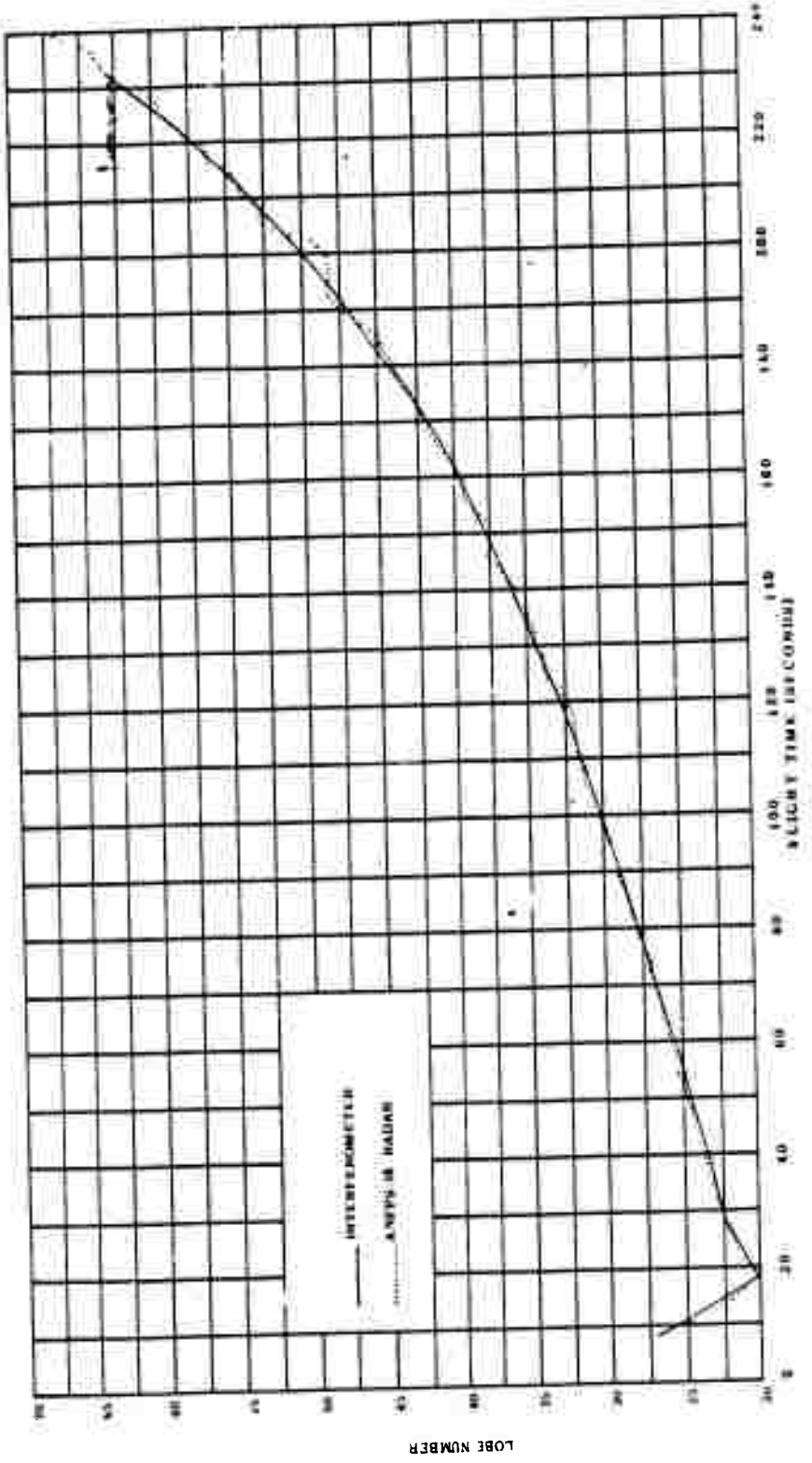

Figure D.11 Trajectory and interferometer lobe numbers, WSMR test, Leg AD.

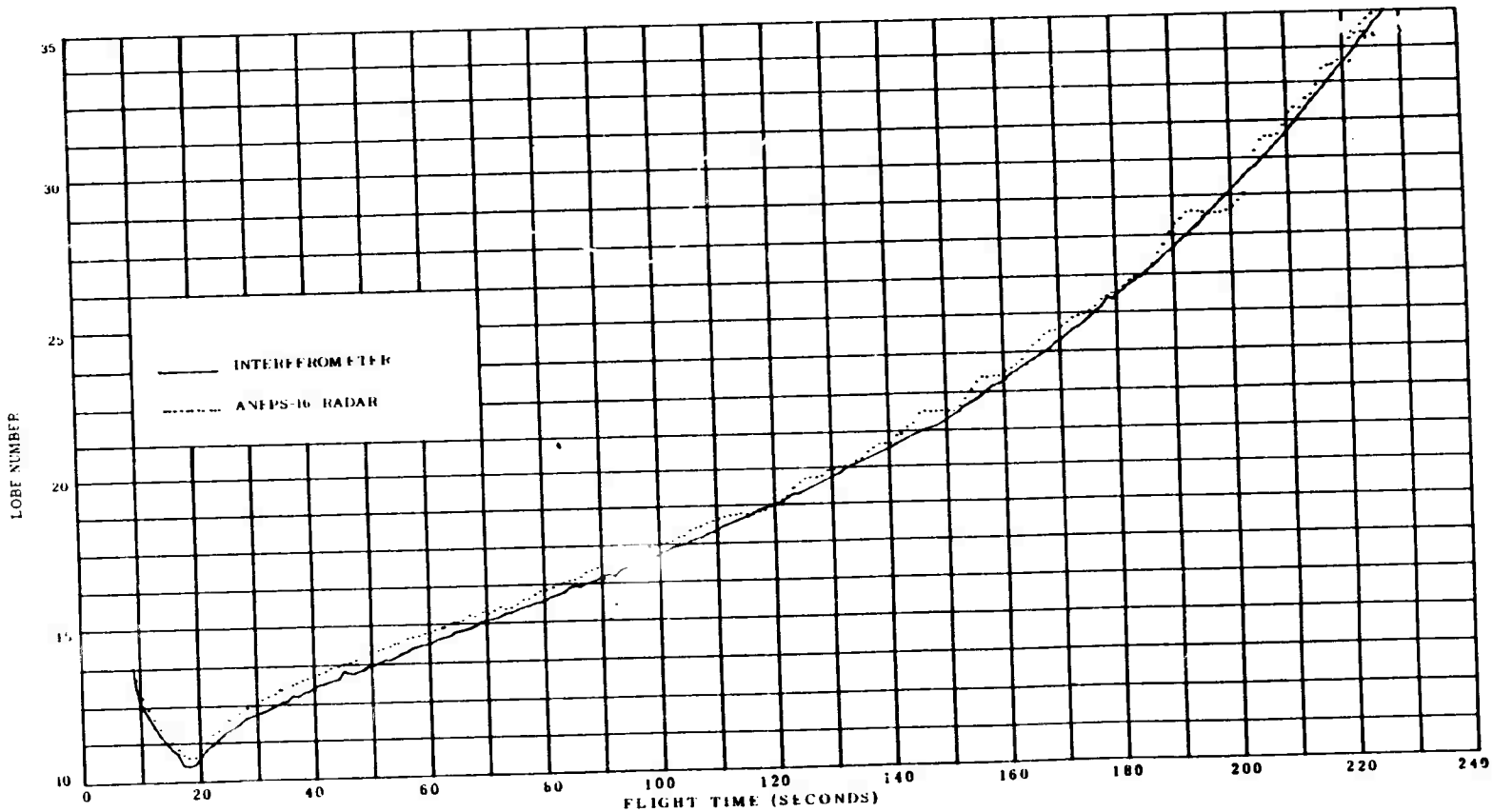

Figure D 12 Trajectory and interferometer lobe numbers, WSMR test, Leg BC.

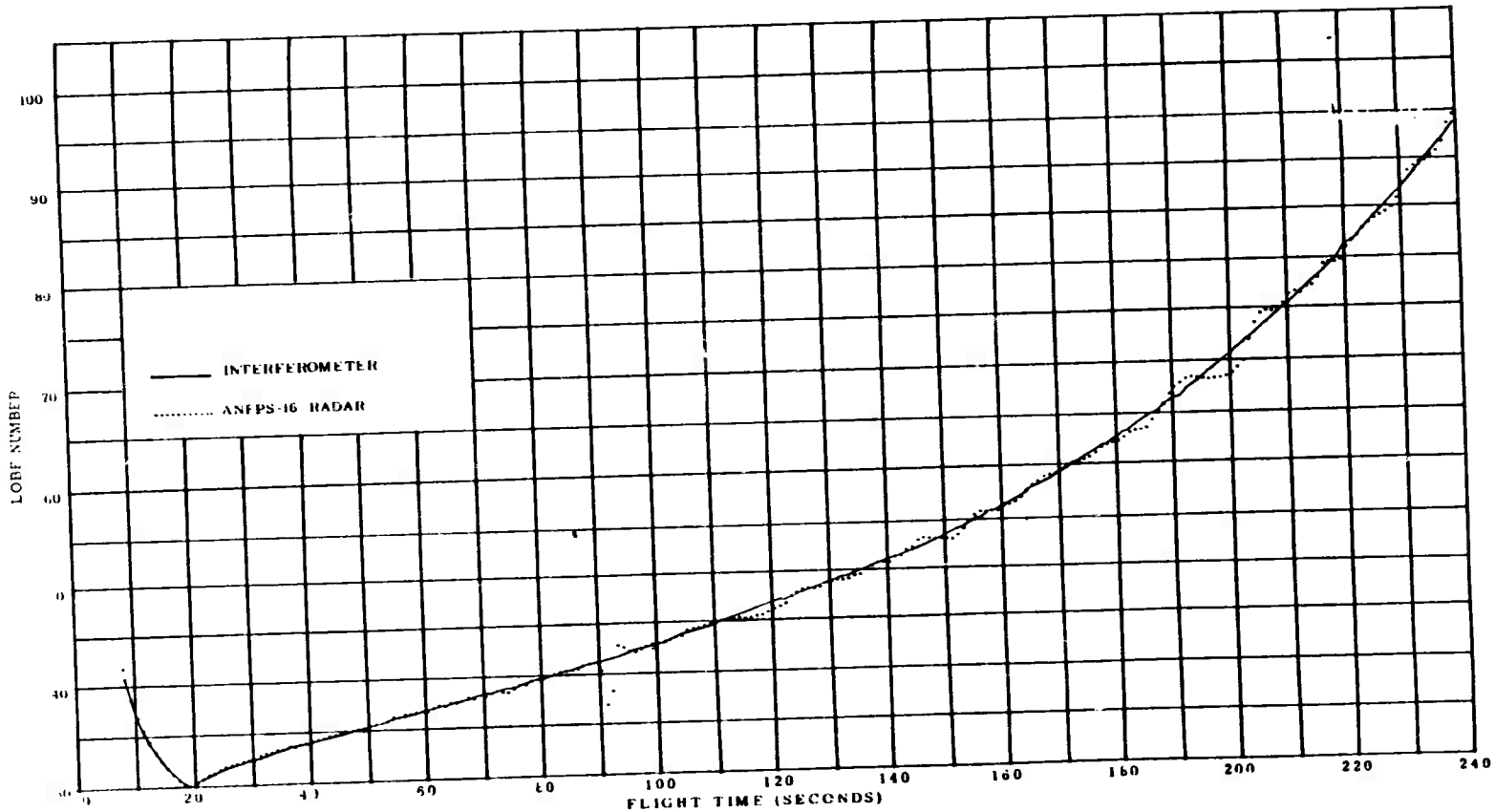

Figure D.13 Trajectory and interferometer lobe numbers, WSMR test, Leg BD.

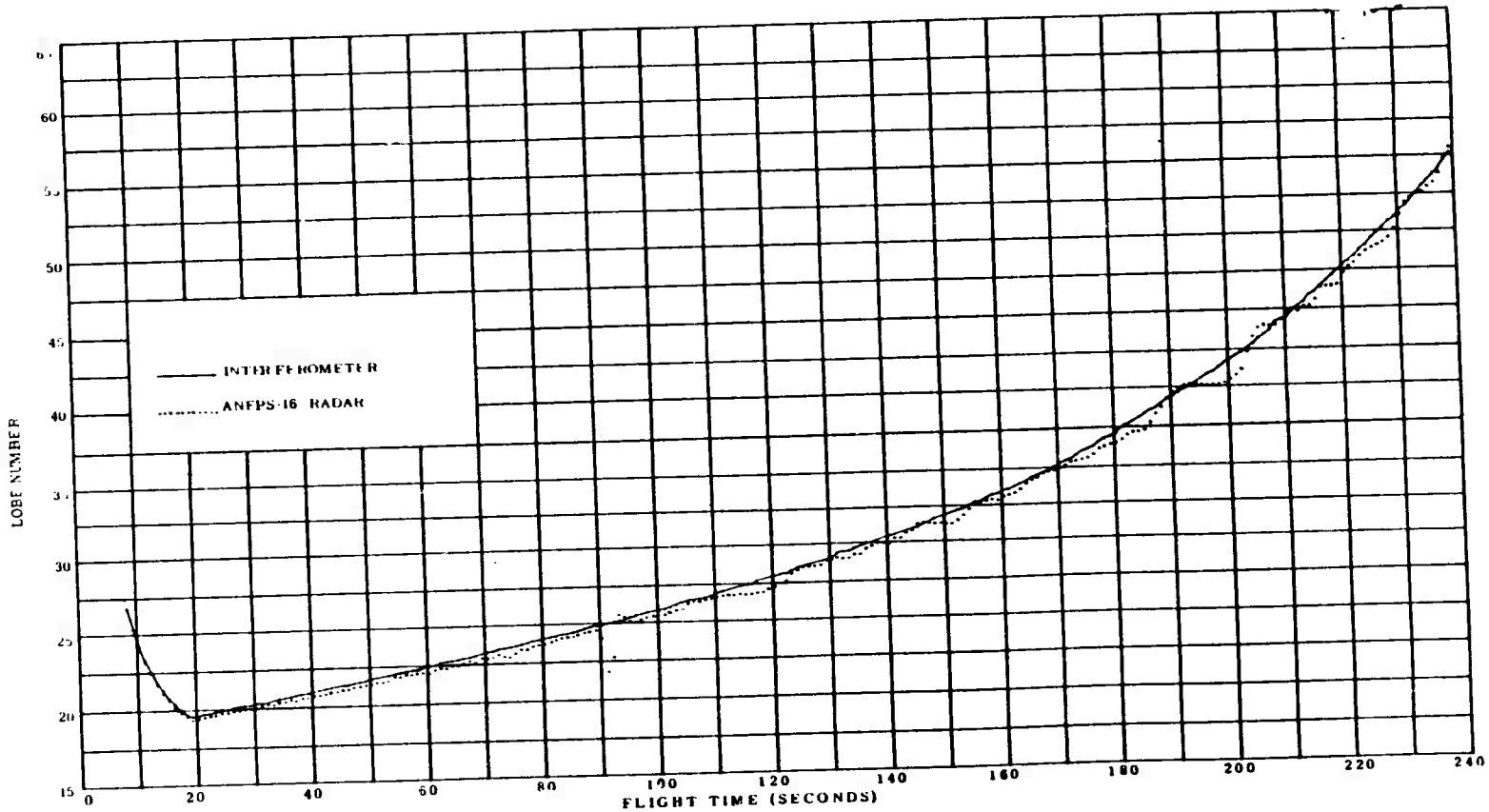

Figure D.14 Trajectory and interferometer lobe numbers, WSMR test, Leg CD.

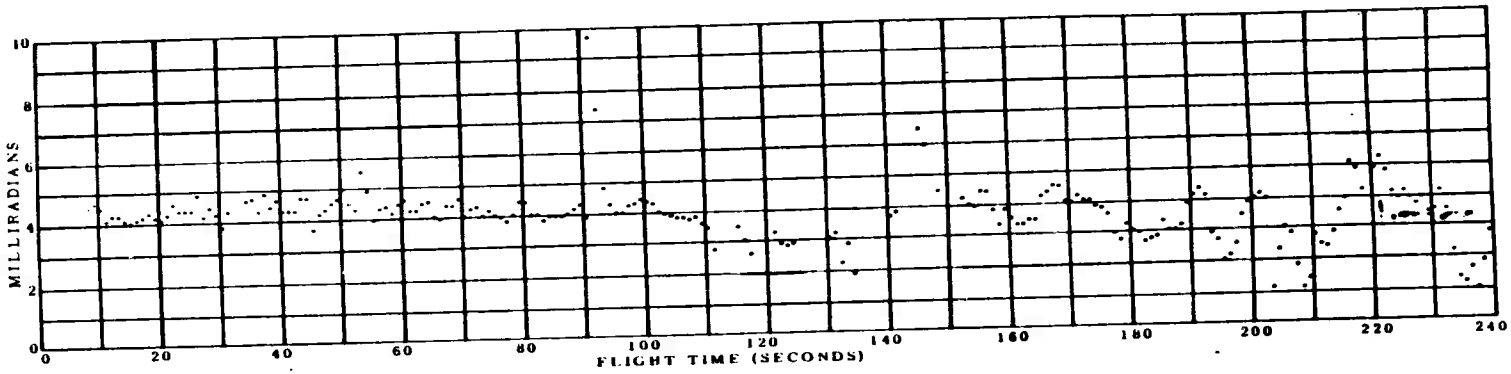

Figure D.15 Interferometer and radar angular comparison, WSMR test, Interferometer Combination AC-BD.

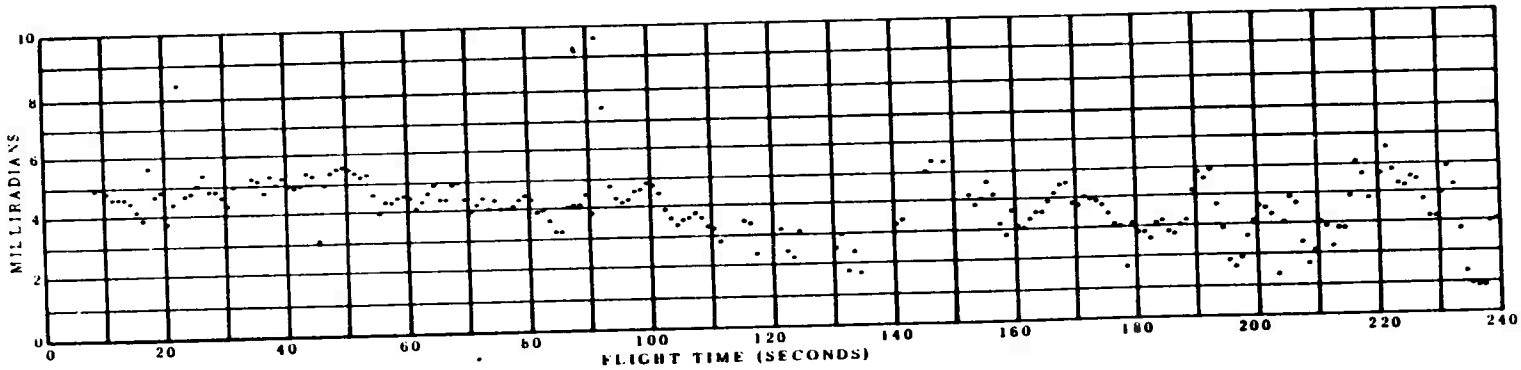

Figure D.16 Interferometer and radar angular comparison, WSMR test, Interferometer Combination AB-BC.

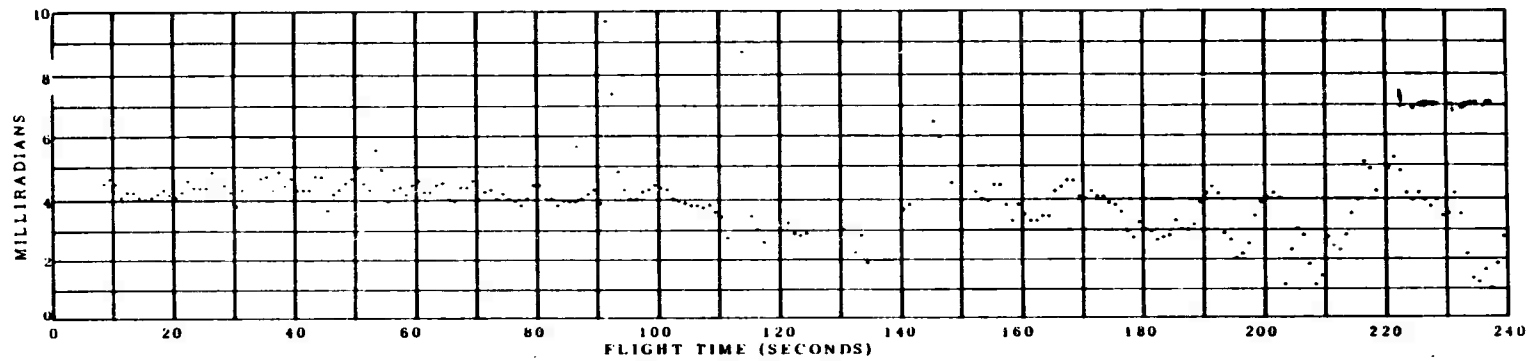

Figure D.17 Interferometer and radar angular comparison, WSMR test, Interferometer Combination AC-CD.

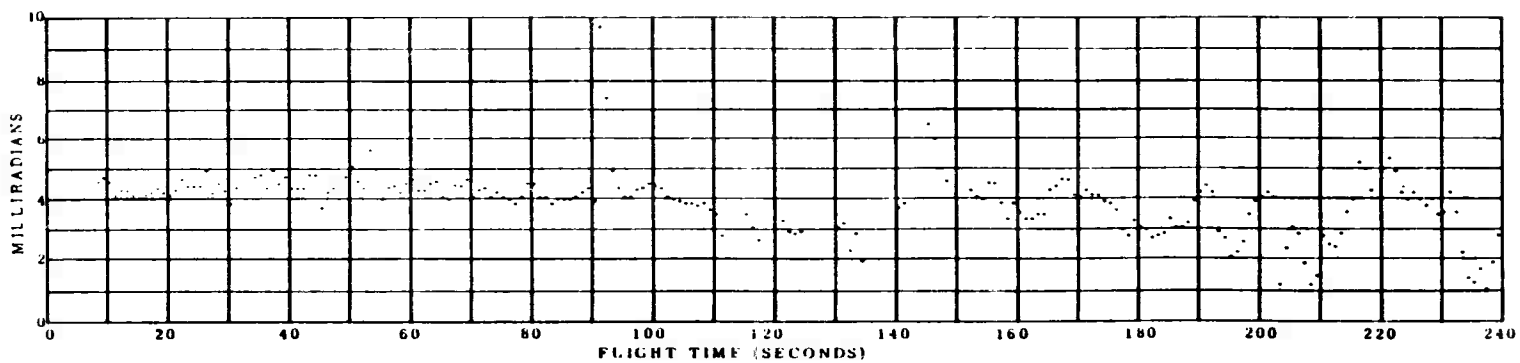

Figure D.18 Interferometer and radar angular comparison, WSMR test, Interferometer Combination AB-BD.

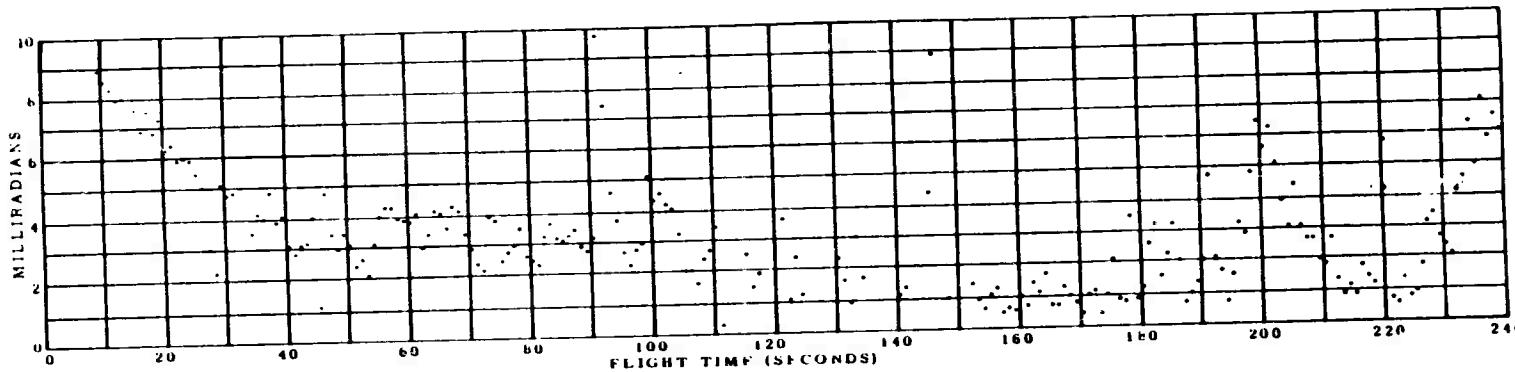

Figure D.19 Interferometer and radar angular comparison, WSMR test, Interferometer Combination AD-BD.

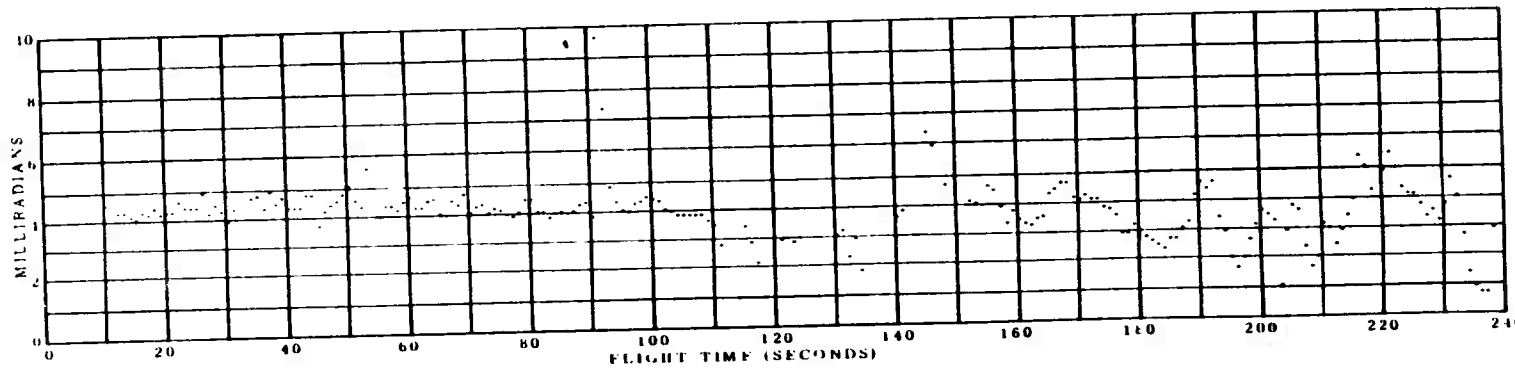

Figure D.20 Interferometer and radar angular comparison, WSMR test, Interferometer Combination BC-AC.

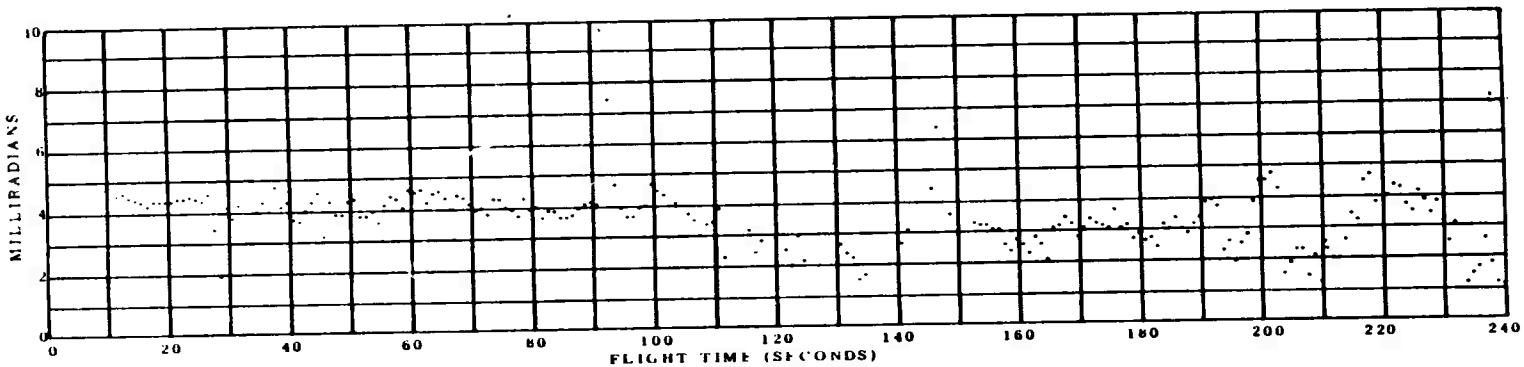

Figure D.21 Interferometer and radar angular comparison, WSMR test, Interferometer Combination AD-CD.

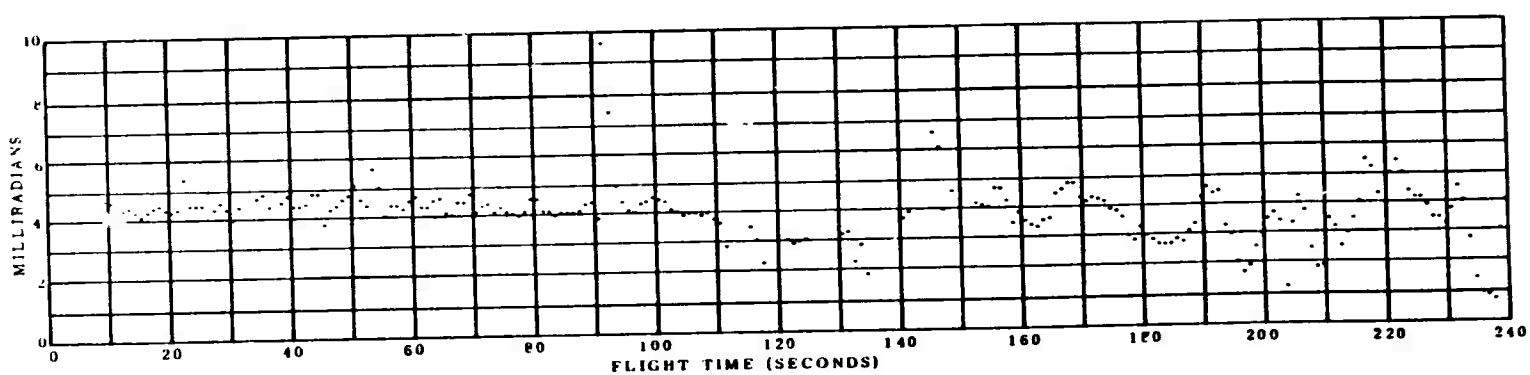

Figure D.22 Interferometer and radar angular comparison, WSMR test, Interferometer Combination AB-AC.

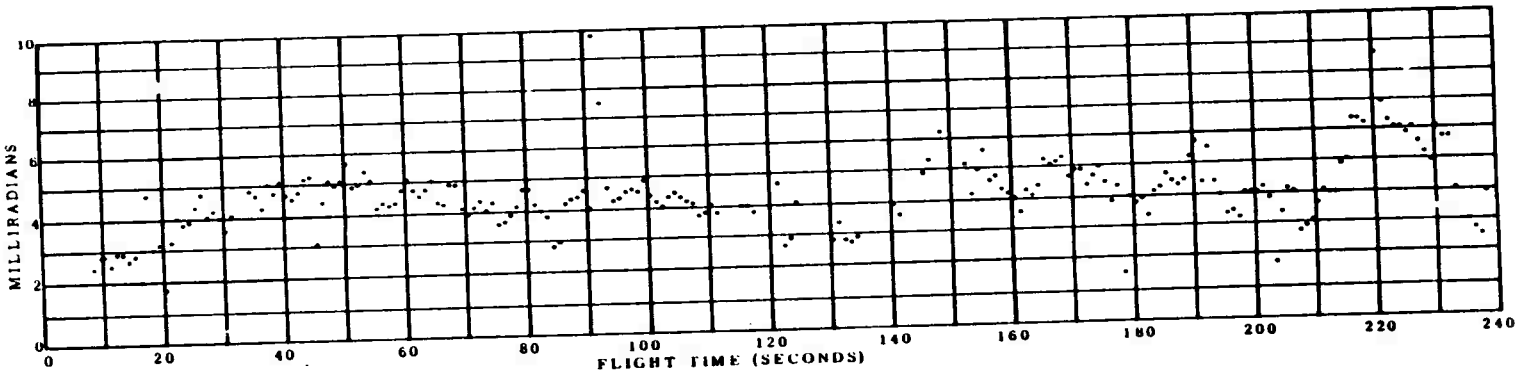

Figure D.23 Interferometer and radar angular comparison, WSMR test, Interferometer Combination BC-BD.

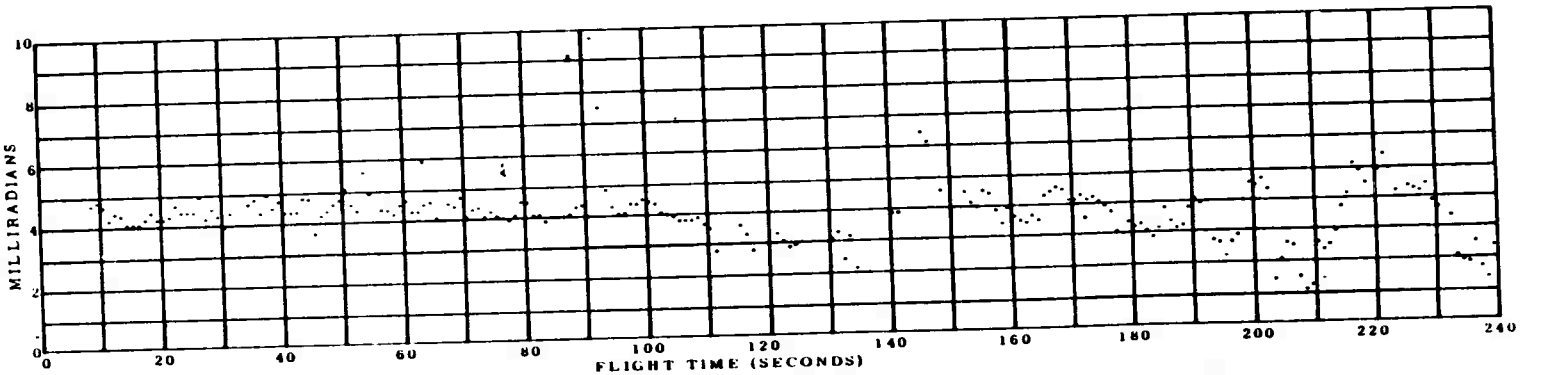

Figure D.24 Interferometer and radar angular comparison, WSMR test, Interferometer Combination AC-AD.

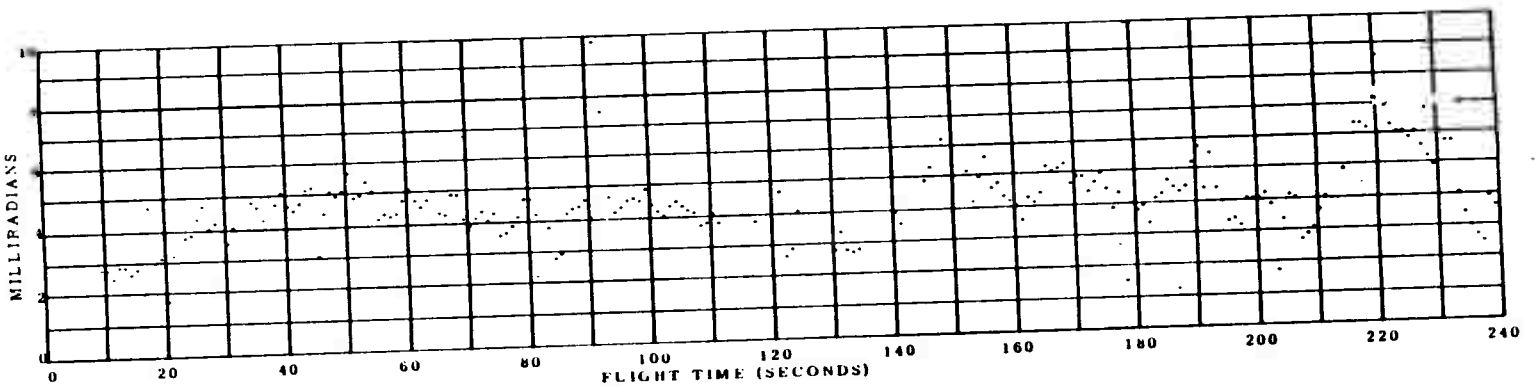

Figure D.25 Interferometer and radar angular comparison, WSMR test, Interferometer Combination BC-CD.

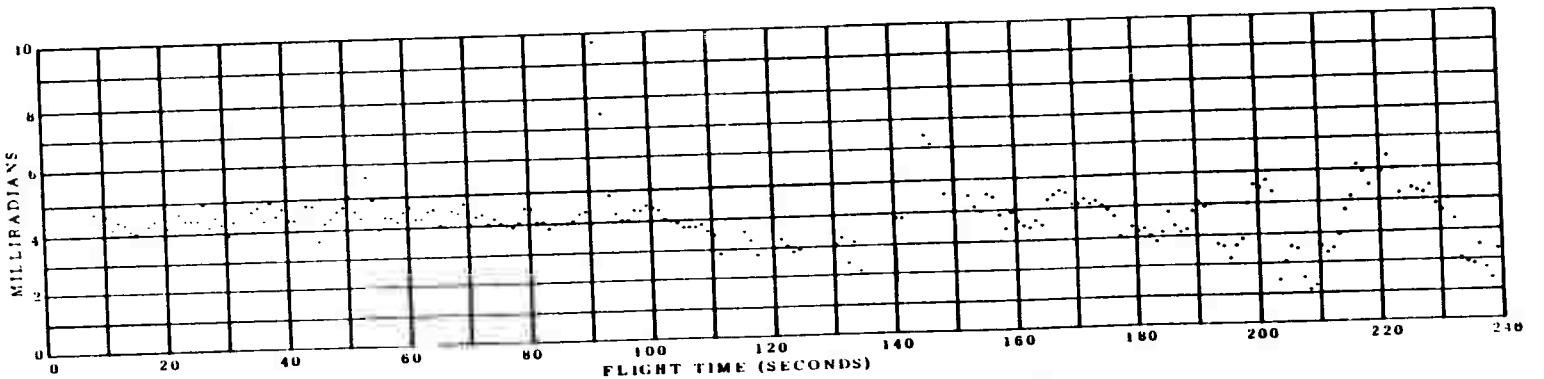

Figure D.26 Interferometer and radar angular comparison, WSMR test, Interferometer Combination AB-AD.

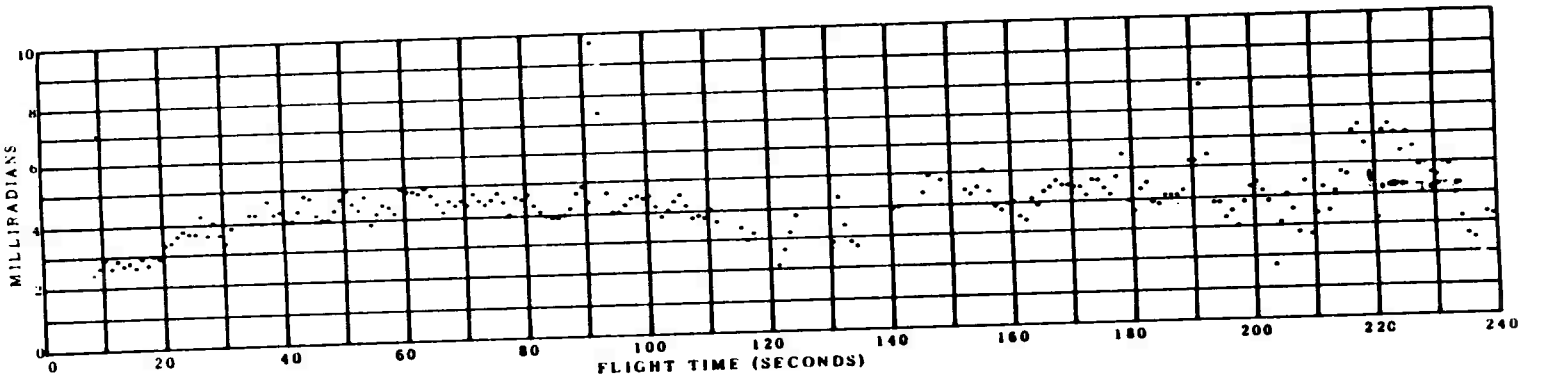

Figure D.27 Interferometer and radar angular comparison, WSMR test, Interferometer Combination BD-CD.

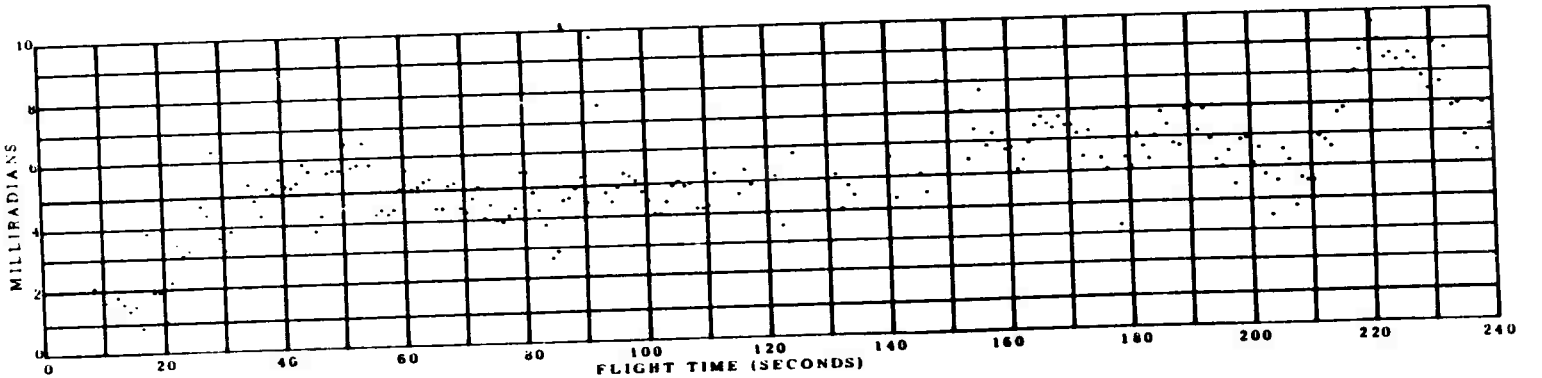

Figure D.28 Interferometer and radar angular comparison, WSMR test, Interferometer Combination BC-AD.

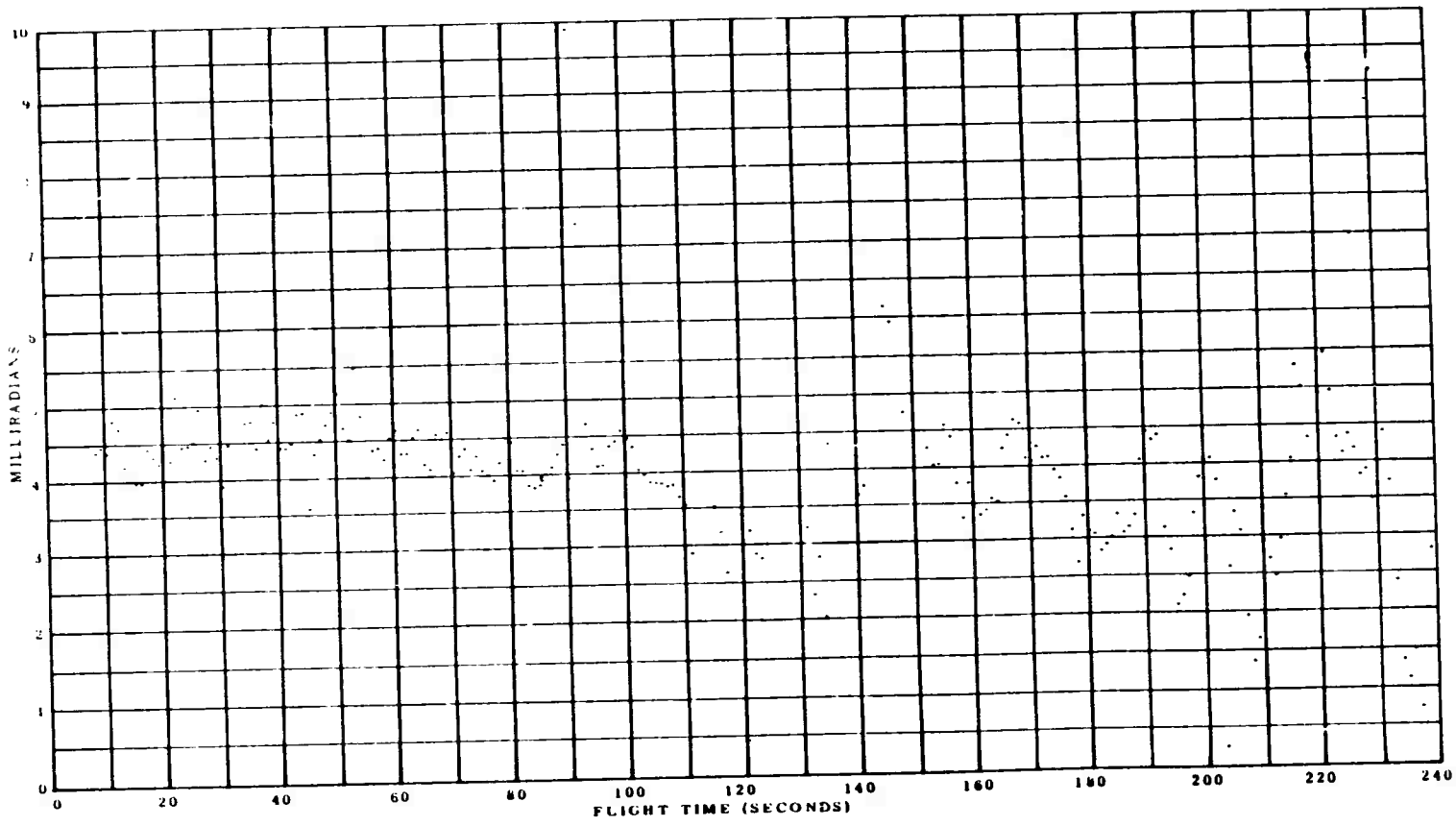

Figure D.29 Interferometer and radar angular comparison, WSMR test, least-squares combination.

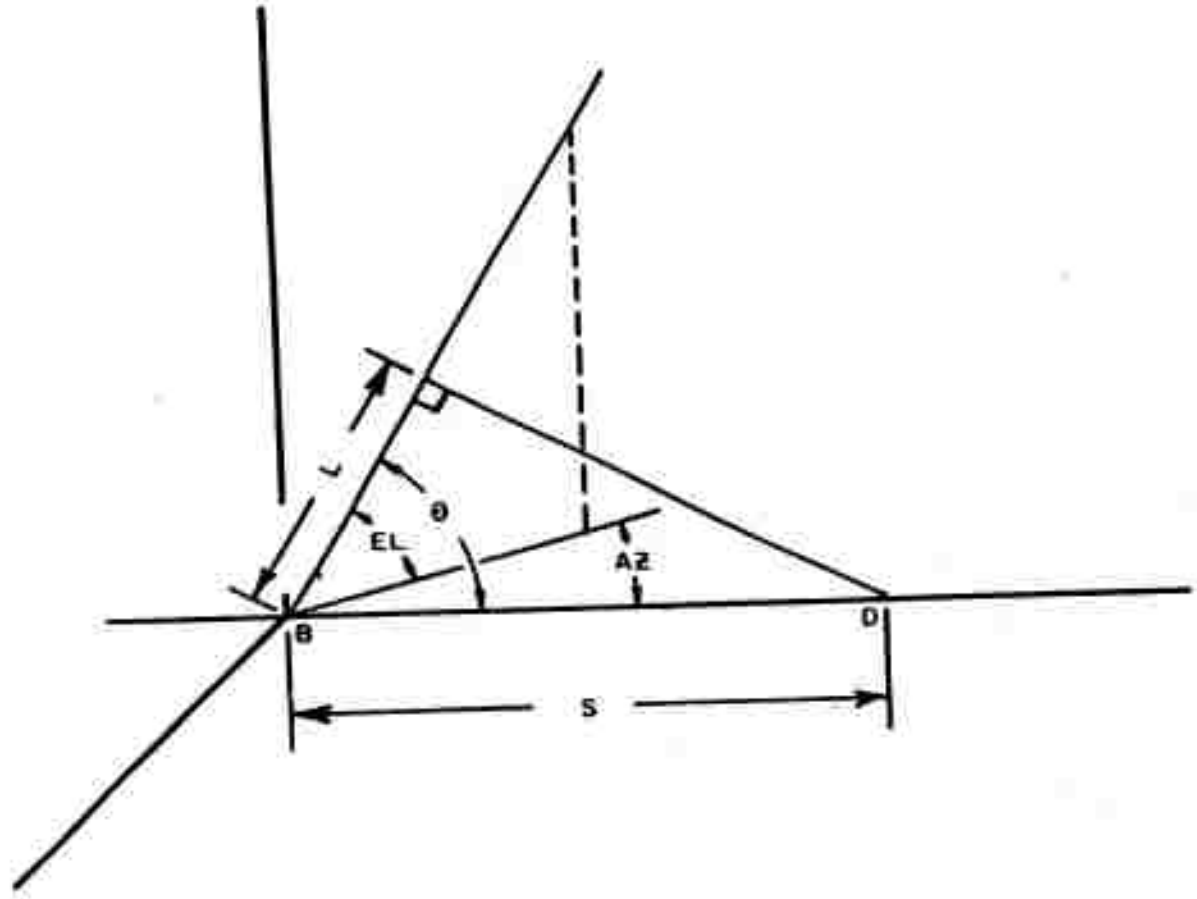

Figure D.30 Ray-path directional components.

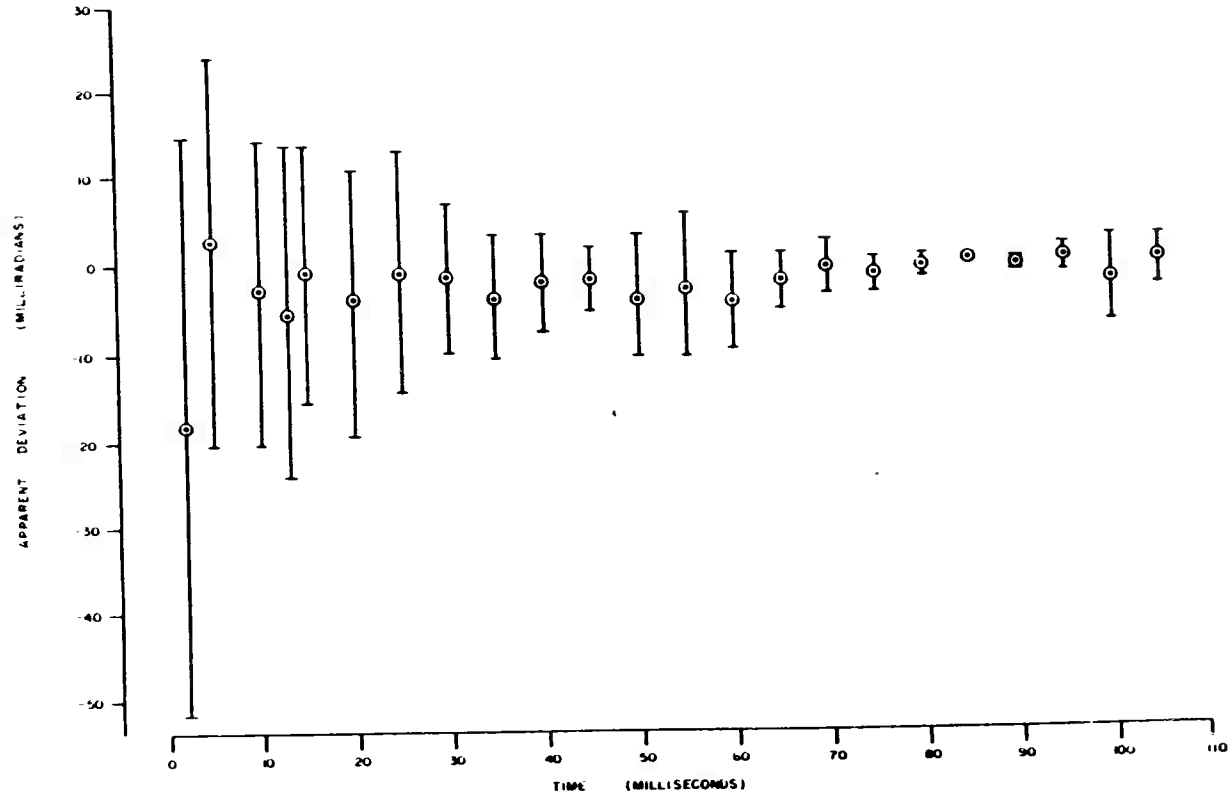

Figure D.31 Perturbation component in azimuth plane, Blue Gill.

REFERENCES

1. W.S. Knapp and others; "Electromagnetic Blackout Handbook"; DASA 1280, May 1962; Defense Atomic Support Agency, Washington, D.C.; Secret Restricted Data.

2. "DASA Project 6.1a, Operation Dominic, Final Report"; EDL-E76, 26 December 1962; Electronic Defense Laboratories, Sylvania Electronic Systems; Mountain View, California; Secret Restricted Data.

3. W. Dudziak and others; "Blue Gill, Third Report of the Fish Bowl Rapid Interpretation Group"; DASA Data Center Special Report 8, 30 November 1962; TEMPO, General Electric Company, Santa Barbara, California; Secret Restricted Data.

4. C.A. Blank and others; "King Fish, Fourth Report of the Fish Bowl Rapid Interpretation Group"; DASA Data Center Special Report 9, 30 November 1962; TEMPO, General Electric Company, Santa Barbara, California; Secret Restricted Data.

5. R. Henrick; "Beta Ray Absorption from King Fish, Symposium Proceedings: Radar Blackout"; DASA 1365, April 1963; Defense Atomic Support Agency, Washington, D.C.; Secret Restricted Data.

6. W. Dudziak and others; "Tight Rope, Fifth Report of the Fish Bowl Rapid Interpretation Group"; DASA Data Center Special Report 10, 30 November 1962; TEMPO, General Electric Company, Santa Barbara, California; Secret Restricted Data.

7. M.P. Shuler; Edgerton, Germeshasen and Grier, Inc., Boston, Massachusetts; private communications, 1963; Secret Restricted Data.

8. "Final Trajectory Data for Fish Bowl Test Series, Operation Dominic"; FER/73-1, 24 April 1963; Cubic Corporation, San Diego, California; Confidential.

Pages 177 and 178 deleted.